~Enhancing Water Supply Reliability~

An Interdisciplinary Research Project to Enhance Predictive Capacity on the Colorado River

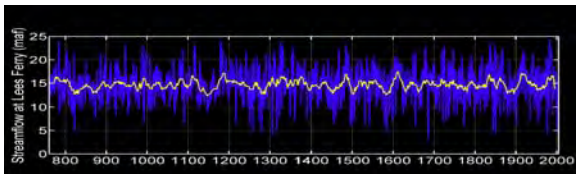

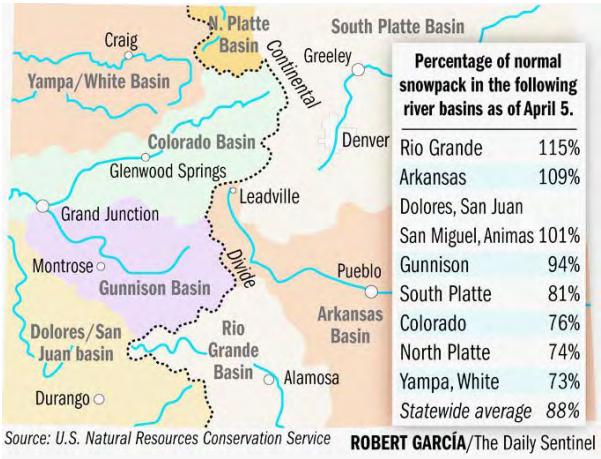

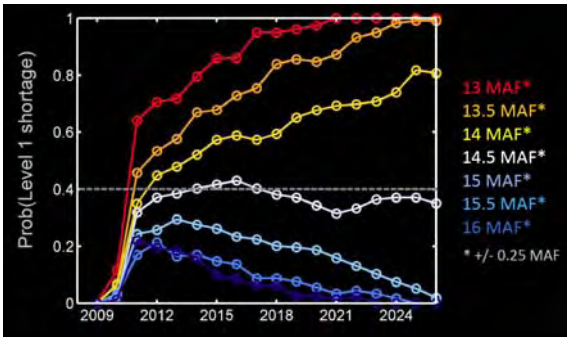

Annual Report Phase III

April 2010

Memorandum

TO: **CAROL ERWIN, ARIZONA PROJECTS OFFICE, RECLAMATION**

TERRY FULP, BOULDER CANYON OPERATIONS OFFICE, RECLAMATION

FROM: **ROSALIND BARK ON BEHALF OF BONNIE COLBY, DAVE MEKO, PETER TROCH AND CONNIE WOODHOUSE, UNIVERSITY OF ARIZONA.**

DATE: **April 20, 2010**

RE: **ANNUAL REPORT, PHASE III**

ENHANCING WATER SUPPLY RELIABILITY PROJECT

The enclosed materials constitute the annual report for Phase III of the University of Arizona – Reclamation *Enhancing Water Supply Reliability through Enhanced Use of Climate Information* study. This ongoing collaboration has brought together an interdisciplinary team that is finding new ways to work together with the end goal to inform better management of water supply risks to end-users in the Lower Colorado River Basin through improved understanding of hydrologic variability, better predictive skills, and the management of supply risk. The project has contributed to the education of six Master's students[1] and four PhD students[2] over the lifetime of the project and it supports two postdocs.[3] Since the last report a number of high-quality products have been developed, including academic manuscripts and guidebooks. Equally important is the ongoing collaboration between Reclamation staff and the University of Arizona faculty, postdoctoral research associates, and graduate students.

[1] Agricultural and Resource Economics: Katie Pittenger MSc 2006, Lana Jones MSc 2008, Michael O'Donnell MSc expected 2010. Hydrology: Laura Lindenmeyer MSc 2006, Matthew Switanek MSc 2008, and Racheal Beagles MSc expected 2010.

[2] Dendrochronology: Scott St. George PhD 2007, Kiyomi Morino PhD 2008. Water management and policy: Dustin Garrick PhD 2010 (a section of his dissertation was related to this project, for which he co-wrote a JAWRA publication that won AWRA's Boggess Award in 2009). Hydrology: Matthew Switanek PhD expected 2011.

[3] Dr. Kiyomi Morino (dendrochronology) and Dr. Rosalind Bark (water management).

Research Update

Phase III of our project comprises research in disciplinary areas as well as interdisciplinary efforts. Interdisciplinary efforts have focused on using the tree-ring reconstructed streamflows in assessing the effectiveness of various Intentional Created Surplus scenarios in reducing and postponing system shortages. This is a collaborative research effort between Rosalind Bark and Kioymi Morino, with Reclamation personnel. This research has been presented at a number of academic venues and also at workshops for Arizona water managers. These research efforts have been made possible in large part by the training Dr. Kiyomi Morino has completed to run Reclamation's Colorado River Simulation System (CRSS) model. This training was funded by the EWSR grant.

The economics sub-group, of Dr. Bonnie Colby and Michael O'Donnell, focused on research and preparation of stakeholder materials on innovative transfer mechanisms to enhance supply reliability for urban and habitat water needs in the Lower Colorado River Basin. Three recently completed guidebooks for stakeholders provide practical information for water supply climate change adaptation through water banks, water auctions, and dry-year contracts. The guidebooks provide a review of where and how these mechanisms have been used, implementation steps, and their strengths and weaknesses.

The paleo-hydrology team of Drs. Mary Glueck and Connie Woodhouse has been investigating droughts in the Upper Colorado River Basin (UCRB). The goal has been to develop a drought atlas of the major droughts in the basin. Their strategy has been to: 1) define droughts; 2) examine characteristics of monthly seasonal precipitation and temperature and annual runoff sequences corresponding to each drought; 3) the associated conditions (sea surface temperatures (SST), sea level pressures (SLP), circulation indices, storm trajectories for each drought); and 4) the spatial footprint/extent of these droughts beyond the UCRB. The droughts in the atlas will be assessed and compared to determine whether it is possible to identify drought "types" with respect to spatial and temporal patterns and associated circulation (and potential causes). Results to date will be presented at the Boulder meeting in May 2010, and a research paper will follow.

Meanwhile, Dr. Kiyomi Morino continues with studies incorporating paleo-data into Reclamation's river operations and planning models. She has shifted focus from the 24-month model to CRSS. For this research she collaborates with the other postdoc on this grant, Dr. Rosalind Bark, and also with Carly Jerla, Reclamation. In addition, Drs. Meko and Morino are working towards the objective of extending and improving tree-ring reconstructions for Lower Basin tributaries. Data preparation for this research has been completed. However, heavy snows over the Southwest this winter cut short plans for field research for Lower Basin tree-ring collection sites. The postponed fieldwork effort will begin in June and end in September.

There are two strands to the hydrology group's research program which is directed by Dr. Peter Troch. One focuses on seasonal to decadal predictability of water availability in the Lower Colorado River basin. Although as little as 10% of Colorado River flows are generated in the lower basin, these contributions can influence the amount of water stored or released throughout the reservoir system. Furthermore,

conditions in the lower basin may affect demand. Several approaches are followed, from data analysis of the observed record of ocean and hydrometeorological drivers of streamflow to the use of large scale hydrological models (VIC) and tree ring reconstructions of precipitation and streamflow. The overall aim is to quantify prediction skill using observed correlations between Atlantic Multidecadal Oscillation (AMO), Pacific Decadal Oscillation (PDO), and El Niño/Southern Oscillation (ENSO) and streamflow variability at the tributary level, and to seek physical explanations for these observed correlations.

The second strand of the hydrology research program focuses on the Upper Basin. Attempts were made to improve seasonal climate predictions for the Gunnison and Little Colorado River basins. This was done by keying into the most correlated oceanic regions, given a specified forecast outlook time, using SST and SLP. These most correlated regions' time series were subsequently used as predictors. Different statistical methods were used (multiple linear regression, principal component analysis) to make the forecasts. Varying weights were applied to particular regions and statistical methods to provide the best forecasts over the time period (1931-2008). This work was published in Switanek et al., 2009. Although this work initially appeared promising, there seem to be two main problems with the methodology. First and foremost, there are certain outlook times, especially for the Gunnison, that the relationships do not seem to be part of a larger-scale pattern or a manifestation of some physical event like ENSO. Therefore, it is difficult to establish whether or not the regions of high correlation are informative or only statistical artifacts. Second, in addition to picking up on the larger-scale patterns of heat exchange between the ocean and the atmosphere, we also need to observe the response on land in a broader, dynamical pattern. The researchers are developing methodologies to address these issues.

Project Deliverables: a Summary

For the period April 2009 through March 2010

View http://www.azwaterinstitute.org/ewsr.html to access online versions of all the available publications, presentations, and media coverage of project results

---

The deliverables of this project include a number of manuscripts published in leading journals, posters presented at academic meetings, presentations, a Colorado River Basin Fact Sheet. The majority of our products are linked to this site, please see http://www.azwaterinstitute.org/ewsr.html. We have reproduced journal articles. To respect copyright these articles should not be widely shared. The Woodhouse et al., 2010 is in press: please contact the authors for a pre-print. Note that the three book chapters cited below are not yet in proof format but can be provided as unformatted pdfs, if requested. Copies of Powerpoint presentations can also be made available, on request.

Publications:

Colby B. and G. Frisvold (2010). Risk and Resilience: The Economics Of Climate-Water-Energy Challenges, IN THE ARID SOUTHWEST, Editors B. Colby and G. Frisvold, Resources for the Future Press, forthcoming.

Colby B. and R. **Bark** (2010). Chapter 41: Inter-sectoral water trading as a climate change adaptation strategy, in WATER RESOURCES PLANNING AND MANAGEMENT, Editors Q. Grafton and K. Hussey, Cambridge University Press, in press.

Jerla C., K. **Morino**, R. **Bark** and T. Fulp (2010). Chapter 22: The Role of Research and Development in Drought Adaptation on the Colorado River Basin, in WATER RESOURCES PLANNING AND MANAGEMENT, Editors Q. Grafton and K. Hussey, Cambridge University Press.

Knight, T. A., D. M. **Meko**, and C. H. Baisan (2010). A bimillennial-length tree-ring reconstruction of precipitation for the Tavaputs Plateau, Northeastern Utah. *Quaternary Research*, *73* (1), 107-117. http://www.azwaterinstitute.org/media/EWSR/KMB09_QuaternaryRes.pdf

O'Donnell M. and B. **Colby** (2010). *Water Banks: A Tool for Enhancing Water Supply Reliability,* January 2010, University of Arizona, Department of Agricultural and Resource Economics. http://ag.arizona.edu/arec/pubs/facultypubs/ewsr-Banks-final-2-11-10.pdf

O'Donnell M. and B. **Colby** (2009). *Dry-Year Water Supply Reliability Contracts: A Tool for Water Managers,* October 2009; University of Arizona, Department of Agricultural and Resource Economics, http://ag.arizona.edu/arec/pubs/facultypubs/ewsr-dyo-Final.pdf

O'Donnell M. and B. **Colby** (2009). *Water Auction Design for Supply Reliability: Design, Implementation, and Evaluation,* May 2009. University of Arizona, Department of Agricultural and Resource Economics. http://ag.arizona.edu/arec/pubs/facultypubs/ewsr-AUCTION-5-28-09.pdf

Switanek M.B., P.A. **Troch** and C.L. Castro (2009). Improving seasonal predictions of climate variability and water availability at the catchment scale. *Journal of Hydrometeorology* 10: 1521-1533, DOI: 10.1175/2009JHM1073.1 http://journals.ametsoc.org/doi/pdf/10.1175/2009JHM1073.1

Woodhouse, C.A., D.M. **Meko**, G. M, MacDonald, D. W. Stahle, and E. R. Cook. In press. A 1200-year perspective on the 21st century drought in southwestern North America. *Proceedings of the National Academies of Science* (PNAS).

Woodhouse, C. A., and D. M. **Meko**, Contributors (2010). *Tree-ring reconstructions of streamflow for Colorado and implications for the future of the Colorado River* in Policy Focus Report/Code PF024, Planning for Climate Change in the West, by Rebecca Carter and Susan Culp, 57 pp (Lincoln Institute of Land Policy, 113 Brattle St., Cambridge, MA 02138-3400, USA), p. 7.

Woodhouse, C.A., J.L. Russell, and E.R. Cook (2009). Two modes of North American drought from instrumental and paleoclimatic data. *Journal of Climate* 22, 4336–4347.

Workshops:

Paleohydrology Workshop, September 11, 2009. Part of a series of workshops: Planning for Climate Change Through an Integrative Approach to Water-Planning, Climate Downscaling, and Robust Decision-Making: A Workshop Series, Decision Center for a Desert City & Decision Theater, Arizona State University. This workshop series is funded by Reclamation and other state agencies. The Paleohydrology Workshop was organized by Connie **Woodhouse**. The program included presentations on results from the Reclamation EWSR project by Carly Jerla, Kiyomi **Morino** and Rosalind **Bark**.

Workshop web page on TreeFlow web site: http://treeflow.info/asu2009.html.

Workshop web page on UA Decision Center for a Desert City web page, with white paper: http://dcdc.asu.edu/dcdcmain/detail.php?cid=18,26,28&ID=384

Presentations:

Beagles, R. and P.A. **Troch** (2010). Two ocean's influence on lower Colorado River water supply. El Dia del Agua, University of Arizona, Tucson, AZ, 31 March, 2010. Poster.

Colby, B. (2009). Climate Science and Economics in Tribal Water Negotiations and Management, Effects of Climate Change on Ecosystems and Societies: Native American and Hispanic Communities, Albuquerque, NM, October, 2009.

Colby, B. (2010). Sharing Best Economic Practices in Adaptation Planning. Eighth Annual Climate Prediction Applications Science Workshop, Managing Water Resources and Drought in a Changing Climate, San Diego, CA, March, 2010.

Meko, D. M. (2009). Paleo drought on the Colorado River, Border Governors' Conference Water Work Table, Binational Drought Science Conference (San Diego: Water Education Foundation, in cooperation with the California Department of Water Resources), 26-27 March 2009.

Morino K. and R. **Bark** (2009). Paleo-Climate Data and Adaptation Measures On The Lower Colorado. 34th Annual Climate Diagnostics and Prediction Workshop. Monterey, CA, 26-30 October, 2009.

Morino K. and R. **Bark** (2010). Using Paleo-Data to Assess Shortage Risk and Management Options on the Lower Colorado River. American Meteorological Society Annual Meeting Atlanta, GA, 17-21, January 2010.

Switanek, M. and P.A. **Troch** (2010). Decadal Predictability in the Colorado River Basin. El Dia del Agua, University of Arizona, Tucson, AZ, 31 March, 2010. Poster

Switanek, M., P.A. **Troch**, and C. Castro (2009). Improving seasonal predictions of climate variability and water availability at the catchment scale. 34th Annual Climate Diagnostics and Prediction Workshop. Monterey, CA, 26-30 October, 2009.

The following presentation included results from Morino and Bark's work on tree-ring reconstructed data to assess ICS management strategies:
Woodhouse, C.A. (2010). Tree-Ring Reconstructions of Streamflow: Applications to Water Management in the Western US. 8th Annual Climate Prediction Applications Science Workshop, San Diego, CA. March 2-4, 2010.

Other presentations on the Colorado River reconstruction(s):

Meko, D. (2009). Tree-Ring Perspective on Colorado Basin Water Supply. Brown Bag Water Speaker Series: The University of Arizona Cooperative Extension, Maricopa County, Phoenix, AZ., Aug 26, 2009.

Morino, K. (2010). How will ICS impact Colorado water deliveries to Tucson? Tucson Water, Tucson, AZ, April 16, 2010.

Woodhouse, C.A. (2010). Tree Rings and Colorado River Drought: A Message from the Past with Implications for the Future. Biosphere 2 Science Series, Biosphere 2, Oracle, AZ, Mar 13, 2010.

Woodhouse, C.A. (2010). Extended Records of Streamflow from Tree Rings and Applications to Water Resource Management. Osher Lifelong Learning Institute, Jan. 29, 2010

Woodhouse, C.A. (2009). Introduction to Dendrochronology and Tree-Ring Reconstructions of Streamflow for the Colorado River Basin. Tucson Water, Tucson, AZ, Nov. 11, 2009.

Media coverage:

Everett-Haynes, L. White House appointment for UA professor, Jan 6, 2010
http://westernfarmpress.com/news/white-house-appointement-0106/

Evans, M.B. UA Professor Earns White House Appointment, Jan 04, 2010
http://tucsoncitizen.com/hot-off-the-press-release/2010/01/04/ua-professor-earns-white-house-appointment/

Woodberry J. Research shows AZ drying up, Feb 4, 2010
http://wildcat.arizona.edu/news/research-shows-az-drying-up-1.1113774

Best, A. New storage eyed as Colorado confronts more people & less water, Oct 19, 2009
http://www.summitdaily.com/article/20091019/NEWS/910189983/-1/rss04

Associated Press. Researchers to get award on river analysis, Jul 20, 2009
http://ktar.com/?nid=6&sid=1191050

Honors:

American Water Resources Association Boggess Award for **Garrick**, D, K **Jacobs**, and G Garfin. (2008) Models, Assumptions, and Stakeholders: Planning for Water Supply Variability in the Colorado River Basin. *Journal of American Water Resources Association,* 44(2)*:* 381-398.

Connie **Woodhouse** appointment to the National Academy of Sciences panel on opportunities and challenges in the hydrologic sciences

Kathy **Jacobs** earned an appointment with the National Oceanic and Atmospheric Administration, from which she is serving with the White House Office of Science and Technology Policy (OSTP), as OSTP's assistant director for climate adaptation and assessment within the office's Energy and Environment Division.

Project leveraging:

NSF-funded North American Monsoon project (PI **Woodhouse**, co-PI **Meko**, Touchan, Leavitt, Castro): shared chronology collection and development for both projects

NOAA-funded Economic Strategies to Address Climate-related Water Supply Variability, Co-PI **Colby** on RISA CLIMAS project, National Atmospheric and Oceanic Administration, 2002-2012.

USDA-funded Agricultural Water Management for Economic Viability and Environmental Quality Under Climate Change, Co-PI **Colby**, U.S. Dept. of Agriculture, Western Regional Project W-190.

Partners:

Public agencies: U.S. Dept. of Agriculture, Arizona Department of Water Resources, Central Arizona Project, Salt River Project

Other collaborators: The Nature Conservancy, Western Regional Office; Western Resource Advocates, Environmental Defense

Future Research

The EWSR research team continues to find new avenues for both internal collaboration and external collaboration with Reclamation staff. A key mechanism for promoting interdisciplinarity has been fortnightly meetings hosted by postdocs Bark and Morino with the graduate students, as well as, research meetings across disciplines and with the entire research team. For our next group meeting in May, Jim Prairie, from Reclamation will participate remotely. This builds on efforts to enhance on-going collaboration with Reclamation staff that has been realized through face-to-face meetings, telephone conferences, and emails.

The two postdocs will continue their collaboration to assess the effectiveness of various Intentionally Created Surplus scenarios on shortage risk. Their research utilizes paleo-reconstructed streamflow records resampled as input into CRSS. They are working with Reclamation staff and plan to write a research paper. Over the next year the economics sub-team plans to collaborate with Reclamation staff on research related to improving cost effectiveness in various aspects of supply reliability arrangements, particularly on the costs of monitoring and enforcing irrigation forbearance agreements.

The hydrology team will continue to work to investigate whether large-scale oceanic variability influences spatial climatic variability of precipitation across the basins. In particular, they wish to investigate how when these fields become structured and prominent, it changes the likelihood for a particular spatial distribution of above or below average precipitation. Meanwhile, refinement of current research in the Lower Basin will involve separating streamflow by season. Finally, further review of the literature, and collaboration with Dr. Connie Woodhouse, is needed to develop a stronger mechanistic explanation for what may be occurring.

In the fall, Dr. Connie Woodhouse, and either a new grad student, or her current postdoc, plan to examine the reconstructed Colorado River streamflow and gridded PDSI to determine if 20th century drought “types” can be identified in the reconstructed data over the past 1200 years to assess frequency and distribution of drought types. A peer-reviewed paper (and potentially a thesis) will be generated based on these results.

Dr. Kiyomi Mornino will pursue further studies with CRSS and paleo-reconstructed streamflow input. Part of this research includes using paleo data to develop inflow scenarios and comparing direct paleo and paleo conditioned data for a subset of these scenarios. Meanwhile, in the coming year, Meko and Morino’s Lower Basin tributary research objectives are to: 1) convert existing time series of annual ring-widths to tree-ring site chronologies and analyze the chronologies for preliminary estimates of spatial covariation of runoff in Lower-Basin tributaries; 2) develop a set of 10-13 new or updated tree-ring chronologies; and (3) apply augmented network of tree-ring data to generate reconstructions of annual flow for at least the Little Colorado, Virgin, Paria, and Bill Williams rivers.

Improving Seasonal Predictions of Climate Variability and Water Availability at the Catchment Scale

MATTHEW B. SWITANEK AND PETER A. TROCH

Department of Hydrology and Water Resources, The University of Arizona, Tucson, Arizona

CHRISTOPHER L. CASTRO

Department of Atmospheric Sciences, The University of Arizona, Tucson, Arizona

(Manuscript received 9 July 2008, in final form 22 May 2009)

ABSTRACT

In a water-stressed region, such as the southwestern United States, it is essential to improve current seasonal hydroclimatic predictions. Typically, seasonal hydroclimatic predictions have been conditioned by standard climate indices, for example, Niño-3 and Pacific decadal oscillation (PDO). In this work, the statistically unique relationships between sea surface temperatures (SSTs) and particular basins' hydroclimates are explored. The regions where global SSTs are most correlated with the Little Colorado River and Gunnison River basins' hydroclimates are located throughout the year and at varying time lags. The SSTs, from these regions of highest correlation, are subsequently used as hydroclimatic predictors for the two basins. This methodology, named basin-specific climate prediction (BSCP), is further used to perform hindcasts. The hydroclimatic hindcasts obtained using BSCP are shown to be closer to the historical record, for both basins, than using the standard climate indices as predictors.

1. Introduction

Lake Powell divides the upper and lower Colorado River basins and has historically had sufficient storage to provide both regions with the quantities of water set by the Colorado River Compact. The current drought, which began in 2000, however, has shown that Lake Powell's storage is susceptible to natural climate variability and cannot always be relied upon. In April 2005, Lake Powell's storage was 33% of live capacity because of yearly inflows that were, on average, approximately 59% below normal. Rising temperatures across the southwestern United States, associated with global climate change, could further exacerbate droughts in the Colorado River basin (Barnett et al. 2005, 2008; McCabe and Wolock 2007; Hoerling and Eischeid 2007). The projected temperature increase and accompanying increase in evapotranspiration are anticipated to decrease runoff in the Colorado River basin between 6%–30% over the next 50 years (Milly et al. 2005; Christensen et al. 2004; Christensen and Lettenmaier 2007). Since the signing of the Colorado River Compact in 1922, the demand for water to be used for municipality, agriculture, and hydropower has grown rapidly. In addition to this increase in demand, climate projections are expected to decrease supply and further stress the water resources in the Colorado River basin. To aid decision makers and stakeholders in the allocation of this stressed resource in the Southwest, it is essential to improve hydroclimatic seasonal predictions.

Most of the variability in Lake Mead's pool elevation is governed by releases from Lake Powell. In the event that a drought restricts Lake Powell's releases to an amount less than required by the Colorado River Compact, tributaries between Powell and Mead will play a significant role in the Lower Colorado basin states' water supply. Therefore, development and improvement of hydroclimatic predictions needs to take place at the subbasin scale (e.g., Little Colorado River basin or Paria River basin). Improving these subbasin predictions can provide a more detailed map of water availability for the entire Colorado River basin, thus reducing potential uncertainty confronting water managers.

Corresponding author address: M. B. Switanek, Department of Hydrology and Water Resources, The University of Arizona, 1133 E. James E. Rogers Way, Rm. 320A, Tucson, AZ 85721.
E-mail: mbswitan@email.arizona.edu

DOI: 10.1175/2009JHM1073.1

The earth's oceans have a vast storage of energy that helps drive global climatic variability. Sea surface temperatures (SSTs) are one manifestation of this energy storage. Given the oceanic mass and water's large specific heat, SSTs' effect on ocean–atmosphere heat and water vapor exchange can be on seasonal to annual time scales. Consequently, variability in SSTs can help provide predictive information about the hydroclimate in regions across the globe. Over the past several decades, the statistical link between regional SST variability [e.g., the El Niño–Southern Oscillation (ENSO), the Pacific decadal oscillation (PDO) and the Atlantic multidecadal oscillation (AMO)] and global surface hydroclimatic variability has been well established (Trenberth 1997; Namias and Cayan 1984; Redmond and Koch 1991; Ropelewski and Halpert 1996; Enfield et al. 2001). Niño-3 is a commonly used index of ENSO, in which Niño-3 is the area average of the SSTs over the domain between 5°N and 5°S latitude and between 210° and 270°E longitude (east of the prime meridian). The PDO index is calculated to be the first principal component [derived from a principal component analysis (PCA)] of detrended SST anomalies northward of 20°N latitude in the Pacific Ocean (Mantua et al. 1997), whereas the AMO is essentially the detrended, area-weighted average of SSTs over the North Atlantic Ocean.

At seasonal to interannual time scales, there are numerous studies documenting the statistical connectivity of ENSO to land surface variables affecting hydroclimatic variability, including temperature (Higgins et al. 2000), precipitation (Ropelewski and Halpert 1996; McCabe and Dettinger 1999; Kim et al. 2005), and streamflow (Piechota et al. 1997; Cayan et al. 1999; Gochis et al. 2007). McCabe and Dettinger (1999) correlate Niño-3 with western U.S. precipitation and show statistically significant regions (these regions have correlation coefficients that are not a result of chance, at the 95% confidence interval). They, in addition to other studies, observe a negative correlation between Niño-3 and winter precipitation in the Northwest, whereas Niño-3 and winter precipitation in the Southwest exhibit a positive correlation.

Forecasts of precipitation and temperature, made by the Climate Prediction Center (CPC), are typically used by the River Forecast Centers to force statistical and hydrological models to simulate naturalized streamflows across the western United States. The CPC currently uses the present state of ENSO to condition these seasonal climatic forecasts. There are two potential problems with using standard climate indices—such as Niño-3, PDO, and AMO—for hydroclimatic prediction. The first problem is that the hydroclimate of a specific terrestrial region (e.g., a river basin) may be more strongly correlated with an oceanic region's SSTs, which is different from the predetermined regions that are used to calculate the standard indices. Historically, there have been numerous studies that have documented broad-scale ocean–atmosphere teleconnections that are not directly tied to standard climate indices (Namias 1969, 1974, 1978; Kutzbach 1970; Nicholls 1980). More recently, Tootle and Piechota (2006) use SSTs for an entire region, such as the Pacific Ocean. They use singular value decomposition (SVD) to identify and delineate statistically significant, covarying regions between U.S. streamflow and Pacific SSTs. The second problem with some of the standard indices is that a matrix methods approach (e.g., PCA and SVD) might not preserve enough information from an original dataset. Some recent hydroclimatic studies—such as Dettinger and Cayan (1995), Rucong et al. (2001) and Grantz et al. (2005)—have abandoned a matrix methods approach.

The study herein extends the Grantz et al. (2005) methodology in the following ways. First, Grantz et al. (2005) only use streamflow in their analysis, whereas we also use precipitation and temperature. Given the level of human influence along most of the rivers in the western United States, it is important to have climatic values to force a hydrological model, thereby obtaining an expected naturalized volume of water. A natural streamflow time series needs to be long enough in the past to calibrate the model. However, if model calibration is possible, then precipitation and temperature offer another way to independently obtain expected water availability for a particular basin. Second, they try to establish unique correlative relationships and potential predictors exclusively for spring discharge at lead times of up to six months. We include all trimonthly seasons through the entire year and are developing potential predictors for these seasons at up to a year ahead of time. Third, Grantz et al. (2005) use SSTs for predicting spring discharge at six and five months' lead time but then condition the predictions with snow water equivalent (SWE) data. We are aware that a snow-dominated system's spring snowmelt will be very strongly influenced by winter SWE; however, we chose to explore the raw potential of using solely SSTs as predictors. We are providing one of the components that assists in constraining expected seasonal hydroclimatic distributions. Lastly, we use the entire oceanic domain, whereas Grantz et al. (2005) observe the correlative structures mostly in the Pacific and the western Atlantic Oceans.

The objective of this study is to outline a methodology that has the capacity to improve current basin-specific hydroclimatic predictions at the seasonal to annual time scale. The section ''Materials'' describes the Little Colorado River and Gunnison River basins and the data

used in the study. The section ''Methodology'' outlines the basin-specific climate prediction (BSCP) approach. The precipitation, temperature, and streamflow data from the Little Colorado and the Gunnison are correlated with global SSTs. The statistical correlative oceanic patterns, using BSCP, are observed at different months of the year and at different time lags. Using these statistical patterns, the SSTs from the regions that exhibit the strongest correlation are subsequently used as predictors to perform hindcasts of each basin's hydroclimate. Niño-3, Niño-3.4 (5°N–5°S, 190°–240°E), Multivariate ENSO index (MEI), and PDO are also used as predictors to perform hindcasts. The section ''Results'' compares the hindcast skill of BSCP to the standard climate indices. The section ''Discussion and conclusions'' highlights the results and concludes with a few recommendations for further research on seasonal hydroclimatic prediction.

2. Materials

a. Regions of study

The Little Colorado River is located in the Lower Colorado River basin and comprises approximately 68 500 km^2. The basin's elevation ranges between 3850 m in the San Francisco peaks to approximately 840 m at the outlet. The Little Colorado receives as little as 36 mm of average seasonal total precipitation during the April–June season and as much as 127 mm for July–September. Average seasonal temperatures historically have ranged between 0.3°C for the December–February season and 20.8°C for June–August. Streamflow for the Little Colorado River originates in eastern Arizona and flows northwest for almost 507 km until meeting the Colorado River in the Grand Canyon (Fig. 1). The average yearly streamflow volume totals approximately 220×10^6 m^3, with average seasonal rates being highly variable between 80 m^3 s^{-1} to essentially no flow.

The Gunnison River is located in the upper Colorado River basin and is approximately 20 800 km^2. The basin's elevation ranges between 4400 to approximately 1390 m at its junction with the Colorado River. The Gunnison average seasonal total precipitation ranges between 115 mm during the June–August season and 160 mm for February–April. Average seasonal temperatures historically have ranged between −9.2°C for the December–February season and 13.8°C for June–August. Streamflow originates in the Rocky Mountains and flows west–northwest for almost 290 km until meeting the Colorado River. The average yearly streamflow volume totals approximately 2.76×10^9 m^3, with average seasonal rates ranging between 215 and 38 m^3 s^{-1}.

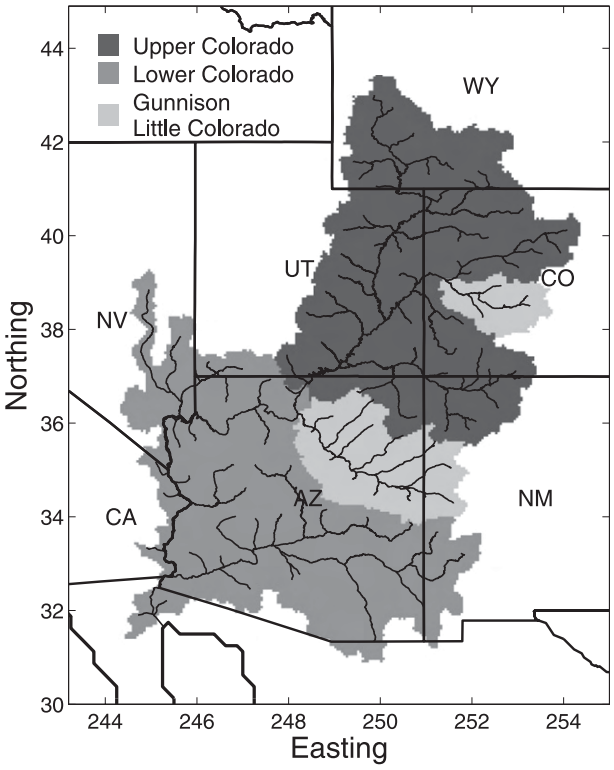

FIG. 1. The Gunnison River basin shown in light gray in the state of Colorado. The Little Colorado River basin is also shown in light gray and residing in Arizona and New Mexico.

b. Data

The precipitation and temperature data for the Little Colorado and Gunnison are obtained from an interpolated, gridded dataset (Maurer et al. 2002). The dataset was created as inputs to force the Variable Infiltration Capacity (VIC) hydrological model and provides data at a 3-h time step with a spatial resolution of $\frac{1}{8}° \times \frac{1}{8}°$. The dataset covers the conterminous United States, and this study uses the years 1951–2005. Naturalized volumetric discharge data for the basins were obtained from the Bureau of Reclamation (available online at http://www.usbr.gov/lc/region/g4000/NaturalFlow/index.html). The discharge data are provided at a monthly time step and are used for the same overlapping 55 years as the temperature and precipitation data, and the streamflows are assumed to reflect the contribution of the whole basin.

Mean monthly SSTs were obtained from the International Comprehensive Ocean–Atmosphere Data Set (ICOADS) through the University Corporation for Atmospheric Research site (available online at http://dss.ucar.edu/). The resolution of the SST data is $2° \times 2°$, and the entire oceanic domain is used. To have the same temporal domain for all of the data, the SSTs corresponding to 1951–2005 are used.

c. Data preparation

To effectively and efficiently ascertain a seasonal quantitative prediction for the Little Colorado and Gunnison basins, seasonal values for precipitation, temperature, and discharge at the basin scale are required. First, spatial averages are calculated. For discharge, it is simply a matter of dividing the volume of water for a given month by the area of the basin. For precipitation and temperature, a file containing the fractional contributions of each 1/8° grid cell is used, where the boundary of the basin is not delineated at the gridcell size but rather more accurate digital elevation maps [30-m resolution obtained through the U.S. Geological Survey (USGS) site (available online at http://seamless.usgs.gov/)], thus only fractional amounts of the bordering grid cells will contribute. By performing a weighted spatial average, the climatic values are not affected by fractions of grid cells that drain out of the basin. Each variable's weighted averages are obtained for their respective time steps. Second, average seasonal temperatures and seasonal totals of precipitation and discharge are obtained. Seasonal hydroclimate variables are averaged or integrated values at a trimonthly resolution. There are 12 trimonthly seasons, corresponding to January–March, February–April continuing through December–February. This yields the total seasonal sums of precipitation and discharge, averaged across the basin, and the seasonal averages of temperature.

In the southwestern United States, seasonal temperature generally exhibits a normal (Gaussian) distribution, whereas seasonal precipitation and discharge exhibit skewness that corresponds well with a gamma distribution. The z values, or z scores, for seasonal temperatures are computed by subtracting the population mean and dividing by the standard deviation. The standardized precipitation index (SPI) has previously been used to convert precipitation, which exhibits a gamma distribution, to normally distributed data (McKee et al. 1993; Kim et al. 2005). We convert cumulative densities from the gamma distribution to SPI values by means of an approximation provided by Abramovitz and Stegun (1972). The same SPI algorithm is applied to obtain z scores of discharge. There are two reasons why we choose to normalize precipitation and discharge. First, this allows a more accurate climate regime comparison between two different basins. Second, our methodology later requires Gaussian distributed data.

As a way to decrease the sparseness of the global SSTs, and to have a second level of quality control, the SSTs were spatially averaged on 10° × 20° latitude by longitude moving windows. As a result, we have more densely populated SSTs across the Pacific, at a 2° × 2° resolution, where each grid cell corresponds to a larger 10° latitude by 20° longitude window. Though we are advocating using SST windows that are not fixed like the Niño-3 domain, we want some consistency with the climate indices. As previously stated, the Niño-3 index is a regional SST average between 5°N and 5°S and between 210° and 270°E. Indices like Niño-3 are using anomalies in regions greater than the gridcell size (2° × 2°) to help describe ocean–atmosphere phenomena. Using a larger sample size in space, we can be more confident that the regional variance is more accurately depicted, thus reducing the randomness associated with individual grid cells.

3. Methodology

a. SST–basins' climate and discharge correlation maps

Using SSTs as a predictor of the climate and discharge in the Little Colorado and Gunnison, we observe the spatial correlative structure between global SSTs and seasonal basin variables at different temporal lags. For example, we use January SSTs in conjunction with the Little Colorado's January–March precipitation to obtain Pearson's correlation coefficients at each grid cell in the oceanic domain. Pearson's product moment correlation coefficients take the form

$$r = \frac{\sum_{i=1}^{n} (x_i - \overline{x})(y_i - \overline{y})}{(n-1)s_x s_y}, \tag{1}$$

where x_i and y_i are individual measurements in the sample size n, $\overline{x}$ and $\overline{y}$ are the sample means of $\mathbf{x}$ and $\mathbf{y}$ with standard deviations of s_x and s_y. The correlation coefficients range from −1 to 1, where the two variables are most well correlated when closest to −1 and 1, with 0 having no correlation. Pearson's correlation coefficients are commonly used with Gaussian distributed data. The correlation map that is created is identified by JAN-PL1 (where JAN corresponds to January SSTs, P is precipitation and L1 is the lag of the middle month of the seasonal precipitation with respect to the SST month). The temporal correlative structure is observed next. Correlation maps are created for the other 11 seasons, at different temporal lags behind January SSTs. Now we have maps corresponding to JAN-PL2 through JAN-PL12. The procedure is repeated for the other 11 months of SSTs as our predictors. Seasonal basin precipitation corresponds to 144 correlation maps (12 SST months × 12 seasonal lags). The same procedure is performed for the Little Colorado's temperature and discharge, which provides 144 correlation maps for each of these variables (432 maps total). The map

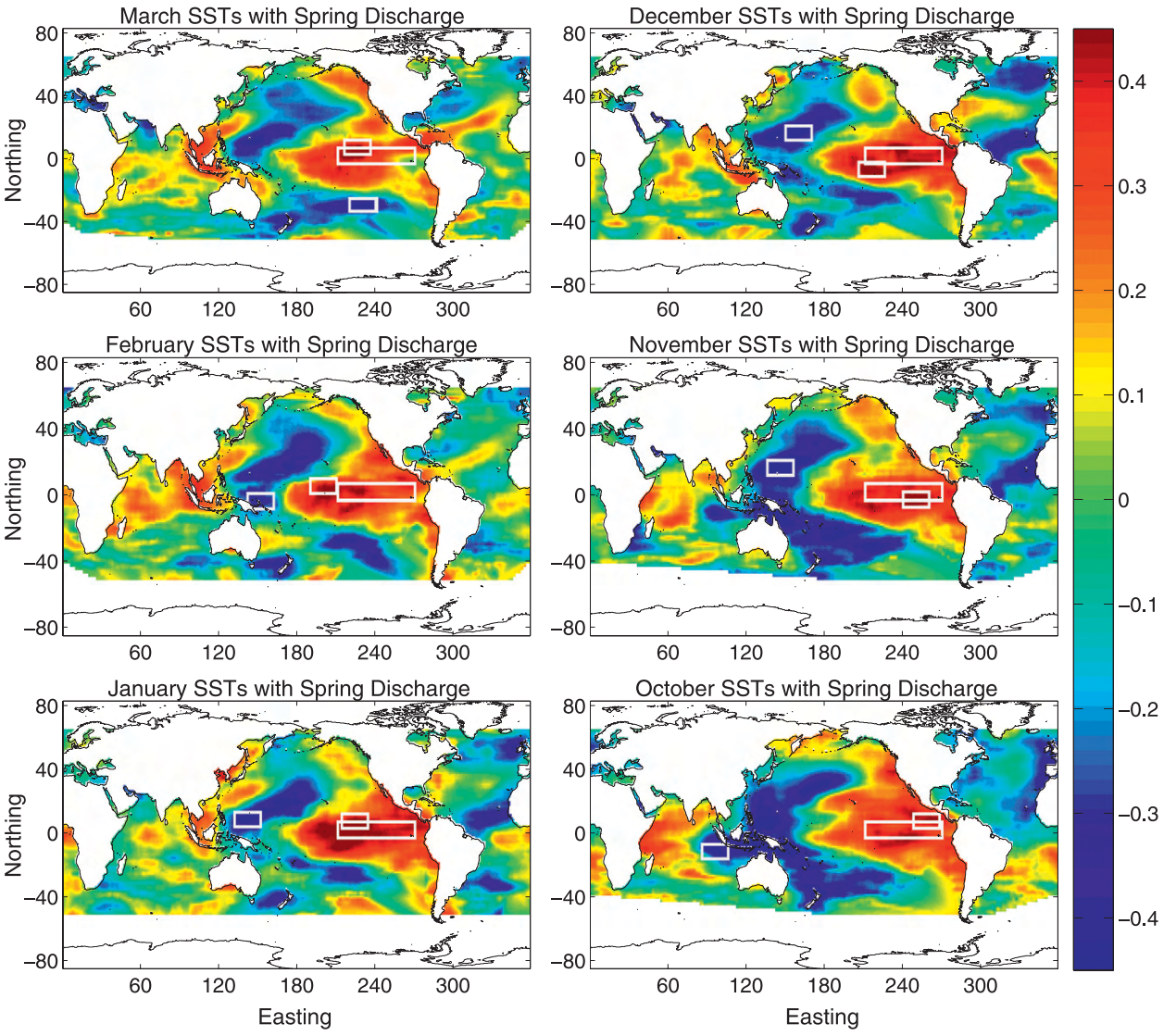

FIG. 2. Little Colorado's structure of correlation coefficients for SST months and March–May (spring) discharge at increasing lag times. The smaller rectangles correspond to the most positively and negatively correlated regions, while the larger rectangle is that of the Niño-3 domain.

identification follows the same structure—for example, FEB-TL1 and MAY-DL9 (where T is temperature and D is discharge). The entire process is then repeated using the Gunnison's unique seasonal hydroclimatic time series.

Figures 2 and 3 show examples of the progression of the oceanic correlative structures for the Little Colorado and Gunnison, respectively. One can observe the robustness of these structures, by the consistency of the patterns, when spring discharge is correlated with increasingly earlier monthly SSTs. The most correlated windows for the Little Colorado are predominantly located around the equatorial Pacific. The Gunnison, however, has a consistent correlation structure in the North Pacific. As a result, one expects for these cases that the ENSO indices and the PDO will be well correlated with the Little Colorado and Gunnison, respectively.

b. Regions of high correlation

Using the correlation coefficients, the most positively and negatively correlated windows (the 10° × 20° latitude by longitude SST windows) across the globe are identified for all combinations of months, lags, and basin variables. Most likely, a different window will correspond to each combination (although different combinations do not necessitate a different window, they could overlap, or be identical in space). Next, the larger of the two most correlated windows, by absolute magnitude, is used to extract the most predictive power from the

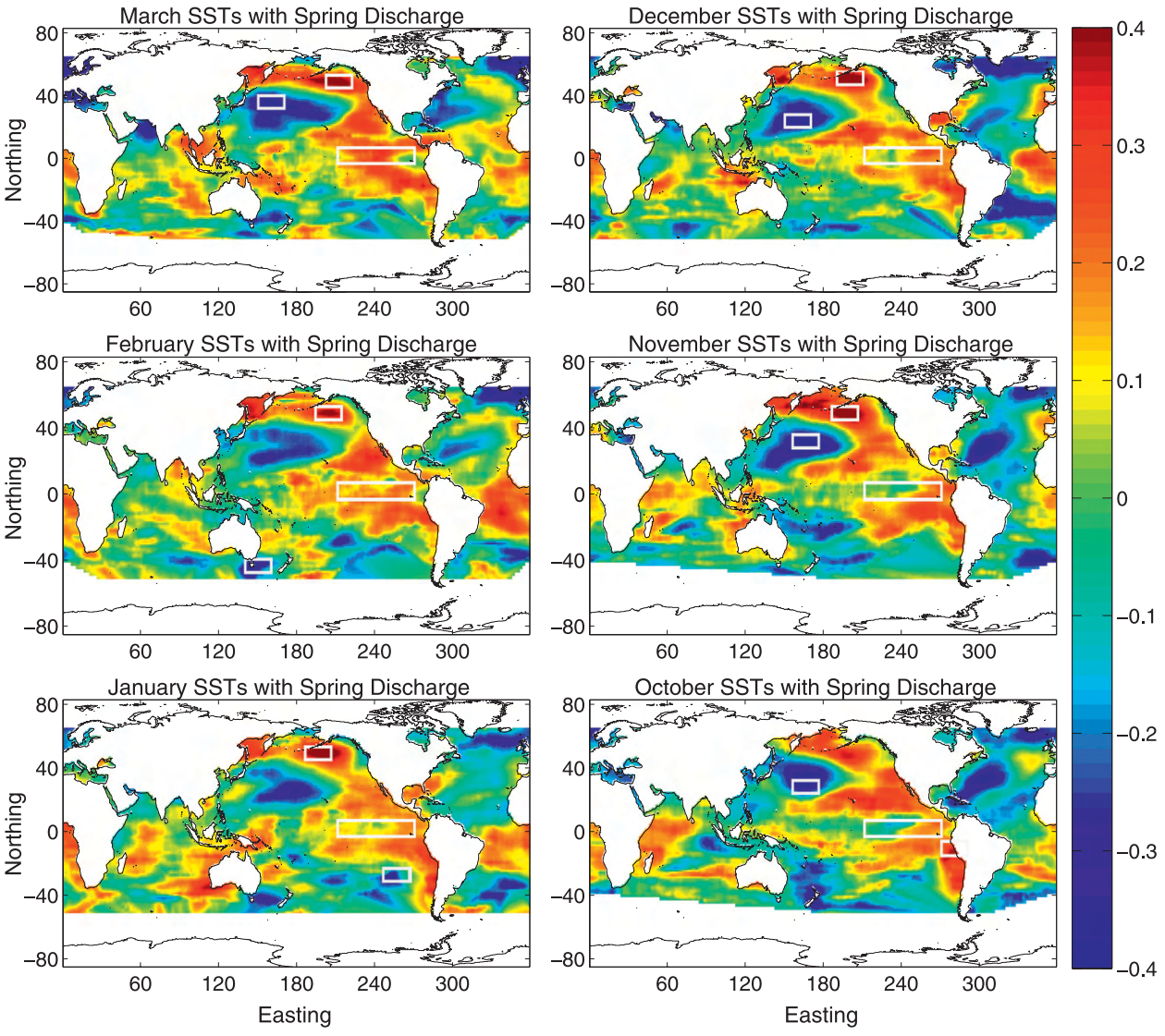

FIG. 3. Same as Fig. 2 but for Gunnison.

corresponding SSTs. There are now 432 SST windows that can be used to quantitatively predict the seasonal hydroclimates in the Little Colorado and Gunnison—as much as a year in advance.

How do the magnitudes of the correlation coefficients change through the year at different lags for both basins? Figures 4 and 5 contrast the correlative magnitude using BSCP (the most correlated SSTs) to Niño-3, Niño-3.4, MEI, and PDO for the Little Colorado and Gunnison, respectively. Using only SSTs as our predictors, at regions that we allow to vary in space, we find stronger correlations than when using the other four standard climate indices as predictors. As mentioned in the previous section, the ENSO indices have a fairly strong correlation with spring discharge in the Little Colorado. However, Gunnison's spring discharge is only significantly correlated with the PDO at lag 1. The statistical correlation using the standard indices is further reduced for almost all other seasons and lags. In the Little Colorado, there are only two instances when one of the standard indices is more strongly correlated than BSCP. The MEI has correlation coefficients of 0.57 for OCT-PL5 and 0.49 for FEB-DL2, whereas BSCP has 0.56 and 0.46, respectively. The BSCP observes stronger correlation for all cases in the Gunnison.

c. *Assessing uncertainty*

An efficient way to assess the uncertainty associated with individual predictions is by using a mixture of Gaussians (McLachlan and Peel 2000; Wójcik et al.

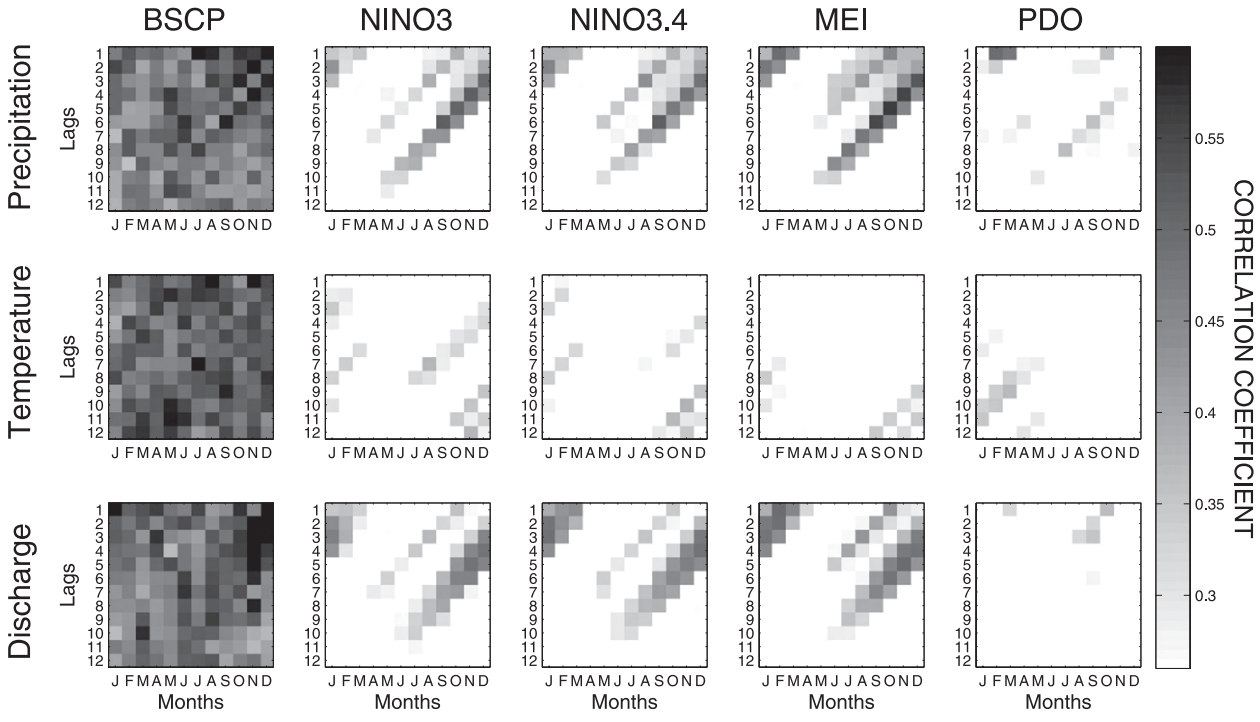

FIG. 4. Absolute magnitude of the correlation coefficients for the Little Colorado through the year and at different lags for the hydroclimatic variables using BSCP vs the standard climate indices. The lower limit of the colorbar is 0.27, which is statistically significant at the 95% confidence level.

2006). Gaussian mixture models (GMMs) form clusters by representing the probability density function (PDF) of observed variables as a mixture of multivariate Gaussian densities. The distribution is fit to the data using an expectation maximization (EM) algorithm (McLachlan and Peel 2000), which assigns joint probabilities across x and y space in the case of a two-dimensional scatterplot. GMMs are most appropriate to use when it is obvious that there is more than one distinct region where the data have gravitated—for example, there is bimodality in the aggregation of the scatter. In our analysis, we did not observe more than one distinct cluster for the hydroclimatic data in the Little Colorado and Gunnison. Hence, a GMM with one cluster is used. It should be made clear that the GMM's results with one cluster are the same as would be obtained with a linear regression. Our methodology, however, uses GMMs instead of linear regression, to be more broadly applicable to basins that could have data exhibiting nonlinearity.

The strength of the GMM regression by itself does not say much about the predictive/hindcast skill. Therefore, a series of Monte Carlo simulations are performed as a robust measure to assess the model's skill. Figure 6 provides an example of one of the simulations using the GMM. The data in Fig. 6 corresponds to the positively correlated window's December SST time series and the Gunnison's spring discharge (upper-right plot in Fig. 3). This scatter has a correlation coefficient of 0.54. The bold circles in Fig. 6a, which constitute 30 randomly chosen points from the scatter, are used to predict the other lighter circles. These 30 points are used to obtain the GMM (Fig. 6b). Next, a slice of the GMM is taken at the December SST z score of one of the lighter circles (surrounded by the larger circle in Fig. 6a). Normalizing this slice gives the PDF and the cumulative distribution function (CDF) of March–May discharge (Figs. 6c and 6d, respectively). The highest peak on the PDF is the most probable discharge, whereas the corresponding CDF is used to assess the 5% and 95% nonexceedence discharges. Similarly, PDFs and CDFs are obtained for all other lighter circles. These hindcasts of the lighter circles are stored, and the points are reshuffled to yield another random 30 bold circles to predict a new set of lighter circles. One hundred different simulations are performed. All of the stored values at each point are then used to obtain average quantities of the most probable 5% and 95% nonexceedence discharges. Lastly, the normally distributed data is converted back to a gamma distribution. This approach of using GMM regression with Monte Carlo simulations was also used to perform the hindcasts with the different climate indices' time series as predictors.

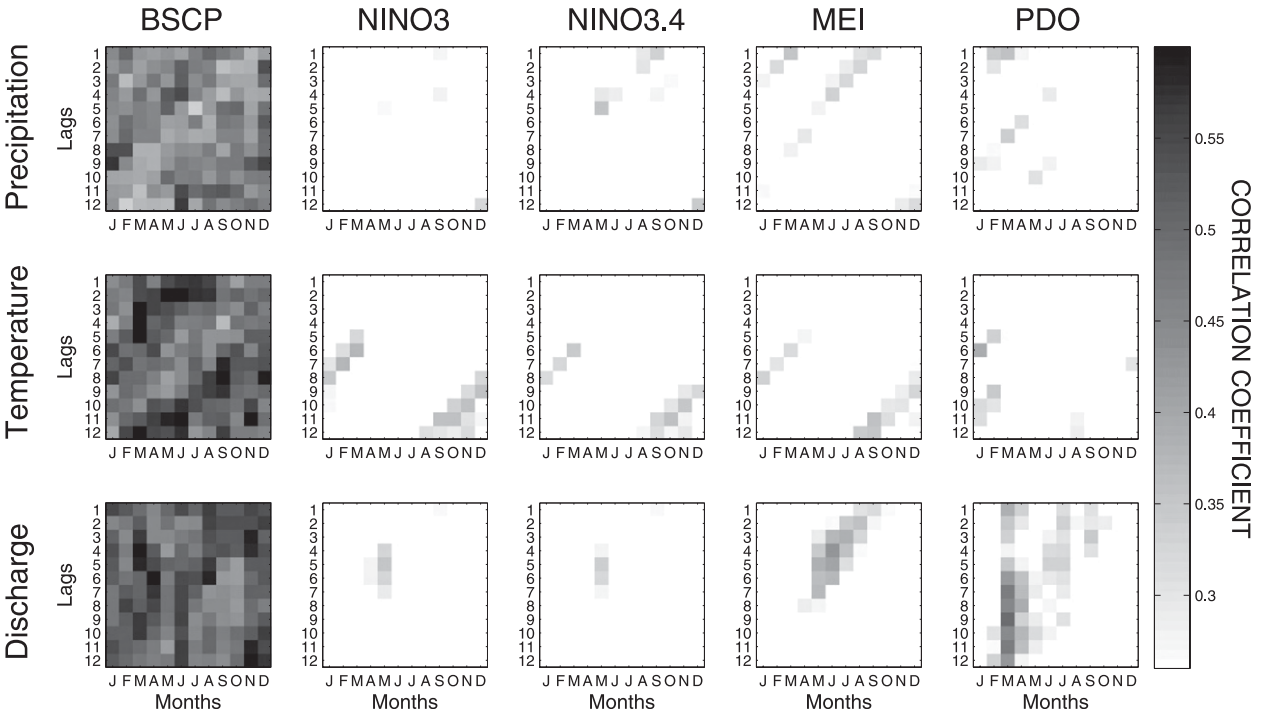

FIG. 5. Same as Fig. 4 but for Gunnison.

Figure 7 shows the hindcasts of the March–May discharge volume (average depth of water over the Gunnison basin) given December SSTs. The dark line shows the observed discharge, whereas the light gray line going through the middle is the observed mean discharge. The circles are the most probable hindcasts, whereas the error bars correspond to the 5% and 95% nonexceedence values. The skill of these hindcasts in contrast to the standard climate indices and the historic hydroclimatology is addressed in the next section.

4. Results

Two parameters are used to assess the predictive skill of each set of hindcasts. The parameters are model correlation coefficient and the Nash–Sutcliffe efficiency (NSE). The model correlation coefficient is calculated with Eq. (1) using modeled versus observed data. NSE is defined as

$$\mathrm{NSE} = 1 - \frac{\sum_{t=1}^{T} (x_o^t - x_m^t)^2}{\sum_{t=1}^{T} (x_o^t - \overline{x}_o)^2}, \qquad (2)$$

where $\overline{x}_o$ is the mean of observed values and x_o^t and x_m^t are the observed and modeled values at time t, respectively. The NSE has historically been used to assess the skill that a hydrologic model has in matching observed hydrographs. It is used here, more generally, to assess the hindcast skill in contrast to simply using the hydroclimatic means of discharge, precipitation, and temperature. NSE ranges from negative infinity to one. A value of one is for perfect hindcasts, whereas values greater than zero indicate when the model is performing better, or hindcasting better, than the hydroclimatic mean. Conversely, values fewer than zero delineate instances when the hydroclimatic mean would give better results than the model.

Figure 8 shows the model's performance, for the Little Colorado, expressed as correlation coefficients that are obtained from observed versus modeled hydroclimate values. With darker shading, the model is more skillfully hindcasting. Figure 9 uses the NSE to give a perspective into how well the hindcasts are doing in contrast to the Little Colorado's hydroclimatic mean. Figures 10 and 11 similarly show the correlation coefficients (observed versus modeled) and NSE values for the Gunnison, respectively. Moderate hindcast skill is observed in both basins, using BSCP, for winter precipitation and temperature throughout the year at a variety of lags. BSCP also hindcasts discharge better in both basins than using the standard indices, though there is substantial difference in skill between the Little Colorado and the Gunnison. The discharge hindcasts using BSCP are much better for the Gunnison. Possible explanations as to why we observe significant differences in the basins' discharge hindcasts is discussed in the following section.

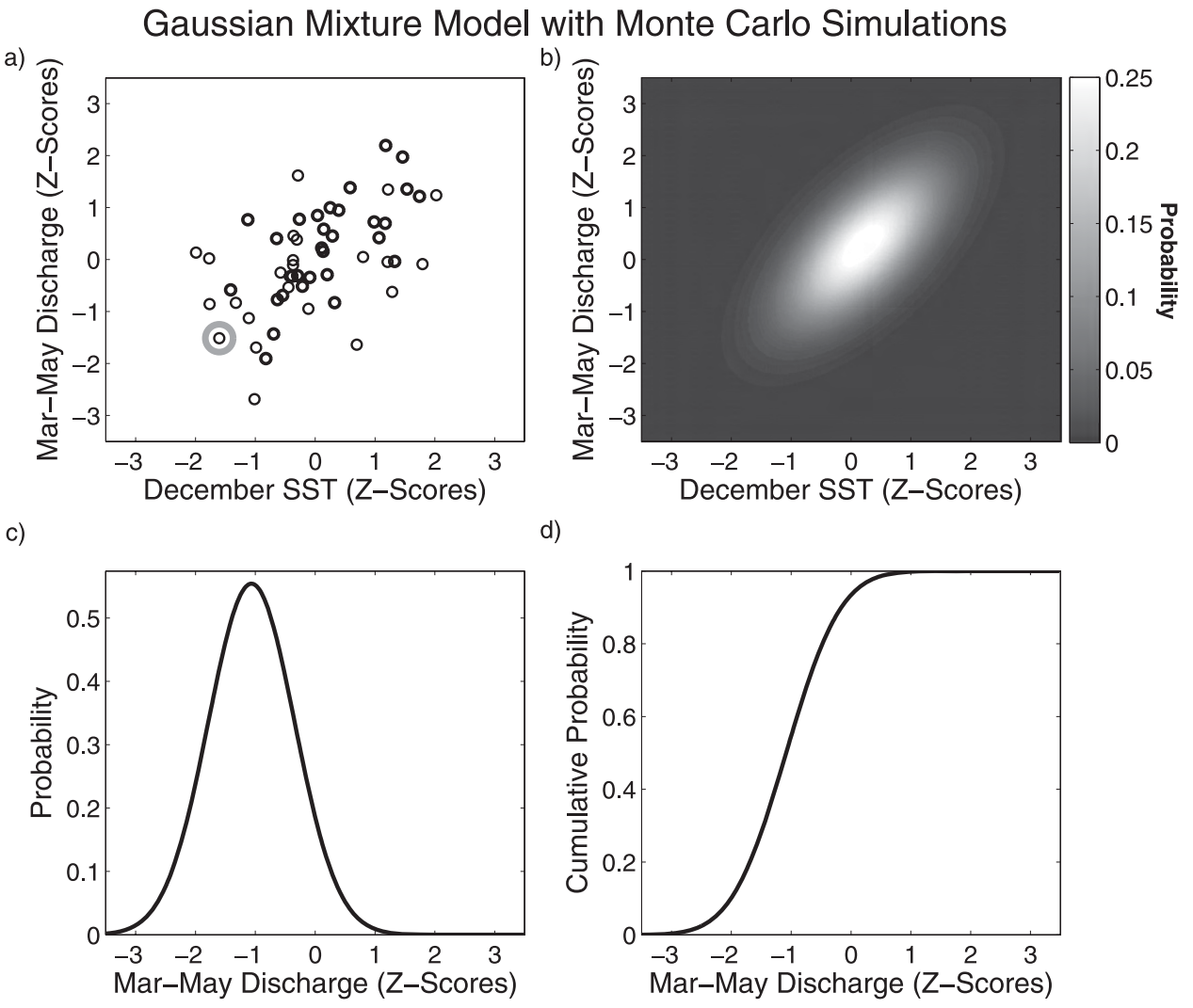

FIG. 6. Applying the GMM with Monte Carlo simulations: (a) the scatter of December SSTs and Gunnison's March–May discharge, where the more bold points are used to hindcast the lighter points; the lighter point that is circled will be the first point to be hindcasted; (b) the resulting GMM; (c) the PDF that corresponds to the slice along the SST z score of the point that is circled; and (d) CDF of the same slice.

5. Discussion and conclusions

This paper has explored the unique statistical relationships that relate global SSTs with the Little Colorado and Gunnison basins' hydroclimates. The advantage of BSCP is that it targets an oceanic region that maximizes the correlation for a specific basin at a given time. As a result, improvement in hydroclimatic seasonal hindcasts has been shown over the standard climate indices.

The work presented here raises several issues that require further analysis and can be improved in three ways. First, the weak-to-moderate skill observed for the Little Colorado's discharge requires improvement. This is the result of the basin's antecedent conditions upon entering the hindcast/forecast season [e.g., soil moisture and snow water equivalent (SWE)]. A basin's storage acts as a nonlinear filter for discharge in response to precipitation and temperature forcings (Troch et al. 2007). During the seasons with significant snowmelt, the Gunnison receives on average approximately 4 times the amount of precipitation than the Little Colorado. Additionally, the Gunnison's temperatures are substantially lower than in the Little Colorado. These conditions create a likely scenario for the Little Colorado's snowpack to quickly melt and subsequently dry out the soil. On the other hand, the Gunnison's soil rarely becomes depleted of moisture. These fluctuations in the Little Colorado's soil moisture have a significant effect on its discharge,

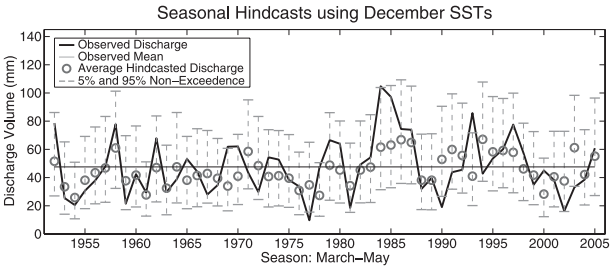

FIG. 7. Hindcasts of Gunnison's March–May total discharge volume using December SSTs.

ultimately reducing the observed hindcast skill level. A hydrological model can better capture the physical processes of precipitation and temperature interacting with differing ranges of soil moisture and SWE to produce a given discharge. Therefore, a hydrological model could be forced with precipitation and temperature hindcasts/forecasts from the BSCP model to produce physically viable realizations of discharge. Seasonal forecasts of basin discharges, which are significantly affected by SWE, can also be updated throughout the winter and early spring as new SWE data becomes available. Second, the predictors (SSTs) can be supplemented with additional oceanic or atmospheric variables (e.g., sea level pressures, wind vectors, geopotential heights). The current scope of this work provides a methodology that obtains the most correlated SST regions and essentially uses a linear regression for hindcasting. This alone has shown potential skill in forecasting. However, rooting the predictors in multiple variables can improve forecast skill by increasing the robustness of the methodology. Furthermore, using an objective combination of a variety of statistical methods [e.g., PCA, screening multiple linear regression (SMLR), optimal climate normals (OCN) or some other trend detection] on a set of time series obtained from multiple variables using BSCP can further increase hindcast/forecast skill similarly to the CPC (O'Lenic et al. 2008). Lastly, the nonstationarity of the correlative statistical patterns requires consideration (Milly et al. 2008). Though adding one additional scatter point will change the correlation in a given location (in most cases), this is a relatively slow process. With the inclusion of an additional year of data, the correlation maps will not be drastically altered. However, the locations of strongest correlation will shift over time because of system dynamics and trending. Both SSTs and land surface temperatures appear to be exhibiting trending (Moron et al. 1998; Jones et al. 1999; Stott et al. 2000). If we are going to successfully translate the BSCP methodology from hindcasting to forecasting, then the nonstationarity exhibited by the ocean–atmosphere–land system must be accounted for in the process. Additionally, to better

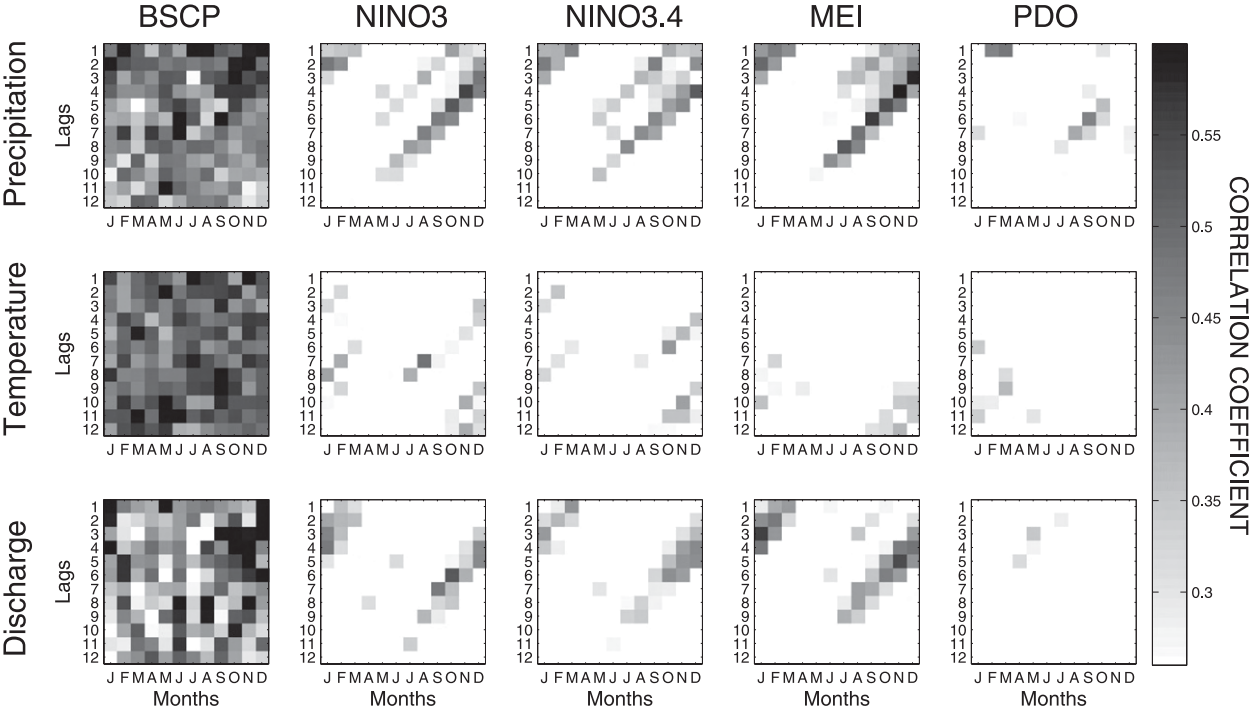

FIG. 8. Little Colorado's correlation coefficients for the hindcasts vs observed hydroclimatic values.

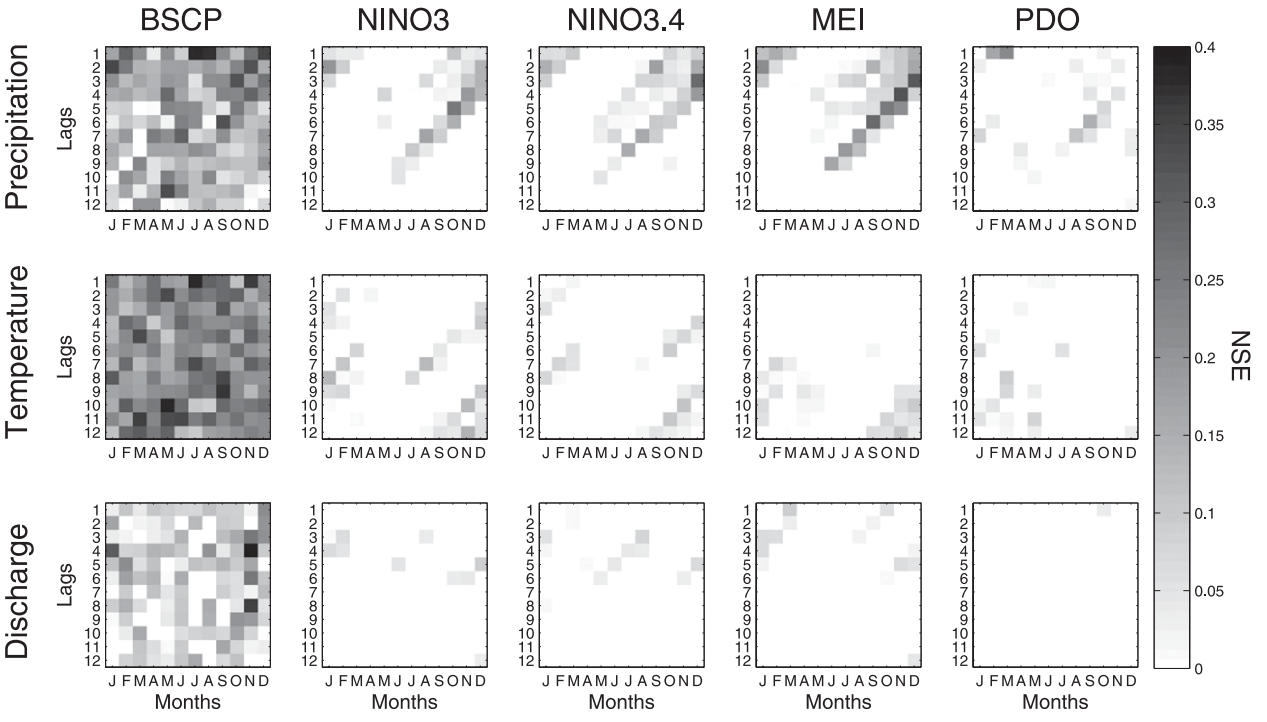

FIG. 9. NSE for the Little Colorado. The darker the shading, the more skillful the hindcasts are in comparison to the hydroclimatic mean.

observe the evolution of these patterns, given trending, it would be advantageous to drop or less heavily weight older data. For example, the last 30–40 years of data (updated each year, adding an additional year, and dropping the last one) can be used to forecast next year's hydroclimate.

Applying BSCP across a multitude of basins, in varying climate regions, has the potential to improve seasonal

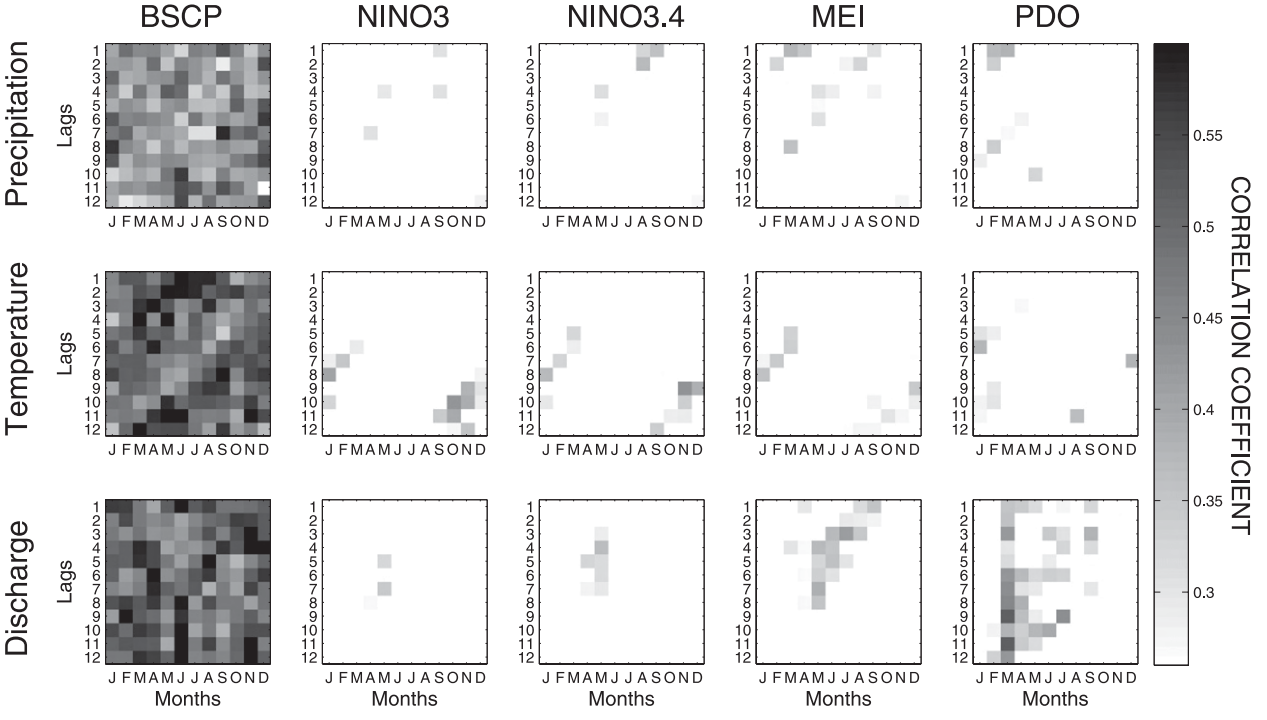

FIG. 10. Same as Fig. 8 but for Gunnison.

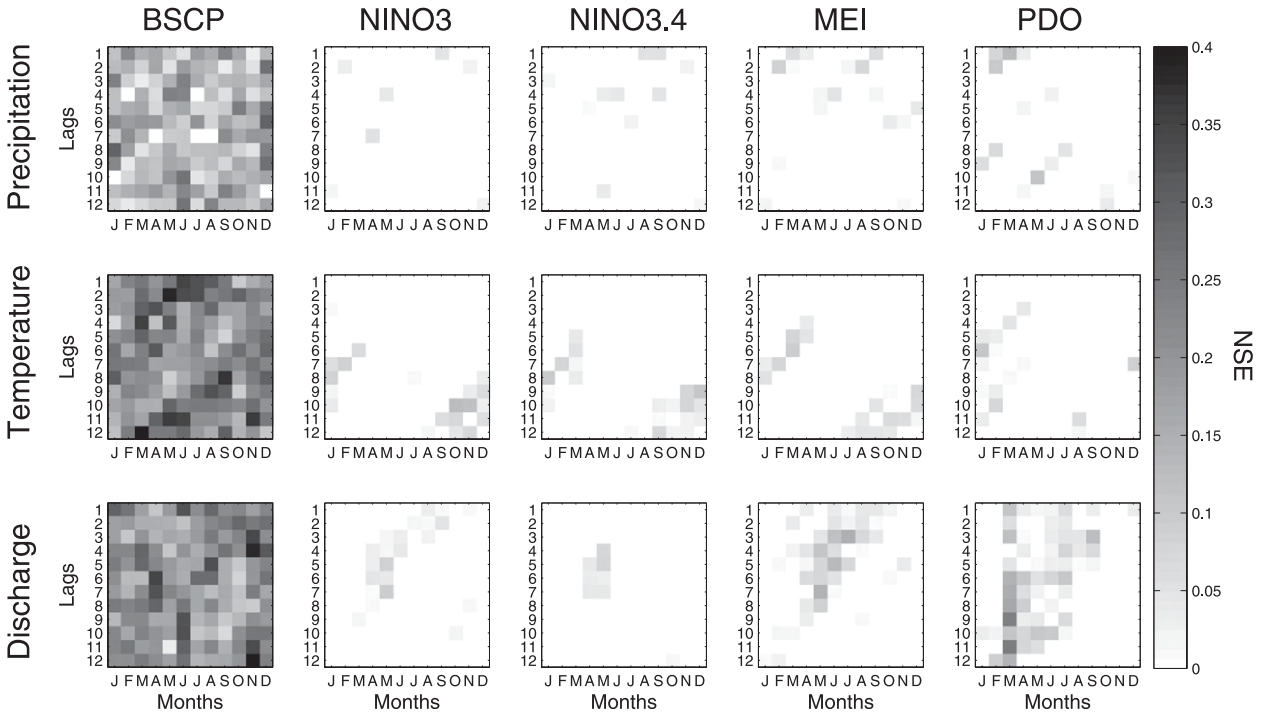

FIG. 11. Same as Fig. 9 but for Gunnison.

hydroclimatic predictions across the globe. Ultimately, we want to know the dynamical interactions that govern the observed statistical patterns. We are currently observing how these spatiotemporal statistical patterns shift between basins, though this is a work in progress. The cross-basin statistical relationships that arise could assist in formulating a new physical understanding of ocean–atmosphere–land interactions. If attained, improved understanding of the causes of seasonal hydroclimatic variability will greatly benefit water resources management.

Acknowledgments. The authors thank the Bureau of Reclamation, Lower Colorado Regional Office, for funding this study. Terry Fulp and Kathy Jacobs have offered invaluable advice and support. We wish to acknowledge Dennis Lettenmaier and Edwin Maurer for the use of Maurer's dataset. Useful discussions with Matej Durcik, Maite Guardiola-Claramont, and Seshadri Rajagopal are very much appreciated.

REFERENCES

Abramovitz, M., and I. A. Stegun, 1972: *Handbook of Mathematical Functions*. 9th ed. Dover, 1046 pp.

Barnett, T. P., J. C. Adam, and D. P. Lettenmaier, 2005: Potential impacts of a warming climate on water availability in snow-dominated regions. *Nature,* **438,** 303–309.

——, and Coauthors, 2008: Human-induced changes in the hydrology of the western United States. *Science,* **319,** 1080–1083.

Cayan, D. R., K. T. Redmond, and L. G. Riddle, 1999: ENSO and hydrologic extremes in the western United States. *J. Climate,* **12,** 2881–2893.

Christensen, N. S., and D. P. Lettenmaier, 2007: A multimodel ensemble approach to climate change impacts on the hydrology and water resources of the Colorado River Basin. *Hydrol. Earth Syst. Sci.,* **11,** 1417–1434.

——, A. W. Wood, N. Voisin, D. P. Lettenmaier, and R. N. Palmer, 2004: Effects of climate change on the hydrology and water resources of the Colorado basin. *Climatic Change,* **62,** 337–363.

Dettinger, M. D., and D. R. Cayan, 1995: Large-scale atmospheric forcing of recent trends toward early snowmelt runoff in California. *J. Climate,* **8,** 606–623.

Enfield, D. B., A. M. Mestas-Nuñez, and P. J. Trimble, 2001: The Atlantic multidecadal oscillation and its relation to rainfall and river flows in the continental U.S. *Geophys. Res. Lett.,* **28,** 2077–2080.

Gochis, D. J., L. Brito-Castillo, and W. J. Shuttleworth, 2007: Correlations between sea-surface temperatures and warm season streamflow in northwest mexico. *Int. J. Climatol.,* **27,** 883–901.

Grantz, K., B. Rajagopalan, M. Clark, and E. Zagona, 2005: A technique for incorporating large-scale climate information in basin-scale ensemble streamflow forecasts. *Water Resour. Res.,* **41,** W10410, doi:10.1029/2004WR003467.

Higgins, R. W., Y. X. Leetmaa, and A. Barnston, 2000: Dominant factors influencing the seasonal predictability of U.S. precipitation and surface air temperature. *J. Climate,* **13,** 3994–4017.

Hoerling, M., and J. Eischeid, 2007: Past peak water in the Southwest. *Southwest Hydrol.,* **6,** 18–19.

Jones, P. D., M. New, D. E. Parker, S. Martin, and I. G. Rigor, 1999: Surface air temperature and its changes over the past 150 years. *Rev. Geophys.,* **32,** 173–199.

Kim, T. W., J. B. Valdés, B. Nijssen, and D. Roncayolo, 2005: Quantification of linkages between large-scale climatic patterns and precipitation in the Colorado River Basin. *J. Hydrol.,* **321,** 173–186.

Kutzbach, J. E., 1970: Large-scale features of monthly mean Northern Hemisphere anomaly maps of sea-level pressure. *Mon. Wea. Rev.,* **98,** 708–716.

Mantua, N. J., S. R. Hare, Y. Zhang, J. M. Wallace, and R. C. Francis, 1997: A Pacific interdecadal climate oscillation with impacts on salmon production. *Bull. Amer. Meteor. Soc.,* **78,** 1069–1079.

Maurer, E. P., A. W. Wood, J. C. Adam, D. P. Lettenmaier, and B. Nijssen, 2002: A long-term hydrologically based dataset of land surface fluxes and states for the conterminous United States. *J. Climate,* **15,** 3237–3251.

McCabe, G. J., and M. D. Dettinger, 1999: Decadal variations in the strength of ENSO teleconnections with precipitation in the western United States. *Int. J. Climatol.,* **19,** 1399–1410.

——, and D. M. Wolock, 2007: Warming may create substantial water supply shortages in the Colorado River basin. *Geophys. Res. Lett.,* **34,** L22708, doi:10.1029/2007GL031764.

McKee, T. B., N. J. Doesken, and J. Kleist, 1993: The relationship of drought frequency and duration to time scales. Preprints, *Eighth Conf. on Applied Climatology,* Anaheim, CA, Amer. Meteor. Soc., 179–184.

McLachlan, G., and D. Peel, 2000: *Finite Mixture Models*. John Wiley & Sons, 419 pp.

Milly, P. C. D., K. A. Dunne, and A. V. Vecchia, 2005: Global pattern of trends in streamflow and water availability in a changing climate. *Nature,* **438,** 347–350.

——, J. Betancourt, M. Falkenmark, R. M. Hirsch, Z. W. Kundzewicz, D. P. Lettenmaier, and R. J. Stouffer, 2008: Stationarity is dead: Whither water management? *Science,* **319,** 573–574.

Moron, V., R. Vautard, and M. Ghil, 1998: Trends, interdecadal and interannual oscillations in global sea-surface temperatures. *Climate Dyn.,* **14,** 545–569.

Namias, J., 1969: Seasonal interactions between North Pacific Ocean and the atmosphere during the 1960's. *Mon. Wea. Rev.,* **97,** 173–192.

——, 1974: Longevity of a coupled air–sea–continent system. *Mon. Wea. Rev.,* **102,** 638–648.

——, 1978: Multiple causes of the North American abnormal winter 1976–1977. *Mon. Wea. Rev.,* **106,** 279–295.

——, and D. R. Cayan, 1984: El Niño: Implications for forecasting. *Oceanus,* **27,** 41–47.

Nicholls, N., 1980: Long-range weather forecasting: Value, status, and prospects. *Rev. Geophys.,* **18,** 771–788.

O'Lenic, E. A., D. A. Unger, M. S. Halpert, and K. S. Pelman, 2008: Developments in operational long-range climate prediction at CPC. *Wea. Forecasting,* **23,** 496–515.

Piechota, T. C., J. A. Dracup, and R. G. Fovell, 1997: Western US streamflow and atmospheric circulation patterns during El Niño-Southern Oscillation. *J. Hydrol.,* **201,** 249–271.

Redmond, K. T., and R. W. Koch, 1991: Surface climate and streamflow variability in the western United States and their relationship to large-scale circulation indices. *Water Resour. Res.,* **27,** 2381–2399.

Ropelewski, C. F., and M. S. Halpert, 1996: Quantifying Southern Oscillation precipitation relationships. *J. Climate,* **9,** 1043–1059.

Rucong, Y., Z. Minghua, Y. Yongqiang, and L. Yimin, 2001: Summer monsoon rainfalls over mid-eastern China lagged correlated with global SSTs. *Adv. Atmos. Sci.,* **18,** 179–196.

Stott, P. A., S. F. Tett, G. S. Jones, M. R. Allen, J. F. Mitchell, and G. J. Jenkins, 2000: External control of 20th century temperature by natural and anthropogenic forcings. *Science,* **290,** 2133–2137.

Tootle, G. A., and T. C. Piechota, 2006: Relationships between Pacific and Atlantic ocean sea surface temperatures and U.S. streamflow variability. *Water Resour. Res.,* **42,** W07411, doi:10.1029/2005WR004184.

Trenberth, K. E., 1997: The definition of El Niño. *Bull. Amer. Meteor. Soc.,* **78,** 2771–2777.

Troch, P. A., M. Durcik, S. Seneviratne, M. Hirschi, A. Tueling, R. Hurkmans, and S. Hasan, 2007: New data sets to estimate terrestrial water storage change. *Eos, Trans. Amer. Geophys. Union,* **88,** doi:10.1029/2007EO450001.

Wójcik, R., P. A. Troch, H. Stricker, P. Torfs, E. Wood, H. Su, and Z. Su, 2006: Mixtures of Gaussians for uncertainty description in bivariate latent heat flux proxies. *J. Hydrometeor.,* **7,** 330–345.

Two Modes of North American Drought from Instrumental and Paleoclimatic Data*

C. A. WOODHOUSE

Department of Geography and Regional Development, The University of Arizona, Tucson, Arizona

J. L. RUSSELL

Department of Geosciences, The University of Arizona, Tucson, Arizona

E. R. COOK

Lamont-Doherty Earth Observatory, Palisades, New York

(Manuscript received 2 July 2008, in final form 17 February 2009)

ABSTRACT

Droughts, which occur as a part of natural climate variability, are expected to increase in frequency and/or severity with global climate change. An improved understanding of droughts and their association with atmospheric circulation will add to the knowledge about the controls on drought, and the ways in which changes in climate may impact droughts. In this study, 1) major drought patterns across the United States have been defined, 2) the robustness of these patterns over time using tree-ring-based drought reconstructions have been evaluated, and 3) the drought patterns with respect to global atmospheric pressure patterns have been assessed. From this simple assessment, it is suggested that there are two major drought patterns across North America, which together account for about 30% of the total variance in drought patterns—one resembles the classic ENSO teleconnection, and the other displays an east–west drought dipole. The same two patterns are evident in the instrumental data and the reconstructed drought data for two different periods, 1404–2003 and 900–1350. The 500-mb circulation patterns associated with the two drought patterns suggest that the controls on drought may come from both Northern Hemisphere and tropical sources. The two drought patterns, and presumably their associated circulation patterns, vary in strength over time, indicating the combined effects of the two patterns on droughts over the past millennium.

1. Introduction

Drought is a feature of natural climate variability and a condition expected to be exacerbated by global climate change, particularly in the subtropical regions of the world (Arblaster et al. 2007; Seager et al. 2007). Droughts are receiving an increasing amount of attention in areas such as the western United States, where greater demands on water supplies due to increases in population, changing water demands, and recent droughts have converged, resulting in a heightened vulnerability to the impacts of drought (e.g., National Research Council 2007). Understanding the spatial and temporal characteristics of drought, and the controls on these characteristics, is critical to planning for and mitigating the impacts of regional drought. A great deal of research has been focused on improving this understanding over the past decades, utilizing information from instrumental and paleoclimatic data as well as climate modeling.

Spatial pattern of drought across North America have been investigated to identify both regions that tend to be homogeneous with respect to drought, and the spatial footprint of drought, such as those that characterized the 1930s Dust Bowl and 1950s droughts. The first study to address homogenous regions that incorporated data from the entire United States over the twentieth century defined nine distinct drought regions (Karl and Koscielny 1982). The nine regions had different frequency characteristics, with drought more persistent in the U.S. interior (Karl and Koscielny 1982), a finding that was

* Lamont-Doherty Earth Observatory Publication Number 7277.

Corresponding author address: C. A. Woodhouse, 412 Harvill Building, Box 2, Department of Geography and Regional Development, The University of Arizona, Tucson, AZ 85721-0076.
E-mail: conniew1@email.arizona.edu

DOI: 10.1175/2009JCLI2705.1

confirmed in further analysis (Karl 1983; Diaz 1983). Nine drought regions very similar to these were also identified in drought reconstructions based on moisture-sensitive tree-ring data, extending back to 1700 (Cook et al. 1999), an indication of the stability of these regions over time. The nature of wet and dry regimes in five areas representing regions of different synoptic-scale forcing across the contiguous United States was investigated by Diaz (1991). The regionally variable distribution of precipitation during wet and dry periods, as well as seasonal tendencies for initiation and termination, was suggested as an indication of both synoptic- and larger-scale circulation further modulated by seasonal atmospheric circulation and teleconnections (Diaz 1991; Barnston and Livesey 1987).

Spatial and temporal analyses of droughts and pluvials over the coterminous United States have been undertaken using highly resolved, gridded precipitation data [Parameter-Elevation Regressions on Independent Slopes Model (PRISM); Daly et al. 1997] for 1895–2003 (Kangas and Brown 2007). The increased spatial resolution of the data used in this study indicated a more heterogeneous coverage of droughts and pluvials than suggested by some previous studies. Results showed dependence on the time scales used to define drought, with short-duration droughts characterized by high temporal and spatial variability, and large areas under drought for very short periods (e.g., a month), while droughts evaluated at longer time scales, such as 12- and 24-month periods, showed more persistence. Indices of short-term droughts indicated a higher frequency of drought in the interior United States, as well as more spatially extensive droughts and pluvials in this region, compared to other regions. More severe extremes occurred in western and some eastern parts of the United States (Kangas and Brown 2007).

Links between the spatial patterns of drought and the mechanisms that control drought have been the topic of much research. El Niño–Southern Oscillation (ENSO) was the first large-scale ocean–atmosphere mechanism to be linked to drought (e.g., Rasmussen and Carpenter 1982; Glantz et al. 1991). ENSO has a distinct footprint on drought in North America (e.g., Cayan 1996; Redmond and Koch 1991), which can also be quite spatially variable (Cole and Cook 1998; Rajagopalan et al. 2000; Brown and Comrie 2004). The interplay between low-frequency and high-frequency variations in Pacific Ocean variability has been shown to be influential to regional climate and drought conditions in North America, resulting in enhanced or diminished regional drought occurrence and severity (Gershunov and Barnett 1998; Barlow et al. 2001; Brown and Comrie 2004; Shabbar and Skinner 2004). Analysis of spatial patterns of U.S. drought associated with the main modes of decadal-scale variability in both the Atlantic and Pacific Oceans suggests that a warm Atlantic, conditioned by Pacific Ocean SSTs, is linked to widespread droughts such as those of the 1930s and 1950s (McCabe et al. 2004). Most recently, modeling studies have further indicated the role of both the North Atlantic and the tropical Pacific in promoting North American drought (Seager et al. 2008; Feng et al. 2008).

Patterns of North American drought have been explored with a rich archive of paleoclimatic data, including tree-ring-based gridded drought reconstructions for North America (Cook et al. 1999, 2004). In addition to defining drought regions (Cook et al. 1999), these and other paleoclimatic data have been used to examine spatial patterns of drought over the past millennia. A number of studies document droughts more persistent and severe than those that have occurred during the period of instrumental records (e.g., Woodhouse and Overpeck 1998; Stahle et al. 1998, 2000; Benson et al. 2002; Cook et al. 2004). An assessment of the spatial analogs of the 1930s and 1950s drought in the context of the past five centuries provided an estimated return interval of 45 yr for a 1950s-type drought (Fye et al. 2003). Millennial-length North American drought reconstructions document drought of unprecedented persistence during the medieval period, but with spatial patterns that are similar to those of twentieth-century droughts (Herweijer et al. 2007). The primary spatial footprint of these medieval droughts implies ENSO as a causal mechanism, and additional modeling and other paleoclimatic data support the important role of persistent and cool tropical Pacific SSTs in these periods of extended drought (Seager et al. 2005; Herweijer et al. 2007; Cook et al. 2007; Graham et al. 2007).

Although far from a complete assessment of the literature, this review documents the rich body of knowledge that supports our understanding of the major drought regions in the United States, the general footprint of major droughts, and possible causal mechanisms. Much research points to the key role of the tropical Pacific Ocean, with indications of the importance of the North Pacific and Atlantic Oceans as controls on regional patterns of drought as well. In this study we take advantage of the gridded North American drought reconstructions for the past millennia to investigate major patterns of drought over three time periods—the twentieth century, the last 500 yr, and the medieval period. Instead of looking for the spatial footprint of the major twentieth-century droughts or the characteristic imprint of known circulation mechanisms on patterns of drought, we let the data define the major patterns, and then draw inferences about the causal

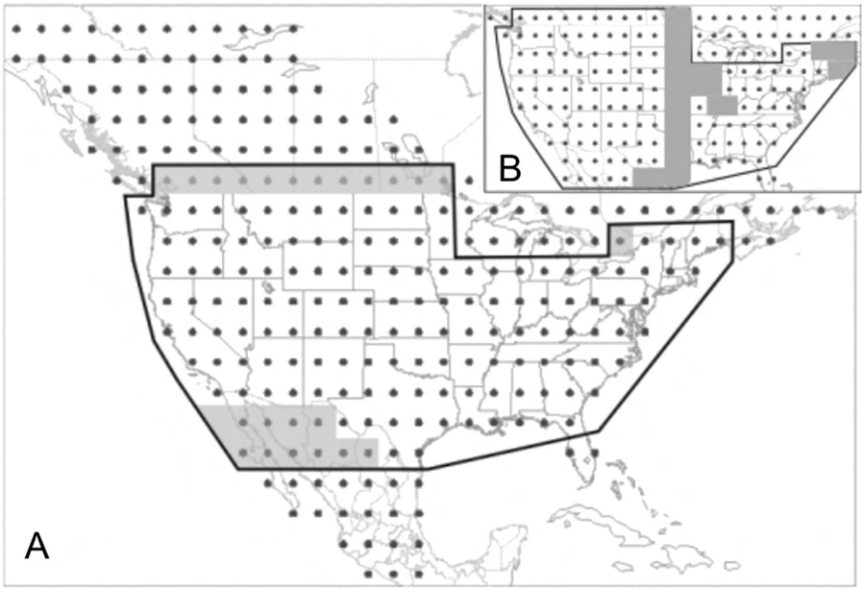

FIG. 1. PDSI grid points used in this study, based on a network of 286 points in a 2.5° × 2.5° grid over North America for both instrumental and reconstructed data (updated from Cook et al. 2004; NOAA/National Climatic Data Center 2008a). Reconstruction data and methods are described in Cook et al. (2004) and associated online supporting materials. (a) Black outline indicates grid points with the common period 1404–2003, selected for the best spatial coverage over the longest period of time; gray shading indicates data points not used in the instrumental data analysis, 1900–2003 (data for non-U.S. points not available to 2003). (b) Inset shows grid points used for the 900–1350 analysis (outlined, nonshaded points).

mechanisms that are associated with these patterns. This approach allows an evaluation of droughts that are identified first in terms of spatial patterns, and then by their association with the atmospheric circulation, rather than examining drought anomaly patterns related to associations with circulation indices. We use gridded instrumental drought data to identify major spatial patterns of drought across the coterminous U.S. and border regions, followed by a similar analysis using reconstructed drought data to assess the robustness and stability of these patterns over two time periods: 1404–2003, and 900–1350, also known as the Medieval Climate Anomaly (e.g., Cook et al. 2004). We then investigate the association between the spatial patterns of drought and atmospheric circulation (500-mb geopotential heights) patterns to infer possible driving mechanisms. Finally, we examine the reconstructed drought patterns for the two time periods to assess the possible role of circulation over time.

2. Data and methods

The two gridded drought datasets for North America used in this study are based on the summer (June–August) Palmer Drought Severity Index (PDSI; Palmer 1965). The PDSI has a lag incorporated into its calculation that results in the summer PDSI reflecting drought conditions of previous seasons (Cook et al. 1999). The PDSI datasets used are from Cook et al. (2004, updated version available online at http://www.ncdc.noaa.gov/paleo/pdsi_ts.html; NOAA National Climatic Data Center 2008a) and are based on a network of 286 points in a 2.5° × 2.5° grid over North America. The instrumental dataset extends from 1900 to 2003, while the tree-ring-reconstructed PDSI extends back 350–2000 yr, depending on location (with the variance adjusted to match the instrumental data in the twentieth and twenty-first centuries). A subset of these data was used for this study. For the reconstruction data, the grid points with the common period 1404–2003 were selected for the best spatial coverage over the longest period of time. The set includes most of the U.S. and bordering parts of Canada and Mexico (Fig. 1). Several grid points from the Great Lakes region and southern Florida were omitted because of the lower validation statistics compared to the instrumental data. A sparser set of grid points was used to examine the medieval period (Fig. 1, inset). For the instrumental data, the same grid points were used as for the 1404–2003 reconstruction dataset, but were restricted to those with the common years 1900–2003 (which excluded the non-U.S. grid points). A total of 160 grid points was retained for the 1404–2003 reconstructed

dataset, 128 for the 900–1350 reconstructed dataset, and 137 grid points for the instrumental dataset (Fig. 1). For the investigation of circulation patterns associated with drought patterns, monthly global 500-mb pressure data from the National Centers for Environmental Prediction–National Center for Atmospheric Research (NCEP–NCAR) reanalysis were used (Kalnay et al. 1996). The average for December through March was selected to represent cold season conditions. Drought patterns in the instrumental data were identified using T-mode principle components analysis (PCA) with a normalized Varimax (orthogonal) rotation (Richman 1986; Yarnal 1993). A T-mode PCA, based on a matrix with columns of years and rows of PDSI gridpoint values, yields principle components (PCs) characterized by years with similar spatial patterns. This approach differs from some previous studies that used PCA to identify drought regions by grouping data spatially (e.g., Karl and Koscielny 1982; Cook et al. 1999). In this study, the focus is not on regions that behave similarly with respect to drought, but on identifying the primary spatial patterns, or footprints, of drought across North America. The number of PCs rotated was based on a cutoff of eigenvalues >1.0 (although several different cutoffs were tried with the same resulting patterns). Scree plots were used to further screen components for analysis. For the analysis of reconstructed PDSI, T-mode PCA with same numbers of PCs rotated was repeated. Composite maps of the five noncontiguous years with the largest positive and negative loadings for the main PCs were used to illustrate spatial patterns of drought for the instrumental period and two paleoperiods. Years in the reconstructed data that also ranked in the top five for the instrumental data were replaced with the next highest ranking year so that the patterns for reconstructed and instrumental periods were independent. This approach is roughly analogous to Blasing's (1975) correlation map–based identification of twentieth-century patterns of surface pressure types, but differs in that years of pressure anomaly types were the basis for the composite precipitation, temperature, and tree-ring-width maps, while here we are using the gridded PSDI to identify patterns in both the instrumental and reconstructed data. The composite maps were generated using data and maps from the National Oceanic and Atmospheric Administration (NOAA)/National Climatic Data Center (2008b) using the full gridded PDSI dataset. To summarize, PC loadings represent time series of the leading drought patterns, while the composite maps of the years with the largest loadings are used to represent the corresponding leading spatial patterns of drought. Time series of the PC loadings were used to explore the relations between PCs over time. The association between drought patterns and atmospheric circulation was examined using correlation maps with PC loadings and global 500-mb heights, 1949–2003 (sea level pressure correlation maps were generated as well, with very similar results). To assess the consistency of the patterns depicted in the composite maps over the three time periods, we also generated maps from the PC scores [analogous to spatial patterns from empirical orthogonal functions (EOFs)]. The PC scores were generated from a normalized varimax rotation in which factor loadings are divided by the square roots of the respective communalities (StatSoft, Inc. 2005).

3. Results

a. Drought patterns in the instrumental and paleodrought data

The PCA, which grouped the PDSI map patterns for the years 1900–2003 into years with similar patterns, resulted in 15 PCs with eigenvalues greater than 1.0. After rotation of the 15 PCs, the first two PCs explained 16% and 14% of the total variance, respectively, and they were targeted for further analysis. When the eigenvalue sampling error is compared to the spacing of eigenvalues assessed using North's rule of thumb (North et al. 1982), the two PCs appear to be separate and unmixed with each other. The loadings of these two PCs were ranked and the five noncontiguous years with the highest negative and positive loadings were used to generate composite maps to illustrate the main spatial features of the two PCs. The composite map for PC1 shows a Pacific Northwest–southwestern U.S. dipole (Fig. 2a, left), a characteristic of the ENSO imprint on the western United States (Dettinger et al. 1998). An examination of the Southern Oscillation index November–March averages (NOAA/Climate Prediction Center 2008) indicates that positive PC1 values coincide with 10 out of the 15 strongest positive SOI years (indicating cool ENSO events) and negative PC1 values correspond with 9 of the 15 most negative SOI winters (indicating warm ENSO events). PC2 displays an eastern–western U.S. drought dipole that is indicative of highly meridional flow (Fig. 2a, right). The reconstructed PDSI data, analyzed for the same years (1900–2003) show the same spatial structure in the first two PCs as the instrumental data (Fig. 2b). The top ranking 5 yr are not identical for both the instrumental and reconstructed data over this common period (cf. Figs. 2a and 2b), but the reconstruction years that are not the same as the instrumental years rank in the top 20% of years in the instrumental analysis (and all but two in the top 15%).

The sensitivity of these patterns to data treatment was assessed by retaining different numbers of PCs for

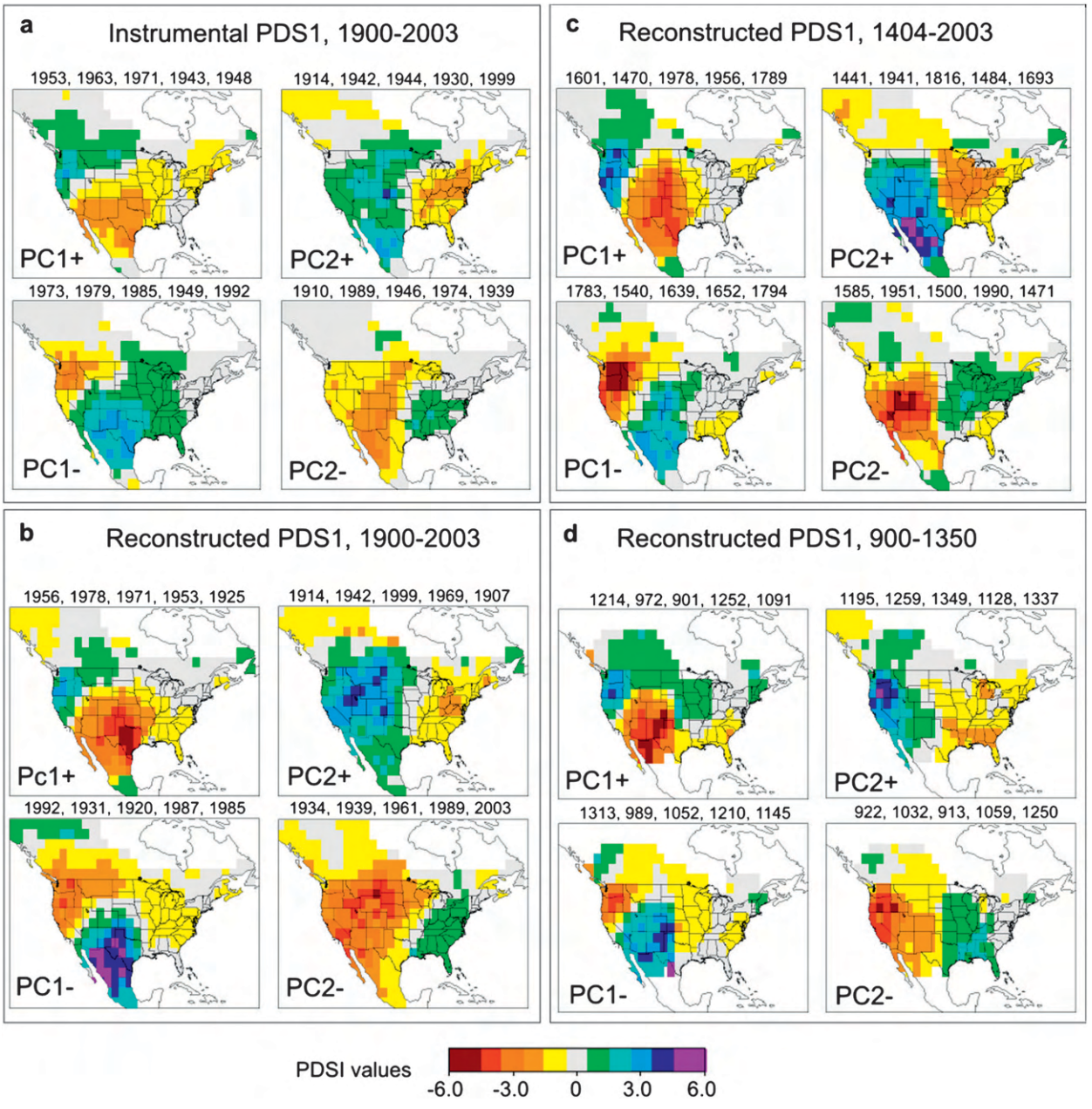

FIG. 2. Composite maps for five noncontiguous years with highest negative and positive loadings, (left) PC1 and (right) PC2, for each set. (a) PCA on instrumental PDSI, 1900–2003. (b) PCA on reconstructed PDSI, 1900–2003. (c) PCA on reconstructed PDSI, 1404–2003. (d) PCA on reconstructed PDSI, 900–1350. The composite maps were generated using the full gridded PDSI dataset.

rotation (nine and five), and by generating composite maps using drought datasets that used different spatial interpolation approaches [NOAA/National Climatic Data Center (2008c) Divisional PDSI and Dai et al. (2004) gridded PDSI]. Resulting maps were all very similar, sharing the southwest–northwest and east–west dipole patterns and most of the same five highest ranking years.

To further test the stability of these two drought patterns, the reconstructed PDSI data with years prior to the twentieth century were subject to the same PCA process. As with the instrumental data, 15 PCs were rotated, and the composite maps of the five highest ranking years for first two PCs were generated. The PCA process was run first on the years 1404–2003 (Fig. 1a), and then on a smaller subset of the gridded data for the years 900–1350 (Fig. 1b). In both cases, as with the instrumental data, the two PCs appear to be separate from each other (North et al. 1982). In the period 1404–2003,

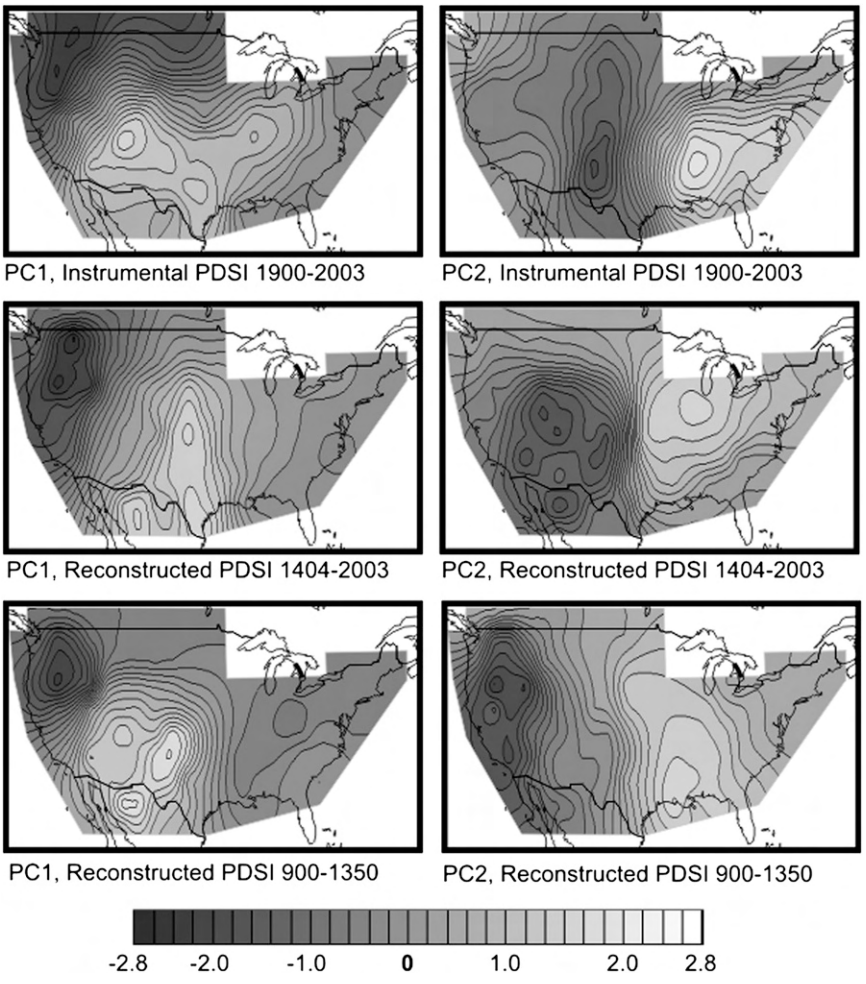

FIG. 3. Maps based on PC scores for (top) instrumental PDSI, 1900–2003, (middle) reconstructed PDSI, 1404–2003, and (bottom) reconstructed PDSI, 900–1350: (left) PC 1 and (right) PC 2.

the first two PCs explained 17% and 18% of the total variance, respectively, while explaining 21% and 14% of the total variance, respectively, for the 900–1350 period. The resulting map patterns were very similar for both the 1404–2003, and 900–1350 periods (the sign of the loadings for both reconstruction periods were reversed for PC1, and for PC2 for the 1404–2003 period, relative to the signs of the instrumental PC loadings; these have been changed in the figures to facilitate comparison; see Figs. 2c,d). The patterns for PC1 are the most consistently similar, especially with regard to western North America. In the medieval period, the pattern over the Midwest is different, but this could be due, at least in part, to the less complete data coverage over this region during this time (see Fig. 1b). The PC2 patterns are characterized by an east–west split in the general vicinity of the Great Plains. The spatial patterns based on the full time series for each of the three time periods, resulting from the PC scores, are very similar (Fig. 3).

The time series of the loadings for the period of time common to the instrumental and reconstructed PDSI PCs were compared to assess the skill of the reconstructed data in replicating the temporal as well as spatial patterns of the instrumental PDSI data (Fig. 4). The loadings were inverted where necessary so that negative values for PC1 indicate dry Southwest and wet Northwest conditions, while negative values for PC2 indicate dry west and wet east conditions (and the reverse for the positive loadings). The time series of the reconstruction loadings closely match the instrumental data. The correlations between instrumental and reconstructed PCs (unsmoothed) are $r = 0.830$ for PC1 and $r = 0.657$ for PC2. The higher correlation for PC1 is likely due to the close match with the instrumental PC from about

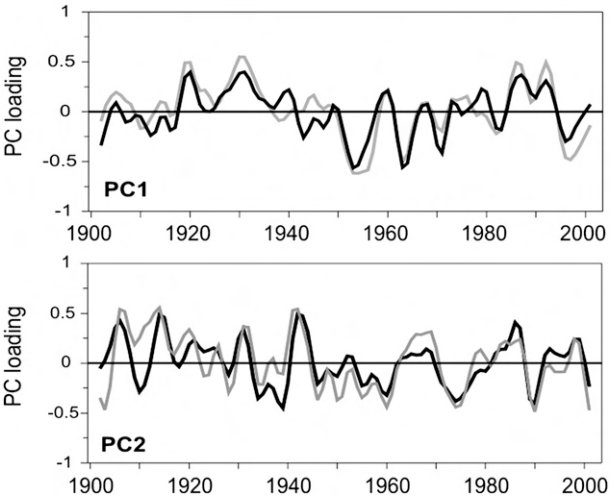

FIG. 4. Instrumental (black lines) and reconstructed (gray lines) PCs (top) 1 and (bottom) 2, 1900–2003, with five-point binomial filter. Loadings have been inverted where necessary so that negative values of PC1 indicate dry southwest–wet northwest and negative values of PC2 indicate dry west–wet east. Positive values are the opposite.

1950 to 1970, when southwestern U.S. droughts of the 1950s and 1960s were very well replicated.

The correlation between the rotated loadings for the PCs shows very a very weak statistically significant relationship between PC1 and PC2 for the analysis period, 1404–2003 ($r = -0.089$, $p < 0.05$), but not for the other two periods. The scores for the two PCs for all three time periods are uncorrelated. Statistically speaking, there is a chance that the two PCs are related to each other during the 1404–2003 period. In reality, such a relationship would not be unexpected, as is discussed in section 4.

b. Drought and atmospheric circulation

Correlation maps of the loadings for the two PCs and global 500-mb heights show the associations between the leading drought patterns and global circulation. The correlation map for PC1 features centers of negative correlation west of the Aleutian Islands and off Southern California and Baja, and positive correlations in the western North Pacific, over northern and eastern North America, and in the eastern North Atlantic (Fig. 5a, top). If shifted east, the two strongest centers of negative correlation would roughly approximate the Aleutian low and Northern Hemisphere 500-mb pattern corresponding to ENSO. The pattern is somewhat more similar to the western Pacific pattern of Wallace and Gutzler (1981) in their set of major teleconnection patterns identified during Northern Hemisphere winters (Figs. 5a,b, top), which is linked to equatorial Pacific conditions (Horel and Wallace 1981).

The main feature of the PC2 map is a center of negative correlation over Hudson Bay and extending east beyond the southern end of Greenland (Fig. 5a, bottom). A weaker center of negative correlation lies over central Asia. Positive correlations are centered over southeastern Europe and also stretch from eastern Siberia across the North Pacific Ocean. This pattern of correlations over northern latitudes is more indicative of the Arctic Oscillation pattern of 500-mb heights, which is dominated by a center of low pressure centered over Greenland, with high pressure stretching from eastern North America to central Europe, and over northeastern Asia. (Figs. 5a,b, bottom).

The circulation anomaly patterns associated with the two PCs do share a center of anomalous pressure off the coast of California. Negative PC1 (dry Southwest) and positive PC2 (dry west) are both associated with high pressure, but the pressure centers are in somewhat different locations. The center associated with PC1 is off the coast of Southern California and Baja, which would block flow into the southwestern United States, corresponding well to the southwestern–northwestern drought dipole pattern. The pressure anomaly off the coast of central to northern California in the PC2 pattern could lead to more west-wide drought, in agreement with the PC2 east–west drought dipole pattern. However, other features in the two anomaly patterns are rather different, which suggests there are two different sets of circulation patterns associated with the west coastal centers of high pressure for PC1 and PC2 droughts.

4. Discussion

The drought map patterns and the 500-mb correlation maps suggest two different North American drought patterns, and two types of circulation features associated with these two patterns that may be influencing drought across North America. The map pattern for PC1 shows a classic ENSO-type signature, and the corresponding correlation map shows the relationship between North American drought patterns and atmospheric circulation that could be expected from ENSO. ENSO has been shown to be a main driver of North American drought, so this result is not unexpected. The second PC is more strongly indicative of a Northern Hemisphere control on drought. The east–west dipole suggests meridional flow across the continent that is typically controlled by the position of the polar jet stream and the Rossby waves that influence its path (Barry and Chorley 2003). The correlation map supports a Northern Hemisphere annular mode (NAM) type of pattern, with centers of one sign over southern Greenland and the opposite sign over the Mediterranean (Thompson and Wallace 2000). Correlations between the PCs and the Southern Oscillation index

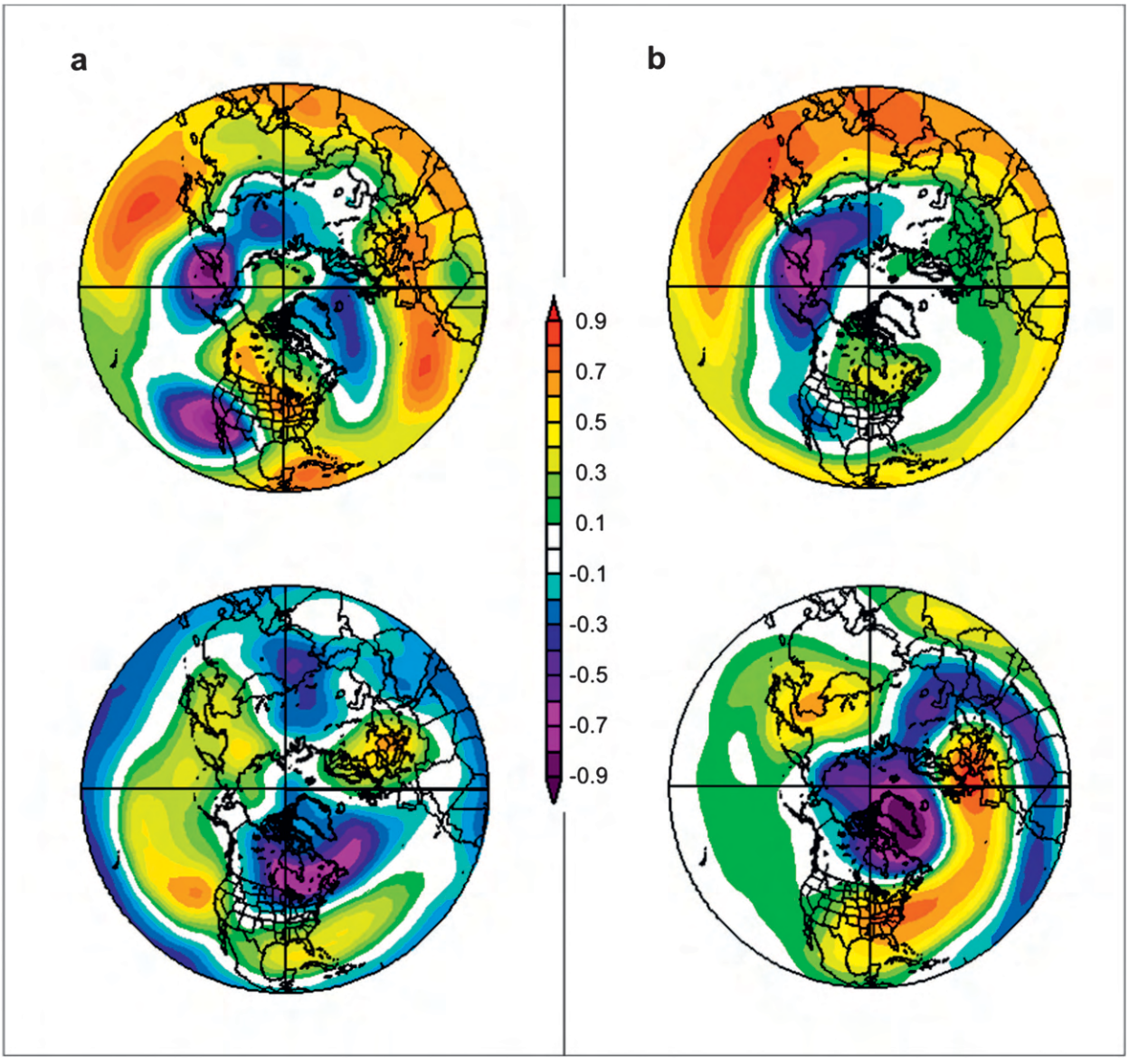

FIG. 5. (a) Correlation fields for December–March 500-mb heights and PC loadings: (top) PC1 and (bottom) PC2. (b) Correlation fields for December–March 500-mb heights and (top) western Pacific index (Wallace and Gutzler 1981) and (bottom) Arctic Oscillation (Thompson and Wallace 2000), 1949–2003. Images provided by NOAA/Earth System Research Laboratory (2008).

(NOAA/Climate Prediction Center 2008) and the Arctic Oscillation index (Thompson and Wallace 1998; data obtained from NOAA/Climate Prediction Center 2008), however, do not indicate a clear association based on these circulation indices, suggesting that the relationship is not a simple teleconnection. The two patterns—ENSO type and NAM type—do correspond well to the two main patterns of Northern Hemisphere winter climate variability identified by Quadrelli and Wallace (2004), related to the NAM and the Pacific–North American (PNA) pattern, with PNA representing an EOF that includes the Southern Oscillation index. If these two PCs do indeed represent major patterns of drought and reflect the influences on North American drought related to Northern Hemisphere atmospheric and equatorial Pacific Ocean–atmospheric circulation, then time series of the two PCs could be used to show variations in the contribution of these two circulation patterns to North American drought over multidecadal time scales.

In assessing the most recent century in the context of the past six centuries, a prominent feature is the 1950s drought, for which PCs indicate both drought in the Southwest and in the western United States (Fig. 6a). This period of drought coincided with strong La Niña

conditions from 1954 to 1956 (Wolter and Timlin 1993), indicated by the deeply negative PC1, but also with negative PC2 loadings suggesting an additional influence. The most recent drought also shows a combination of negative values for the two PCs, but in this case the east–west PC shows a more negative loading. The early twentieth century is characterized by widespread and persistently wet conditions throughout much of the western United States (Fye et al. 2003; Woodhouse et al. 2005). Corresponding to this pluvial period is a peak in PC1 loadings, followed by a peak in PC2 loadings, suggesting that this wet period was first due to favorable conditions in the equatorial Pacific, followed by favorable conditions in Northern Hemisphere circulation. The strongly and persistently positive PC loadings for this period are unprecedented going back to at least 1400, in agreement with reconstructions of Colorado River flow for the past five centuries (Stockton and Jacoby 1976; Woodhouse et al. 2006), which is perhaps another indication of just how anomalous the hydroclimatic conditions were that formed the basis of Colorado River allocations.

The end of the sixteenth century has been noted for severe, persistent, and widespread drought conditions that occurred over many parts of North America (Woodhouse and Overpeck 1998; Stahle et al. 2000). It has been hypothesized that this drought was due to persistent La Niña conditions (Stahle et al. 2000). The loadings for PC1 are strongly negative for much of the second half of the sixteenth century, in agreement with a possible link to ENSO (Fig. 6a). However, PC2 loadings are also deeply negative within this period, indicating that west-wide drought was possibly also influenced by Northern Hemisphere circulation. PC2 shifts abruptly to positive values at the turn of the century and into the first part of the seventeenth century. The dry conditions in the eastern United States associated with positive loadings of PC2 are in good agreement with the documented drought in the early part of the seventeenth century that likely devastated the Jamestown Colony (Stahle et al. 1998). The Colorado River basin and other parts of the western United States were documented to be quite wet in the early seventeenth century, also in agreement with positive PC2 loadings (e.g., Fye et al. 2003; Cook et al. 2004; Woodhouse et al. 2006).

While the two PCs are only very weakly correlated at annual times scales ($r = 0.089$, 1404–2003), the decadally smoothed time series show a closer association between the two PCs after about 1620 (1404–1619, $r = 0.149$; 1620–2003, $r = 0.454$). This suggests that over the last four centuries, at decadal time scales, both circulation patterns may often contribute to the wet or dry conditions in areas with drought anomalies of the same sign in both PCs, such as in the U.S. intermountain west, the western Great Plains, and northern Mexico. This could also be an indication of periods when the relationship between tropical Pacific Ocean and Northern Hemisphere circulation is more closely linked. Before this time, which appears to be characterized by lower-frequency variability and more persistent drought, one pattern appears to dominate over the other at these time scales.

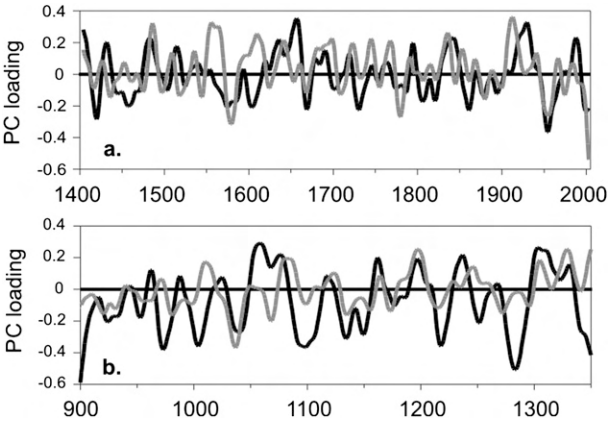

FIG. 6. Reconstructed PDSI loadings for PC1 (black line) and PC2 (gray line), smoothed with a 20-yr spline. Negative values of PC1 indicate a dry southwest–wet northwest, while negative values of PC2 indicate a dry west–wet east. Positive values indicate the opposite conditions: (a) 1404–2003 and (b) 900–1350.

During the Medieval period, the loadings of both PCs are often negative, with few extended periods of positive loadings (Fig. 6b). Periods when PCs are in and out of phase are also evident. The twelfth century has been shown to be a period of particularly persistent and widespread drought (Cook et al. 2004; Herweijer and Seager 2008; Meko et al. 2007). In this analysis, negative loadings on PC1 throughout much of the period, indicating drought in the Southwest (Fig. 6b), are in agreement with the studies that have suggested that a causal mechanism for the medieval droughts was a persistent La Niña state in the equatorial Pacific (Cook et al. 2007; Graham et al. 2007). During the medieval period, the percent of variance accounted for by PC1 more strongly suggests the role of ENSO (21% versus 14%) than in either the instrumental period (16% versus 14%) or the more recent reconstruction period (17% versus 18%), in support of previous work. In contrast, while the most persistent period of low flows in the Colorado River between A.D. 762–2005 is reported to be 1118–79 (Meko et al. 2007), and although this analysis suggests ENSO may have been a primary driver into the mid-1100s, neither PC is strongly negative after this point. The two PCs account for only 35% of the total variance, so other circulation features are likely influencing drought at this time period (as well as in other periods).

The numbers of chronologies from which the gridpoint PDSI is reconstructed is much reduced by 900. However, although sparsely distributed across the continent, regions west of the Rocky Mountains are still well represented, including the intermountain west, California, and the Pacific Northwest, with a small handful of eastern chronologies. Thus, the greater variance explained by PC1 during the medieval period is not likely to be due to a dominance of data in the southwestern United States. It should be noted that the comparisons of specific reconstructions with areas under drought are not independent, because virtually all of the tree-ring data have been used in the PDSI reconstructions as well as in the other reconstructions mentioned, but the point is that different circulation patterns may have lead to these regional droughts.

5. Conclusions

This analysis indicates two major patterns of drought across the U.S. and border regions of Canada and Mexico, a classic ENSO drought imprint and an east–west pattern of drought. The two patterns are remarkably robust over time, equally evident in both instrumental and reconstructed PDSI data, for the instrumental period as well as for the past six centuries. The two patterns are still well represented during the more data-scarce medieval period. The patterns seem to be insensitive to the number of components rotated, and composite maps using other sources of PDSI data display very similar patterns. The composite maps are based on the five years that best represent these patterns, and these patterns are supported by the mapped PC scores. In both cases, the resulting patterns are likely more clear-cut than will be the case in reality. The drought pattern for any given year will be a variable blend of the two PC patterns, in addition to other factors. The two patterns only explain about one-third of the total variance, indicating that complex and regional patterns more commonly characterize drought. However, this exercise serves as a starting point to investigate the circulation patterns associated with widespread drought patterns.

The 500-mb circulation patterns associated with the two drought patterns point to different types of circulation features related to drought. The circulation patterns by themselves cannot be interpreted as mechanistic features, but may be indicative of mechanisms. Although the PC1 drought pattern typifies the classic ENSO teleconnection pattern, especially in the western United States, the circulation pattern associated with this PC1 is not as clearly indicative of ENSO. The pattern also shares some features of the West Pacific index, which is related to equatorial Pacific conditions (Horel and Wallace 1981). Much research strongly supports the cool phase ENSO as a driver of drought in western North America, and it is likely that the link to ENSO exists here as well. The circulation associated with PC2 shares some of the main features of the Arctic Oscillation, which is part of a family of circulation modes that are characterized by opposing pressure in the northern middle and high latitudes, know collectively as the Northern Hemisphere annual mode (Thompson and Wallace 2000).

If these circulation patterns do indeed represent both tropical and Northern Hemisphere features, they suggest the role of both types of circulation in the occurrence of North American drought. Studies have suggested circulation typified by the NAM and ENSO are clearly important to midlatitude climate, so the link to major patterns of drought is plausible (Quadrelli and Wallace 2004; Nakamura et al. 2007). Because the two circulation modes are not independent (Nakamura et al. 2007), disentangling the influence of one or the other may be difficult. These results suggest that droughts in North America are influenced by the combined effects from the tropics and high latitudes, with one or the other playing a dominant role at times. Smoothed time series of the PC loadings indicate periods of time when the two are in phase and out of phase over decadal and multidecadal time scales. When in phase, the two patterns could be reinforcing the effects of each other, but may also indicate periods when the two circulation patterns are less independent. A challenge will be to confirm the findings suggested by this study in a way that provides a greater understanding of the drivers of drought under natural climate variability and global climate change.

Acknowledgments. Thanks to all the contributors of tree-ring chronologies that have made the reconstructed PDSI network possible, and to Ed Gille of the NOAA Paleoclimatology Branch for uploading the latest version of the PDSI reconstructions to run on the composite map tool. Our thanks also to Jeffery Lukas who helped with Fig. 3. We greatly appreciated the comments and suggestions of two anonymous reviewers.

REFERENCES

Arblaster, J., and Coauthors, 2007: Summary for policymakers. *Climate Change 2007: The Physical Science Basis,* S. Solomon et al., Eds., Cambridge University Press, 1–21.

Barlow, M., S. Nigam, and E. H. Berbery, 2001: ENSO, Pacific decadal variability, and U.S. summertime precipitation, drought, and stream flow. *J. Climate,* **14,** 2105–2128.

Barnston, A. G., and R. E. Livesey, 1987: Classification, seasonality, and persistence of low-frequency atmospheric circulation patterns. *Mon. Wea. Rev.,* **115,** 1083–1126.

Barry, R. G., and R. J. Chorley, 2003: *Atmosphere, Weather, and Climate*. 8th ed. Routledge, 421 pp.

Benson, L., and Coauthors, 2002: Holocene multidecadal and multicentennial droughts affecting Northern California and Nevada. *Quat. Sci. Rev.,* **21,** 659–682.

Blasing, T. J., 1975: Methods for analyzing climatic variations in the North Pacific sector and western North America for the last few centuries. Ph.D. dissertation, University of Wisconsin—Madison, 177 pp.

Brown, D. B., and A. C. Comrie, 2004: A winter precipitation 'dipole' in the western United States associated with multidecadal ENSO variability. *Geophys. Res. Lett.,* **31,** L09203, doi:10.1029/2003GL018726.

Cayan, D. R., 1996: Interannual climate variability and snow pack in the western United States. *J. Climate,* **9,** 928–948.

Cole, J. E., and E. R. Cook, 1998: The changing relationship between ENSO variability and moisture balance in the continental United States. *Geophys. Res. Lett.,* **25,** 4529–4532.

Cook, E. R., D. M. Meko, D. W. Stahle, and M. K. Cleaveland, 1999: Drought reconstructions for the continental United States. *J. Climate,* **12,** 1145–1162.

——, C. A. Woodhouse, C. M. Eakin, D. M. Meko, and D. W. Stahle, 2004: Long-term aridity changes in the western United States. *Science,* **306,** 1015–1018.

——, R. Seager, M. A. Cane, and D. W. Stahle, 2007: North American drought: Reconstructions, causes, and consequences. *Earth Sci. Rev.,* **81,** 93–134.

Dai, A., K. E. Trenberth, and T. Qian, 2004: A global data set of Palmer Drought Severity Index for 1870–2002: Relationship with soil moisture and effects of surface warming. *J. Hydrometeor.,* **5,** 1117–1130.

Daly, C., G. Taylor, and W. Gibson, 1997: The PRISM approach to mapping precipitation and temperature. *Proc. 10th Conf. on Applied Climatology,* Reno, NV, Amer. Meteor. Soc., 10–12.

Dettinger, M. D., D. R. Cayan, H. F. Diaz, and D. M. Meko, 1998: North–south precipitation patterns in western North America on interannual to decadal time scales. *J. Climate,* **11,** 3095–3111.

Diaz, H. F., 1983: Drought in the United States—Some aspects of major dry and wet periods in the contiguous United States, 1895–1981. *J. Climate Appl. Meteor.,* **22,** 3–16.

——, 1991: Some characteristics of wet and dry regimes in the contiguous United States: Implications for climate change detection efforts. *Greenhouse-Gas-Induced Climatic Change,* M. E. Schlesinger, Ed., Elsevier, 269–296.

Feng, S., R. J. Oglesby, C. M. Rowe, D. B. Loope, and Q. Hu, 2008: Atlantic and Pacific SST influences on Medieval drought in North America simulated by the Community Atmospheric Model. *J. Geophys. Res.,* **113,** D11101, doi:10.1029/2007JD009347.

Fye, F. K., D. W. Stahle, and E. R. Cook, 2003: Paleoclimatic analogs to 20th century moisture regimes across the USA. *Bull. Amer. Meteor. Soc.,* **84,** 901–909.

Gershunov, A., and T. P. Barnett, 1998: Interdecadal modulation of ENSO teleconnections. *Bull. Amer. Meteor. Soc.,* **79,** 2715–2725.

Glantz, M. R., R. W. Katz, and N. Nicholls, Eds., 1991: *Teleconnections Linking Worldwide Climate Anomalies*. Cambridge University Press, 545 pp.

Graham, N. E., and Coauthors, 2007: Tropical Pacific–mid-latitude teleconnections in medieval times. *Climatic Change,* **83,** 241–285, doi:10.1007/s10584-007-9239-2.

Herweijer, C., and R. Seager, 2008: The global footprint of persistent extra-tropical drought in the instrumental era. *Int. J. Climatol.,* **28,** 1761–1774, doi:10.1002/joc.1590.

——, ——, E. R. Cook, and J. Emile-Geay, 2007: North American droughts of the last millennium from a gridded network of tree-ring data. *J. Climate,* **20,** 1353–1376.

Horel, J. D., and J. M. Wallace, 1981: Planetary-scale atmospheric phenomena associated with the Southern Oscillation. *Mon. Wea. Rev.,* **109,** 813–829.

Kalnay, E., and Coauthors, 1996: The NCEP/NCAR 40-Year Reanalysis Project. *Bull. Amer. Meteor. Soc.,* **77,** 437–471.

Kangas, R. S., and T. J. Brown, 2007: Characteristics of U.S. drought and pluvials from a high-resolution spatial dataset. *Int. J. Climatol.,* **27,** 1303–1325.

Karl, T. R., 1983: Some spatial characteristics of drought duration in the United States. *J. Climate Appl. Meteor.,* **22,** 1356–1366.

——, and A. J. Koscielny, 1982: Drought in the United States: 1895-1981. *J. Climatol.,* **2,** 313–329.

McCabe, G. J., M. A. Palecki, and J. L. Betancourt, 2004: Pacific and Atlantic Ocean influences on multidecadal drought frequency in the United States. *Proc. Natl. Acad. Sci. USA,* **101,** 4136–4141.

Meko, D. M., C. A. Woodhouse, C. A. Baisan, T. Knight, J. J. Lukas, M. K. Hughes, and M. W. Salzer, 2007: Medieval drought in the upper Colorado River basin. *Geophys. Res. Lett.,* **34,** L10705, doi:10.1029/2007GL029988.

Nakamura, T., Y. Tachibana, and H. Shimoda, 2007: Importance of cold and dry surges in substantiating the NAM and ENSO relationship. *Geophys. Res. Lett.,* **34,** L22703, doi:10.1029/2007GL031220.

National Research Council, 2007: *Colorado River Basin Water Management: Evaluating and Adjusting to Hydroclimatic Variability*. National Academies Press, 222 pp.

NOAA/Climate Prediction Center, cited 2008: Monthly atmospheric and SST indices. [Available online at http://www.cpc.ncep.noaa.gov/data/indices/.]

NOAA/Earth System Research Laboratory, cited 2008: PSD interactive plotting and analysis pages. [Available online at http://www.cdc.noaa.gov/cgi-bin/data/getpage.pl.]

NOAA/National Climatic Data Center, cited 2008a: North American drought atlas PDSI reconstructions version 2a (2008)—Time series plots. [Available online at http://www.ncdc.noaa.gov/paleo/pdsi08_ts.html.]

——, cited 2008b: Tree-ring reconstructions of Palmer Drought Severity Index across North America over the last 2000 years. [Available online at http://www.ncdc.noaa.gov/cgi-bin/paleo/pd04plot.pl.]

——, cited 2008c: U.S. climate divisions dataset source and information. [Available online at http://www.cdc.noaa.gov/data/usclimdivs/data/.]

North, G. R., T. L. Bell, and R. F. Cahalan, 1982: Sampling errors in the estimation of empirical orthogonal functions. *Mon. Wea. Rev.,* **110,** 699–706.

Palmer, W. C., 1965: Meteorological drought. U.S. Weather Bureau Research Paper 45, 58 pp.

Quadrelli, R., and J. M. Wallace, 2004: Varied expressions of the hemispheric circulation observed in association with contrasting polarities of prescribed patterns of variability. *J. Climate,* **17,** 4245–4253.

Rajagopalan, B., E. Cook, U. Lall, and B. K. Ray, 2000: Spatiotemporal variability of ENSO and SST teleconnections to summer drought over the United States during the twentieth century. *J. Climate,* **13,** 4244–4255.

Rasmusson, E. G., and T. H. Carpenter, 1982: Variations in tropical sea surface temperature and surface wind fields associated with the Southern Oscillation/El Niño. *Mon. Wea. Rev.,* **110,** 354–384.

Redmond, K. T., and R. W. Koch, 1991: Surface climate and streamflow variability in the western United States and their relationship to large scale circulation indices. *Water Resour. Res.,* **27,** 2381–2399.

Richman, M. B., 1986: Rotation of principal components. *J. Climatol.,* **6,** 293–335.

Seager, R., Y. Kushnir, C. Herweijer, N. Naik, and J. Miller, 2005: Modeling of tropical forcing of persistent droughts and pluvials over western North America: 1856–2000. *J. Climate,* **18,** 4065–4088.

——, and Coauthors, 2007: Model projections of an imminent transition to a more arid climate in southwestern North America. *Science,* **316,** 1181–1184, doi:10.1126/science.1139601.

——, Y. Kushnir, M. F. Ting, M. Cane, N. Naik, and J. Velez, 2008: Would advance knowledge of 1930s SSTs have allowed prediction of the Dust Bowl drought? *J. Climate,* **21,** 3261–3281.

Shabbar, A., and W. Skinner, 2004: Summer drought patterns in Canada and the relationship to global sea surface temperatures. *J. Climate,* **17,** 2866–2880.

Stahle, D. W., M. K. Cleaveland, D. B. Blanton, M. D. Therrell, and D. A. Gay, 1998: The Lost Colony and Jamestown droughts. *Science,* **280,** 564–567.

——, E. R. Cook, M. K. Cleaveland, M. D. Therrell, D. M. Meko, H. D. Grissino-Mayer, E. Watson, and B. H. Luckman, 2000: Tree-ring data document 16th century megadrought over North America. *Eos, Trans. Amer. Geophys. Union,* **81,** 121.

StatSoft, Inc., 2005: STATISTICA (data analysis software system), version 7.1. [Available online at http://www.statsoft.com.]

Stockton, C. W., and G. C. Jacoby, 1976: Long-term surface-water supply and streamflow trends in the Upper Colorado River Basin. *Lake Powell Research Project Bulletin 18,* National Science Foundation, 73 pp.

Thompson, D. W. J., and J. M. Wallace, 1998: The Arctic Oscillation signature in the wintertime geopotential height and temperature fields. *Geophys. Res. Lett.,* **25,** 1297–1300.

——, and ——, 2000: Annular modes in the extratropical circulation. Part I: Month-to-month variability. *J. Climate,* **13,** 1000–1016.

Wallace, J. M., and D. S. Gutzler, 1981: Teleconnections in the geopotential height field during the Northern Hemisphere winter. *Mon. Wea. Rev.,* **109,** 784–812.

Wolter, K., and M. S. Timlin, 1993: Monitoring ENSO in COADS with a seasonally adjusted principal component index. *Proc. of the 17th Climate Diagnostics Workshop,* Norman, OK, NOAA/NMC/CAC and Cosponsors, 52–57.

Woodhouse, C. A., and J. T. Overpeck, 1998: 2000 years of drought variability in the central United States. *Bull. Amer. Meteor. Soc.,* **79,** 2693–2714.

——, K. E. Kunkel, D. R. Easterling, and E. R. Cook, 2005: The twentieth-century pluvial in the western United States. *Geophys. Res. Lett.,* **32,** L07701, doi:10.1029/2005GL022413.

——, S. T. Gray, and D. M. Meko, 2006: Updated streamflow reconstructions for the Upper Colorado River basin. *Water Resour. Res.,* **42,** W05415, doi:10.1029/2005WR004455.

Yarnal, B., 1993: *Synoptic Climatology in Environmental Analysis: A Primer*. Belhaven Press, 256 pp.

Quaternary Research 73 (2010) 107–117

Contents lists available at ScienceDirect

Quaternary Research

journal homepage: www.elsevier.com/locate/yqres

A bimillennial-length tree-ring reconstruction of precipitation for the Tavaputs Plateau, Northeastern Utah

Troy A. Knight [a,b,*], David M. Meko [b], Christopher H. Baisan [b]

[a] Department of Geography and Regional Development, University of Arizona, Tucson, AZ 85721, USA
[b] Laboratory of Tree-Ring Research, University of Arizona, Tucson, AZ 85721, USA

ARTICLE INFO

Article history:
Received 18 December 2008
Available online 3 October 2009

Keywords:
Tree-rings
Dendroclimatology
Drought
Climate
Utah

ABSTRACT

Despite the extensive network of moisture-sensitive tree-ring chronologies in western North America, relatively few are long enough to document climatic variability before and during the Medieval Climate Anomaly (MCA) ca. AD 800-1300. We developed a 2300-yr tree-ring chronology extending to 323 BC utilizing live and remnant Douglas-fir (*Pseudotsuga menziesii*) from the Tavaputs Plateau in northeastern Utah. A resulting regression model accounts for 70% of the variance of precipitation for the AD 1918–2005 calibration period. Extreme wet and dry periods without modern analogues were identified in the reconstruction. The MCA is marked by several prolonged droughts, especially prominent in the mid AD 1100s and late 1200s, and a lack of wet or dry single-year extremes. The frequency of extended droughts is not markedly different, however, than before or after the MCA. A drought in the early AD 500s surpasses in magnitude any other drought during the last 1800 yr. A set of four long high-resolution records suggests this drought decreased in severity toward the south in the western United States. The spatial pattern is consistent with the western dipole of moisture anomaly driven by El Niño and is also similar to the spatial footprint of the AD 1930s "Dust Bowl" drought.

Introduction

One of the most important achievements of North American paleoclimatic research has been the construction and continuing expansion of a continent-wide network of high-resolution climate-sensitive tree-ring chronologies. Despite the improved understanding of late Holocene climate conditions and change afforded by this network, relatively few tree-ring records are available prior to AD 1000, even in the densely sampled semiarid regions of western North America (Cook et al., 2004). Though this region boasts the greatest number of well-replicated millennial-length chronologies, their spatial coverage, species diversity and environmental setting are limited (Stahle et al., 2007). Most millennial-length chronologies are either from high-elevation sites (Hughes and Graumlich, 1996; Hughes and Funkhouser, 1998) or rely on archaeological samples for much of their length (Dean et al., 1985). While both types of chronologies have been useful in illuminating the climatic history of the west, the former is limited by a restricted or mixed environmental response, and the latter by a reduced ability to capture lower frequency (multi-decadal to centennial) climate variability (Cook et al., 1995). Over the past decade, efforts to address these limitations have been made by developing millennial-length, moisture-sensitive chronologies in lower elevation landscapes through utilization of remnant wood (logs, stumps, snags) (e.g., Grissino-Mayer, 1996; Meko et al., 2007).

In this paper we introduce a new tree-ring chronology constructed from living and dead Douglas-fir (*Psuedotsuga menziesii*), and a 2300-yr reconstruction of annual precipitation for the West Tavaputs Plateau of northeastern Utah. Our reconstruction adds 1500 yr to the record of climate history of northeastern Utah, and allows study of modern and past climatic variation from the perspective of the past 2000 yr. A motivation for this work was need for better information on the Medieval Climate Anomaly (MCA) (~AD 800–1300), perhaps the most significant long-term moisture anomaly in the western United States in the past two millennia (Hughes and Diaz, 1994; Cook et al., 2004; Graham et al., 2007). In the American West, numerous proxy records show this period as punctuated by prolonged and severe droughts unlike any in modern times (Stine, 1994; Benson et al., 2002; Cook et al., 2004; Meko et al., 2007). Recent dendroclimatic reconstructions in the Uinta Basin and Uinta Mountains of northeastern Utah highlight unusual wetness in the early 20th century (Carson and Munroe, 2005; Gray et al., 2004; MacDonald and Tingstad, 2007) and agree that some droughts in past centuries were more intense and prolonged than those of the instrumental record. But the longest of these reconstructions extends only to AD 1226, near the end of the MCA. In summarizing the longer record, we focus our analysis on three temporal scales: centennial, decadal, and annual. We identify

* Corresponding author. Fax: +1 520 621 2889.
E-mail address: tak@email.arizona.edu (T.A. Knight).

0033-5894/$ – see front matter
doi:10.1016/j.yqres.2009.08.002

changes in mean conditions and in the frequency and temporal distribution of extremes. We highlight a major drought in the first millennium AD, place droughts of the MCA and the period of modern observations in the context of the past 2000 yr, and examine the relationship between remote atmospheric/oceanic climatic drivers and moisture variability in the Tavaputs region.

Study area

The Tavaputs Plateau lies at about 40°N longitude in northeastern Utah and northwestern Colorado and constitutes the northernmost extent of the Colorado Plateau (Fig. 1). The western sub-plateau, west of the Green River, is the focus of this study. The plateau, whose elevation ranges from 1450 m to 3050 m, is highly dissected and features a labyrinth of steep-walled canyons. Much of the plateau is overlain by sedimentary rocks of the Green River Formation deposited in an Eocene inland lake. Vegetation patterns on the plateau generally depend on elevation and aspect, but are also influenced by cold-air drainage and other factors. Vegetation grades from salt desert scrub (*Atriplex* spp.) at the lowest elevations to mixed conifer and aspen (*Populus tremuloides*) forest at the highest elevations. Piñon (*Pinus edulis*)/juniper (mostly *Juniperus osteosperma*) woodland, sagebrush (*Artemesia spp.*) steppe, and Douglas-fir (*Psuedotsuga menziesii*) forest occupy the middle elevations.

Climate of the plateau and northeastern Utah in general is arid-to-semiarid continental, with precipitation amounts and temperature largely dependent on elevation. The plateau receives precipitation year-round with a high in March, a low in June, and a secondary peak from August through October. Precipitation is most variable in September and October. The primary sources of moisture in the Tavaputs region include frontal systems originating in the Pacific during winter, the North American Monsoon (NAM) in summer, and cutoff lows in late summer and early fall (Mock, 1996). Cutoff lows in September and October may bring excessive and persistent rains to the area and can make the difference between a year being wet or dry. Though this area marks the modern northernmost penetration by the NAM (Mitchell, 1976; Mock, 1996), the northward extent of the NAM has likely shifted through time (Peterson, 1994). Runoff from the plateau contributes to the Green River, a major tributary of the Colorado River.

Data

Tree-ring data

We collected Douglas-fir tree-ring samples from living trees and remnant wood in two side canyons of the plateau's primary drainage, Nine Mile Canyon, at elevations 2130–2225 m. Tree-ring series derived from these two sites are referred to from here on as the Harmon Canyon (HAR) chronology. Cores were taken from living trees by increment borer and cross-sections from remnant wood by chain saw. Both sites have poorly developed soil, sparse ground cover and low density of trees on steep rocky slopes. The conditions are ideal for climate-sensitive ring growth as soil-moisture retention is highly limited and competition among trees and disturbance is minimized (Fritts, 1976). The open-stand conditions and sparse fuels limit fire hazard, allowing extraordinary longevity of trees in addition to the accumulation and preservation of remnant wood. Remnant-wood samples were collected both on slopes where dead trees were found *in situ*, and on the canyon floor where debris-flow deposits emanated from secondary gullies.

Samples were prepared using standard dendrochronological techniques (Stokes and Smiley, 1968). Archaeological reference chronologies for the Four Corners region developed and held at the Laboratory of Tree-Ring Research helped confirm the crossdating of the older portion of the chronology. After measuring rings to the nearest 0.01 mm, we checked crossdating accuracy statistically with the program COFECA (Holmes, 1983).

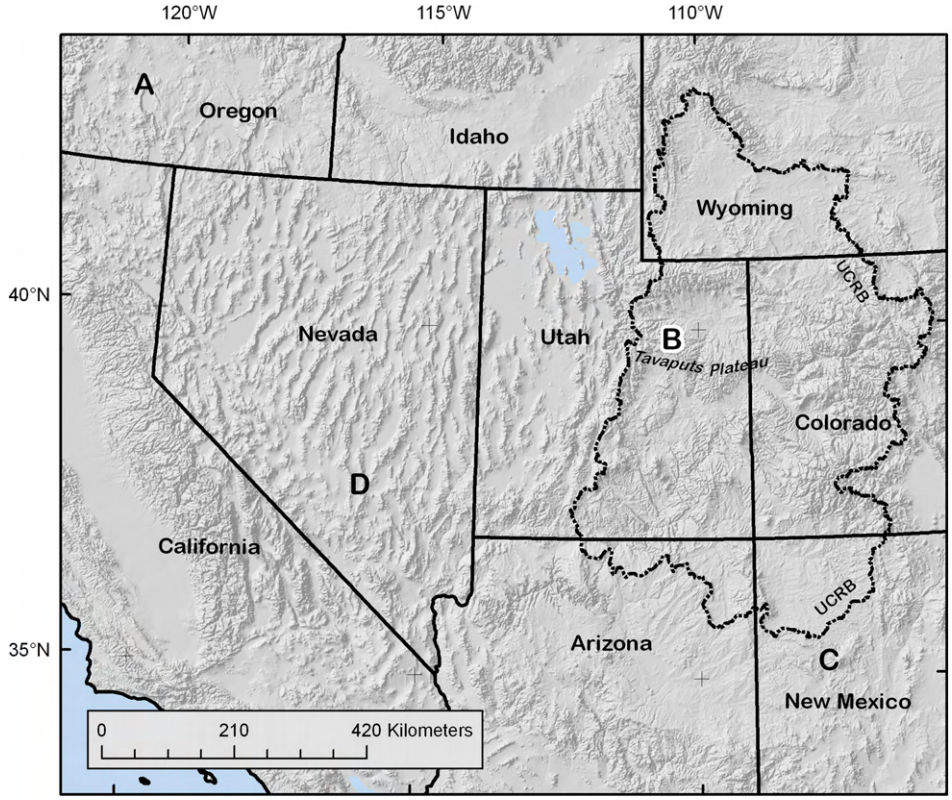

Figure 1. Map of southwestern United States showing site locations. Upper Colorado River basin (UCRB) outlined by dashed line. Letters mark Harmon Canyon tree-ring site on the Tavaputs Plateau (B), and other tree-ring sites and climate reconstructions plotted in Figure 8 (A, C, D). See caption in Figure 8 for details.

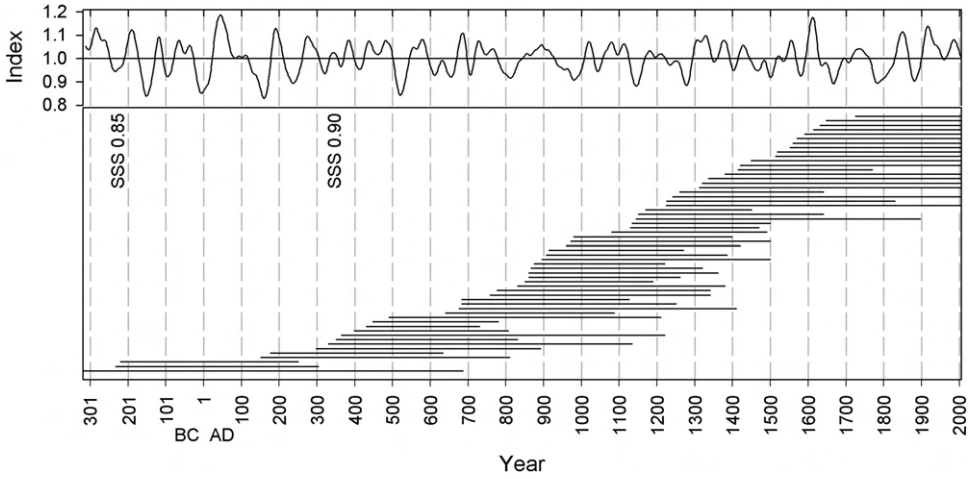

Figure 2. Sample depth of Harmon Canyon tree-ring chronology through time. Top: chronology smoothed with 50-yr spline. Bottom: time coverage by ring-width series for individual trees. These dates do not necessarily reflect establishment and death dates, due to erosion of outer rings, non-presence of pith, etc. Annotated are subsample signal strength (Wigley et al., 1984) thresholds of 0.85 and 0.90.

Measured ring-width series were standardized into a tree-ring chronology using the program ARSTAN (Cook, 1985). We excluded any tree less than 250 yr in age to avoid loss of low-frequency variance associated with detrending of short segments (Cook et al., 1995). Approximately 2/3 of the sampled series were detrended with negative exponential curves or straight lines, and the remainder with a cubic smoothing spline (Cook and Peters, 1981) with a 0.5 frequency response at 70 percent of the series length or 250 yr, whichever was longer. Indices were calculated by the ratio method for each measured radius (Fritts, 1976), and then averaged within trees to produce tree indices. These were then averaged over trees by a biweight mean to generate the site chronology. Variance stabilization options in ARSTAN were explored but not used as they produced inconsequential changes to the chronology. All subsequent analysis uses the "residual" site chronology, which ARSTAN produces by prewhitening (removing autocorrelation from) core indices before averaging over cores or trees.

The high mean between-tree correlation ($r^{-} = 0.86$) of the final HAR chronology indicates that growth variations at the site are driven by a common environmental factor. The mean sensitivity, a measure of high-frequency ring-width variance (Fritts, 1976), is 0.48, which is reasonably high for tree-ring chronologies typically used in climate reconstruction. The chronology includes 58 trees (19 living and 39 dead), and the mean segment-length of the indices for individual trees is 516 yr (Fig. 2). Though the chronology extends to 323 BC, the subsample signal strength does not exceed the suggested minimum threshold of 0.85 (Wigley et al., 1984) until 217 BC, when the sample size reaches two trees.

Climate data

Because the remote Tavaputs Plateau is not well represented by instrumental climate records, we used interpolated climate data to investigate tree growth/climate relationships. Precipitation data came from the Parameter-elevation Regressions on Independent Slopes Model (PRISM) (*http://www.prism.oregonstate.edu/*). PRISM uses weather station data, digital elevation models, and other spatial datasets combined with expert knowledge of climatic processes to derive gridded estimates of monthly precipitation across landscapes (Taylor et al., 1995). PRISM data were downloaded for six grid cells, each with a resolution of 4 km, across the northwestern portion of the plateau and centered on the tree-ring collection sites. The longer axis of the set of cells trends east-west, reflecting the plateau's drop in elevation from east to west. We averaged monthly values from all six points to create a mean Tavaputs precipitation series.

Reconstruction

Correlation analysis was used to identify the season of strongest precipitation signal in the tree-ring chronology. Climate data for this analysis included the PRISM precipitation data summed over 1, 3, 6 and 12 months ending with September of the growth year.

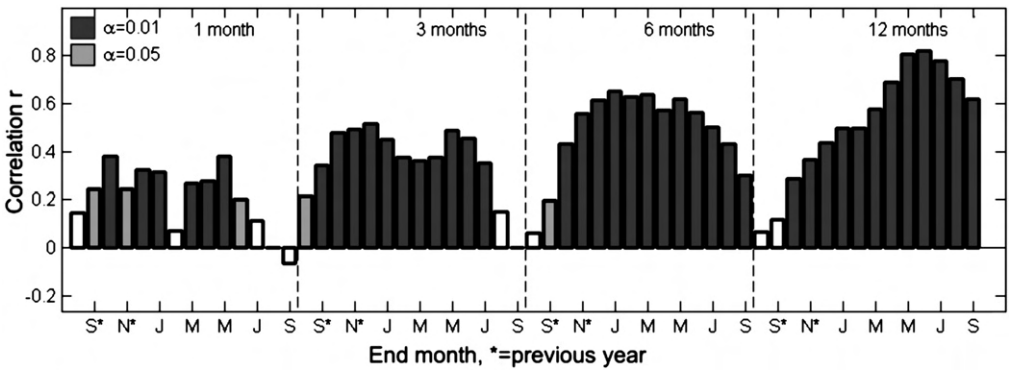

Figure 3. Correlations between the tree-ring chronology and monthly and seasonal PRISM precipitation. Month is end month of the seasonal grouping. Last month is September of growth year. Asterisk indicates months or seasons for year preceding growth year. Significance ($\alpha = 0.01$ and $\alpha = 0.05$) tested by a Monte Carlo method (see text).

Table 1
Calibration and validation statistics of reconstruction model.

Calibration period	Timespan	Calibration		Validation				
		R^2 adjusted	Std error	Sign test hits	Sign test misses	RE	r	RMSE
Late	1962–2005	0.78	42.76	36	8	0.57	0.79	
Early	1918–1961	0.62	47.04	38	6	0.72	0.88	
Full	1918–2005	0.70	46.04					46.6

All validation tests based on split sample method except root-mean-square error (RSME), which is from leave-one-out method.

Significance of correlations was tested by a Monte Carlo approach in which the sample correlations were compared with correlations between precipitation and simulated tree-ring series. The simulated tree-ring series were generated by "exact simulation" following Percival and Constantine (2006). In exact simulation, the spectrum of an observed series is first estimated by one of several possible methods. Circulant imbedding, which uses sampling of Gaussian noise and a frequency-domain approach (Davies and Harte, 1987), is then applied to generate the simulations. In our implementation, we used the periodogram for the spectral estimate (Bloomfield, 2000), and the Deitrich and Newsam (1997) method for circulant embedding. The method was used to generate 1000 simulations of the tree-ring chronology. These were then correlated with the precipitation series, and the 0.95 and 0.99 probability points of the 1000 sample correlations were taken as thresholds for significance.

Correlations reveal a highly significant relationship between the tree-ring chronology and PRISM-derived precipitation. Precipitation in the prior fall and winter appear to be important to Douglas-fir radial growth in the study area (Fig. 3). Correlations of the tree-ring chronology with precipitation increase as months are aggregated into seasons and are highest for the 12-month season grouping of previous July to current June ($r = 0.84$).

The reconstruction model is a regression of annual (July–June) PRISM precipitation on the tree-ring chronology. The model was calibrated on AD 1918–2005. Although PRISM data extends back to AD 1895, station coverage before 1918 was judged too thin to adequately represent climate variations both north and south of the plateau.

The model accounts for more than two-thirds of the variability of precipitation in the calibration period ($R^2_{adj} = 0.70$) (Table 1). Residuals analysis showed no evidence of violation of regression assumptions. Normality of residuals was supported visually by inspection of the histogram and statistically by a Kolmogorov–Smirnov test. Lack of autocorrelation of residuals was supported by the results of a Durbin–Watson statistic and by the plotted autocorrelation function. A scatter plot showed no dependence of residuals on fitted values. The regression was validated by a split-sample method in which the model is fit to one half of the data and tested on the other half (Snee, 1977). Validation included a sign test applied to signs of departures from the mean (Fritts, 1976), the reduction-of-error (RE) statistic, which measures the skill of prediction relative to climatology (the calibration-period mean) (Fritts et al., 1990), and the Pearson correlation between predicted and actual values. The root-mean-square error (RMSE) from cross-validation (Michaelsen, 1987) of the model calibrated on the full AD 1918–2005 period was used as an estimate of uncertainty of the long-term reconstruction.

Validation results show the reconstruction has positive skill (Table 1). The sign test is significant for validation on either half of the data, and RE values are well above 0. Correlation coefficients for the split-sample validation periods are also large and significant. The RMSE of cross-validation of the full model (46.6 mm) is considerably smaller than the standard deviation of the observed precipitation for the AD 1918–2005 full-period calibration (84.2 mm). The reconstruction tracks the observed precipitation closely (Fig. 4). Correspondence is good even for AD 1896–1917, which precedes the period used for computation of calibration and validation statistics and may have somewhat less reliable precipitation data.

Analysis of reconstruction

Methods

We evaluated the Tavaputs precipitation reconstruction, which spans 323 BC to AD 2005, at centennial-to-multidecadal, decadal, and annual scales. We restrict our more detailed analysis of decadal to annual variability of the reconstruction to the period after AD 200, when the chronology consists of 4 or more trees. For multi-decadal to centennial-scale variability we smoothed the reconstruction with 50- and 100-yr splines. At the decadal scale, we quantified duration and severity of wet and dry periods by smoothing the reconstruction with a 19-weight Gaussian filter whose wavelength of 50% frequency response is approximately the same as for an 11-yr moving average (Meko and Woodhouse, 2005). A wet or dry decadal episode was defined as an unbroken interval with the Gaussian-smoothed series above or below its long-term mean.

Within decadal episodes we identified periods of extreme wet or dry conditions as Z-scores of the Gaussian smoothed series exceeding an absolute value of 1.25. This threshold was reached four times

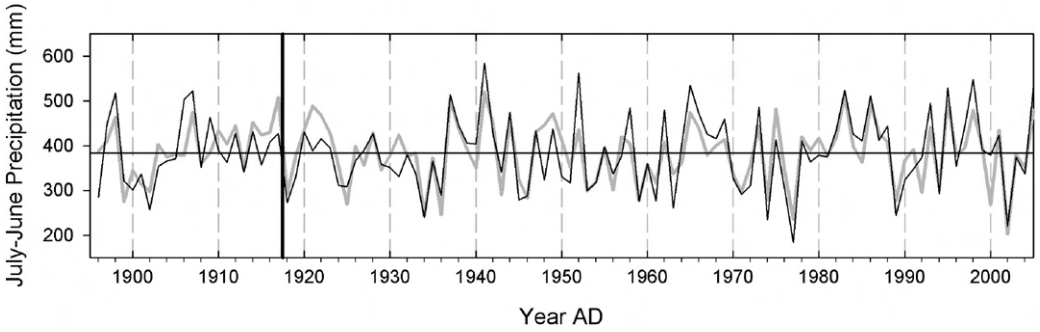

Figure 4. Time series plot showing agreement of observed and reconstructed annual July–June precipitation. Black line is PRISM observed precipitation. Gray line is tree-ring precipitation reconstructed by regression model. Vertical line marks start of calibration period (1918–2005) of model. Horizontal line is the calibration-mean observed precipitation (383 mm).

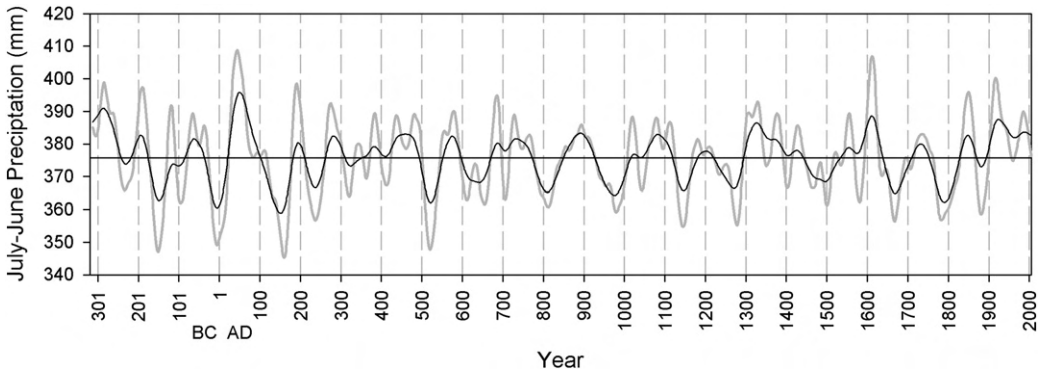

Figure 5. Smoothed long-term reconstruction showing multidecadal-to-centennial variation. Smoothing by 50-yr spline (gray) and 100-yr spline (black). Horizontal line is long-term mean reconstructed precipitation (376 mm).

during the historic period, including the extremely wet conditions of the early AD 1900s and the severe drought of the AD 1890s. We then ranked wet and dry decadal episodes by magnitude, defined as the maximum or minimum smoothed precipitation, and listed the duration and intensity of the episodes. Intensity was defined as the percentage of years exceeding the extreme dry/wet threshold in the episode.

Finally, taking advantage of the annual resolution afforded by tree rings, we identified the most extreme wet and dry years in the reconstruction. Compression of reconstructed values towards the mean, an unavoidable effect of regression, biases the direct comparison of observed and reconstructed precipitation values. Therefore, we based thresholds on reconstructed values. We identified the three wettest and driest reconstructed individual years for AD 1896–2005, the overlap of observed and reconstructed precipitation. The three driest were AD 2002 (202 mm), 1977 (236 mm) and 1934 (243 mm), and the three wettest were AD 1941 (520 mm), 1983 (513 mm), and 1917 (507 mm). Years of the long-term reconstruction were then classified as wet or dry if they were above 507 mm or below 243 mm.

Results

The precipitation reconstruction prior to AD 200 is marked by a dry phase from the early 2nd century BC to the 1st century AD and a sharp oscillation from a very wet phase to very dry phase during the first two centuries AD (Fig. 5). The magnitude of this oscillation is uncertain because the tree-ring chronology is based on only three trees during that period. However, an independently developed piñon (*Pinus edulis*) chronology from the Tavaputs Plateau shows similar oscillations (Knight, Meko, and Basain, unpublished data). After AD

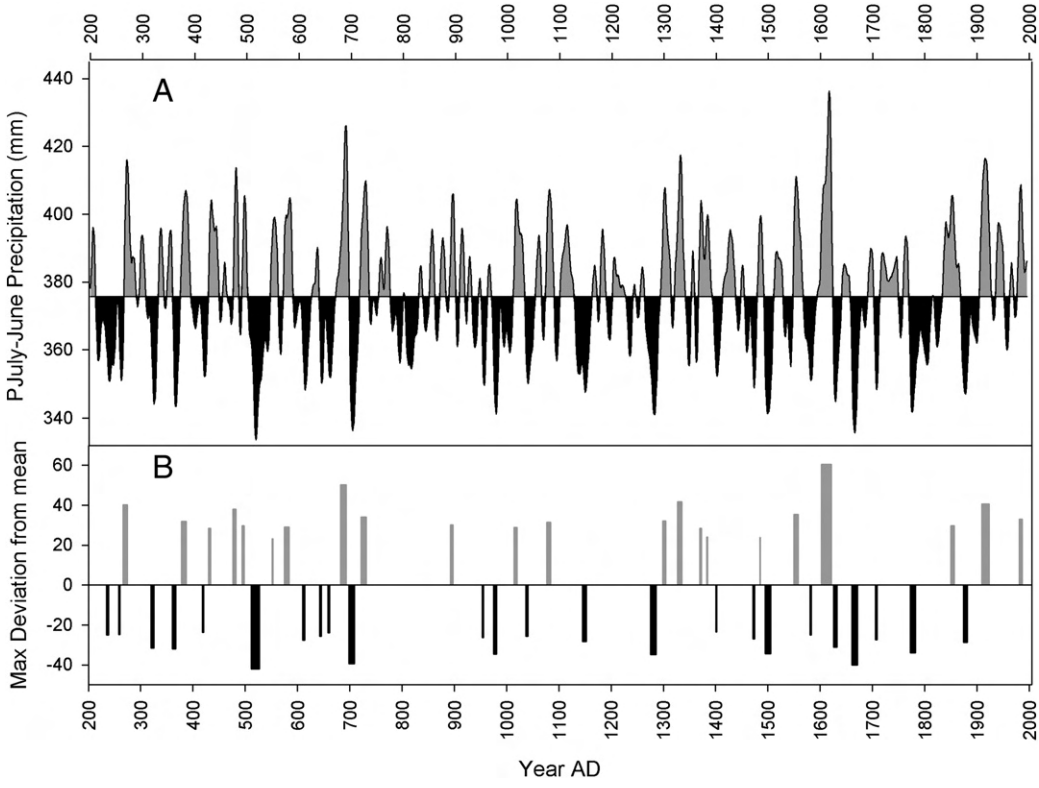

Figure 6. Time series plot showing decadal variation of reconstructed precipitation and timing of droughts and wet periods since AD 200. (A) reconstruction smoothed with 19-weight Gaussian filter. Dry episodes, or smoothed series below long-term mean, shaded black. Wet episodes, or smoothed series above mean, shaded gray. (B) Core droughts and wet periods defined as Gaussian-filtered series with standardized value exceeding 1.25 in absolute value. Height of bar represents maximum deviation of smoothed series from long term mean; width represents duration exceeding threshold.

200, long-term excursions from mean conditions occur during wet phases from AD 1300 to the early 1600s and from the mid-AD 1800s to present, and during dry phases from the early AD 1100s to 1300 and from mid-AD 1600s to mid-1800s. Between AD 500 and 1100 the series is characterized by oscillatory behavior at a wavelength of 70 to 150 yr.

Embedded within the centennial variation are numerous decadal-scale dry and wet episodes characterized by departures from the mean (Fig. 6). Statistics for episodes are listed in Table 2. Extreme magnitude, duration, and intensity of wet and dry episodes do not necessarily coincide. For instance, the dry episode AD 970–1010 lasted 41 yr but included only a 7-yr period below the "extremely dry" threshold. Conversely, the much shorter (19-yr) dry episode AD 1492–1510 included 11 yr below the threshold. Such differences emphasize the variety in time-series signatures of drought; all three properties—magnitude, duration and intensity—may be useful in gauging the strength of a dry or wet episode and its potential consequences for natural and human systems.

Two decadal episodes, one wet and one dry, stand out in terms of all three properties (Table 2). The first is the dry episode AD 502–544. This was the longest and highest magnitude dry episode, and it contained a 16-yr period below the "extremely dry" threshold. The second is the wet episode AD 1594–1623. This was the longest and highest magnitude wet episode and contained a 19-yr segment above the "extremely wet" threshold.

Abrupt transitions between the extreme categories of wet and dry occur several times in the reconstruction. For example, the transition from the wetness in the early AD 1600s (AD 1594–1623) to subsequent drought conditions is only 6 yr. Similarly, conditions switch from wet to dry, and back to wet, in a 49-yr period AD 683–731. In some cases these abrupt transitions are followed by long periods of more stable conditions. After the extreme oscillation ending in AD 731, the frequency and magnitude of extreme dry and wet periods drops and remains low until the dry period beginning in AD 1276 (Fig. 6B). This 500-yr period generally lacks decadal episodes of extreme conditions. After the wet period in the early AD 1600s, extremely wet conditions do not reemerge until the early AD 1900s—except for a brief period of wetness in the 1850s. This same interval of the early AD 1600s to early 1900s does have five extreme droughts (Fig. 6).

Table 2
Listing of ranked decadal-scale dry (A) and wet (B) periods.

Dry period—end year	(a) Max deviation from mean (cm)	(b) Length of period (yr)	(c) Mean annual deviation from mean (cm)	(d) Years below drought threshold	(e) % of period below drought threshold
(A)					
544	−42.19	43	−21.24	16	37
1688	−40.18	32	−16.13	11	34
715	−39.46	20	−33.17	11	55
1292	−34.80	30	−20.99	11	37
1010	−34.61	41	−16.16	7	17
1510	−34.45	19	−36.45	11	58
1833	−33.98	64	−15.06	10	16
372	−32.40	15	−27.72	7	47
329	−31.68	23	−18.08	6	26
1640	−31.10	17	−27.40	7	41
1904	−28.82	36	−18.72	8	22
1161	−28.30	34	−18.83	7	21
623	−27.71	35	−10.93	5	14
1713	−27.54	11	−27.65	4	36
1478	−27.02	24	−16.10	3	13
960	−26.34	29	−11.99	3	10
1052	−25.77	20	−17.68	5	25
669	−25.68	31	−21.04	3	10
263	−25.03	54	−16.98	4	7
1593	−24.93	27	−14.51	3	11
(B)					
Wet Period - end year	(a) Max deviation from mean	(b) Length of period (yr)	(c) Mean annual deviation from mean	(d) Years above pluvial threshold	(e) % of period above pluvial threshold
1623	60.51	30	34.72	19	63
695	50.35	26	28.72	11	42
1341	41.71	22	26.10	9	41
1928	40.73	24	29.11	15	63
306	40.31	43	15.96	8	19
484	38.03	11	45.21	6	55
1566	35.36	20	24.72	9	45
734	34.04	19	27.56	10	53
1996	32.97	20	15.21	6	30
1313	32.06	21	21.54	6	29
1088	31.51	16	29.77	10	63
392	31.29	20	19.03	8	40
900	30.20	13	21.89	5	38
1868	29.78	35	17.97	7	20
501	29.70	11	27.09	5	45
588	29.05	19	27.92	10	53
1032	28.76	22	19.60	6	27
446	28.41	21	26.95	5	24
1392	28.40	27	19.14	4	15
1491	23.87	13	23.50	2	15

Ranking by (a) maximum deviation of the smoothed series from long-term mean during period. Length of period (b) is number of years where smoothed series exceeds or drops below mean as in Figure 6A. Mean annual deviation from mean (c) is calculated from the unsmoothed annual reconstruction values within each period identified using the smoothed series. Years exceeding core threshold (d) is as in Figure 6B. Percentage of period exceeding core threshold (e) is 100 times ratio of (d) to (b).

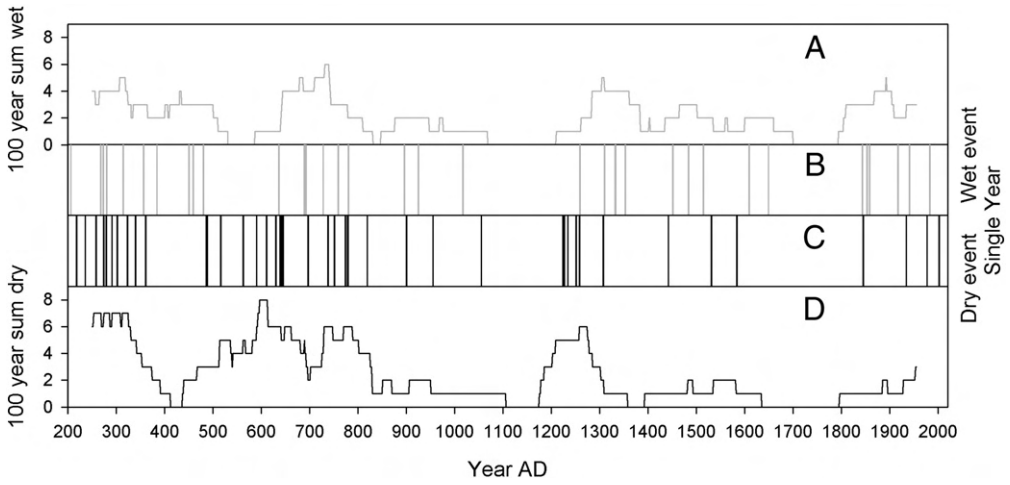

Figure 7. Extreme single-year dry and wet events. Bars indicate individual events, wet (B) and dry (C). See text for definition of events. Line graphs show sum of wet years (A) and dry years (D) in 100-yr moving window.

The identification of single-year extremes yielded 36 wet yr and 44 dry yr (Fig. 7). Extreme single-year events are unevenly distributed through time. Both wet and dry extremes cluster prior to AD 820, between AD 1220 and 1310, and again after AD 1840. Gaps or decreases in frequency of both wet and dry single-year extremes occur near AD 820–1220 and AD 1600–1840. The strong clusters prior to AD 820 are separated by shorter gaps: AD 362–485 for dry years and AD 481–635 for wet years. Consecutive years of single-year dry extremes occur only twice in the reconstruction, AD 562–563 and AD 778–779. The narrowest time-windows with three such events are 7 yr (AD 639–645) and 6 yr (AD 774–779). Extreme single-year events do not necessarily fall within or generate decadal dry and wet episodes. For instance, the wet episodes AD 1593–1623 and AD 1905–1928 are not characterized by large numbers of extreme wet years. Similarly, the severe decadal drought at the end of the AD 1200s is not characterized by a high frequency of single-year dry extremes; the dry extremes in the AD 1200s actually precede the severe decadal drought at the end of the century.

Discussion

The AD 500s drought

By several measures the AD 502–544 drought is the most severe of the Tavaputs reconstruction (Table 2). What was the larger spatial context of this drought? The question is difficult to answer because high-resolution records covering this period are rare. For a crude assessment, we assembled three of the longest and best-replicated tree-ring series, or climatic reconstructions based on them, from other parts of the American West. The series include a reconstruction of central Nevada precipitation based on the Methuselah Walk bristlecone pine (*Pinus longaeva*) chronology (Hughes and Graumlich, 1996), a reconstruction of northwestern New Mexico precipitation based on a Douglas-fir tree-ring chronology from the El Malpais lava flows (Grissino-Mayer, 1996), and a drought-sensitive western juniper chronology (*Juniperus occidentalis*) in south central Oregon (Meko et al., 2001). All three series reflect winter and spring precipitation, though the reconstruction from northwestern New Mexico probably reflects summer rainfall to some extent. All records are smoothed with a 31-yr spline to highlight decadal to multi-decadal variation.

In the Nevada and Oregon records, the early AD 500s are marked by drought, but the initiation appears slightly later than on the Tavaputs (Fig. 8). The annual reconstructed series of Tavaputs precipitation reveals the heart of the early AD 500s drought as two runs of below-average precipitation, AD 515–520 and AD 524–531. In both the Oregon and central Nevada records the AD 510s and 520s are similarly dry. In northwestern New Mexico, reconstructed precipitation is low in the AD 520s but above normal in the AD 510s. Like many other droughts of the tree-ring record, the AD 500s drought does not simultaneously hit all four of the key tree-ring sites. For instance, of the major MCA droughts—late AD 1000s, mid-1100s, and late 1200s—only the drought of the mid-AD 1100s appears at all four sites. The four series are strongly synchronous in the late AD 1500s and early 1600s, when severe drought is followed by a wet period, and in the late AD 100s during a high-magnitude wet period (Fig. 8).

To further refine our view of the extent of the AD 500s drought we looked at several other records available for the period. In two other moisture-sensitive millennial length tree-ring chronologies (not shown) recently developed in eastern and southeastern Utah, the early AD 500s appear as prominent low-growth feature (Knight, Meko, and Basain, unpublished data). Remnant-wood Douglas-fir samples from Eagle, Colorado, near the headwaters of the Colorado River, also show the early AD 500s as a low-growth interval (data provided by Connie Woodhouse).

Farther west, in the Sierra Nevada, evidence for extreme drought in the first half of the AD 500s is lacking. Giant Sequoia (*Sequoiadendron giganteum*) chronologies that cover this interval do no show a marked increase in frequency of very narrow rings (Hughes and Brown, 1992), while fire frequency in giant sequoia groves actually decreases (Swetnam, 1993). Hughes and Brown (1992) note, however, that giant sequoia tree rings are much better recorders of extremely dry single years than of multi-year extended dry periods. The sequoia record cannot therefore be regarded as strong evidence for absence of an early AD 500s drought in the Sierra Nevada.

In summary, a synthesis of information from long chronologies suggests the severe early AD 500s drought on the Tavaputs was part of a larger feature affecting at least parts of the Upper Colorado River Basin (UCRB), Great Basin and Pacific Northwest. This pattern is consistent with a contraction of the westerlies and withdrawal of the winter storm track to the north over western North America. Normal or high growth at tree-ring sites further to the south (e.g., New Mexico, Arizona) could still occur under these conditions with enhanced summer monsoon rainfall, or possibly with low-latitude storms undercutting a ridge over the western United States.

Medieval climate anomaly on the Tavaputs

The Tavaputs reconstruction gives an 1800-yr perspective on the moisture conditions between AD 800 and AD 1300 for a particular

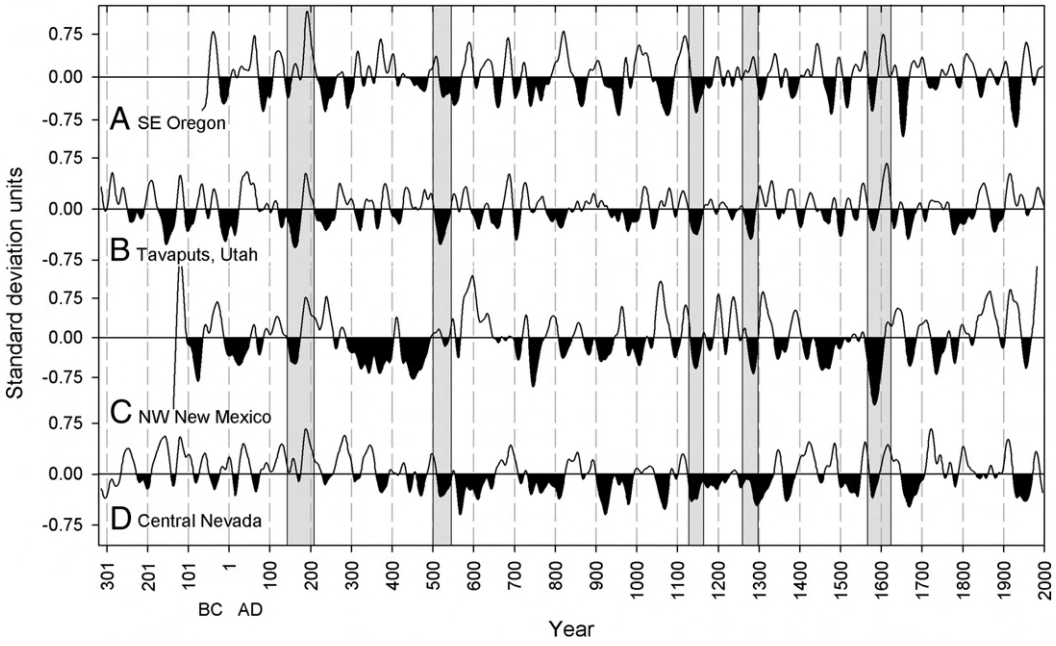

Figure 8. Comparison of Tavaputs precipitation reconstruction with other regional tree-ring climate reconstructions and a long moisture sensitive tree-ring chronology. Periods mentioned in text are shaded gray for emphasis. (A) Table Rock, Oregon, western juniper (*Juniperus occidentalis*) tree-ring chronology (Meko et al., 2001), (B) Tavaputs July–June precipitation reconstruction, (C) northwestern New Mexico climate-division 4 July–June precipitation reconstruction from El Malpais tree-ring chronology (Grissino-Mayer, 1996), (D) central Nevada climate-division 3 July–June precipitation reconstruction, from Methuselah Walk bristlecone pine chronology (Hughes and Graumlich, 1996), All series were converted to standard deviation units and smoothed with a 31-yr spline. See map in Figure 1 for locations of series.

location. From the AD 1130s to 1300 the Tavaputs is indeed dry, contrasting sharply with the wetness after AD 1300 (Fig. 5). Prolonged dry conditions also occur prior to AD 830 and again in the mid-to-late AD 900s, while wetter conditions are especially pronounced in the AD 1000s. High-amplitude low-frequency fluctuation rather than overall dryness characterizes the broader MCA interval. Other centennial-length dry periods, such as the mid-1600s to mid-1800s, rival those of the AD 1100s and 1200s. With decadal-scale smoothing (Fig. 6) droughts in the late AD 900s, mid-1100s and late 1200s are persistent, but their duration and magnitude are not unique (Table 2). Are the prolonged MCA droughts unusually clustered? Of the 20 highest-magnitude dry episodes (Table 2) five occur between AD 800 and 1300; these have an average duration of 33 yr. Five dry periods also occur in the previous 500-yr period, AD 300–800, while six and part of a seventh occur in the subsequent 500-yr period, AD 1300–1800. The average duration of dry periods is 28 yr both for AD 300–800 and AD 1300–1800. While high-magnitude droughts in the MCA are not unusually frequent, they are somewhat atypically long.

Other properties of the MCA as reconstructed on the Tavaputs merit attention. At the decadal scale, the record shows both rapid oscillations such as during the AD 800s and early AD 900s, and broader swings such as during the late AD 900s to mid-1100s. Both single-year (Fig. 7) and decadal-scale (Fig. 6) wet and dry extremes decrease in frequency and magnitude between AD 800 and 1200. Variance of reconstructed precipitation in moving 20- and 100-yr windows reaches its all-time low between AD 950 and 1200, the core of the MCA. Although our reconstruction marks the MCA as unusual in a few aspects of drought variability, the period stands out in the archaeological record of the Tavaputs Plateau. Between AD 1000 and 1300, people who lived a semi-sedentary lifestyle and practiced agriculture flourished in the canyons of the plateau (Spangler, 2000). Several features presented here, such as sustained droughts in the AD 1100s and 1200s and a lack of extremes prior to AD 1200, may have important archaeological implications for the eventual abandonment of agriculture by AD 1300 (Benson et al., 2007; Kloor, 2007).

20th century in long-term perspective

Is the instrumental record reflective of the range of natural climate variability for northeastern Utah? In short, we find the answer mixed. Prolonged and at times extremely intense droughts are a regular part of the Tavaputs long reconstruction but are absent from the modern record. This conclusion is consistent with two recent tree-ring-based moisture reconstructions for northeastern Utah (Gray et al., 2004; MacDonald and Tingstad, 2007). Our reconstruction classifies the modern period as wet in the context of the last 1800 yr, but not as wet as the early AD 1600s or possibly the early AD 1300s. The anomalous wetness of the 20th century has been pointed out in several paleoclimatic reconstructions for the West (Stine, 1994; Grissino-Mayer, 1996; Woodhouse et al., 2006; Stahle et al., 2007).

The implications for water management in the West are significant. Growing populations fueling increased demand have already placed stress on available resources. The current (1999–2008) drought, which sent Lake Powell on the Colorado River to record low levels (U.S. Bureau of Reclamation www.usbr.gov/uc/feature/drought.html), has been relatively brief in the context of the past two millennia. Yet this recent drought has raised the specter of severe water shortages with projected increasing temperatures (McCabe and Wolock, 2007).

The instrumental period does provide examples of what may be the most extreme short-term drought conditions. AD 2002 (6th driest), 1977 (34th driest) and 1934 (45th driest) are among the driest 3% of individual years in the reconstruction since AD 200. The worst-case scenario for water management may be the occurrence of one or more of these extreme years embedded in an extended dry period. An example from the past is the dry AD 600s, when four extremely dry years occur in the 15-yr interval AD 630–645. Such conditions could be stressful even for water-supply systems with considerable multi-year storage.

The extreme drought year AD 2002 emphasizes the potential impact on ecological systems of short-duration extreme events embedded within longer-duration droughts. AD 2002 witnessed both regional and local die-off of pinyon (*Pinus edulis*), a widespread

and ecologically important woodland dominant. The die-off most likely resulted from both direct drought mortality and weakened resistance to lethal bark beetles and other pests (Breshears et al., 2005). This die-off, though primarily driven by short-term extreme conditions, will have consequences that persist on the landscape for decades (Allen and Breshears, 1998). Return to a more persistent drought regime like those seen in past centuries could heighten the effects of such extreme years on water resources and ecosystems.

Drivers of climatic variability on the Tavaputs

Recent studies have linked UCRB precipitation and streamflow variability with remote atmospheric and oceanic oscillations, including the El Niño Southern Oscillation (ENSO), the Pacific Decadal Oscillation (PDO) and the Atlantic Multi-decadal Oscillation (AMO) (Hidalgo and Dracup, 2003; McCabe et al., 2007). On the inter-annual time scale, ENSO is a major contributor to climatic variability in the west. During El Niño episodes (warmer eastern tropical Pacific) the Pacific Northwest tends to be drier than normal and the southwestern US wetter than normal, and vice-versa during La Niña episodes (cooler eastern tropical Pacific) (Brown and Comrie, 2004). The UCRB lies in a transition zone between these poles. Much of Utah and southern Colorado responds as the southwestern US; the upper Green River Basin weakly responds as the Pacific Northwest; and the headwaters area in Colorado shows little correspondence with either pole (Hidalgo and Dracup, 2003; Woodhouse, 2003; Woodhouse et al., 2006). As mapped by Hidalgo and Dracup (2003), the Tavaputs falls clearly within the part of the UCRB whose ENSO response is like that of the southwestern US. We confirmed this through correlation of monthly and seasonal composites of the Tavaputs PRISM derived precipitation data with June-November Southern Oscillation Index (SOI), a measure of ENSO state, downloaded from NOAA's Climate Prediction Center (http://www.cpc.ncep.noaa.gov/data/indices/). Tavaputs precipitation is negatively correlated with SOI (June–July precipitation, 1933–2005, $r=-0.47$, $\alpha=0.01$), indicating wetter (drier) conditions during El Niño (La Niña). Examination of specific El Niño/La Niña events suggests this relationship is dominated by wetter conditions during El Niño, and that dry years are unrelated to La Niña events.

At the decadal to multi-decadal scale, shifts in the PDO and AMO may influence UCRB moisture variability, perhaps changing the spatial pattern of ENSO relationships within the UCRB by shifting the ENSO dipole transition zone (Hidalgo and Dracup, 2003). Anomalies in Tavaputs reconstructed precipitation indeed sometimes track inferred or reconstructed moisture conditions in Oregon (e.g., AD 680s–730s) and other times in New Mexico (e.g., AD 1260s–1340s) (Fig. 8). In general, warm North Atlantic sea-surface temperatures appear to be associated with 20th century UCRB drought (McCabe et al., 2007), while PDO tends to enhance ENSO teleconnections, strengthening El Niño effects during its positive (colder north Pacific) phase, and La Niña effects during its negative (warmer north Pacific) phase (Gershunov and Barnett, 1998; Timilsena et al., 2009). That Tavaputs precipitation is weakly positively correlated with the PDO ($r=0.272$, $\alpha=0.01$) is consistent with enhancement of El Niño effects by colder north Pacific sea-surface temperatures. The two driest decades of the instrumental record, however, AD 1970–1979 and 1926–1935, occurred during opposite PDO phases, suggesting this relationship is complicated by other factors.

Gridded tree-ring reconstructions of moisture conditions for North America have given insights into spatial patterns of drought and their possible forcing factors over the past 1200 yr (Cook et al., 2004; Herweijer et al., 2007; Stahle et al., 2007). The reconstructions can be linked to remote forcing factors either by analogy with modern droughts or by independent reconstruction of the forcing factors themselves (Graham et al., 2007; Seager et al., 2007). For example, MCA droughts in the 10th, 12th, and 13th centuries have been linked to winter-precipitation decreases possibly associated with persistent La Niña-like conditions driven by greater solar forcing and/or a lack of volcanic activity (Graham et al., 2007; Seager et al., 2007).

For earlier droughts, mapping of spatial patterns of drought and attribution of possible forcing factors becomes more and more difficult as the number proxy records diminishes with time. The early AD 500s drought is a case in point. The four records plotted in Fig. 8 suggest the AD 500s drought had a northwest dry/southwest wet pattern, which is consistent with El Niño. That the Tavaputs is one of the dry sites suggests the El Niño transition zone was shifted to the south.

For a broader spatial footprint of drought during years with New Mexico being wet and the other three locations dry (below −0.5 standard units), we examined gridded PDSI maps of Cook et al. (2008). For the common period of the four series (66 BC to AD 1992) such conditions occurred in a total of 28 yr, including 3 yr during the early AD 500s drought. The analysis of PDSI maps was restricted to the period after AD 800, when the number of tree-ring chronologies contributing to the PDSI reconstructions increases sharply. Fourteen of the 28 selected spatial-contrast years occurred after AD 800. The PDSI maps for those years were consistent with the moisture anomalies at the four key locations in showing Oregon dry and New Mexico wet. Three distinct larger scale patterns of drought were represented in the 14 maps: (1) drought centered on the interior northwest and extending south into central California and east into the northern and central Rockies, (2) drought similar to the first pattern but shifted southwards, with normal to wet conditions in western Canada and Washington, and (3) dry across nearly the entire continent, with strongest drought in a band across the northern and central Rockies and Plains, and less dry to neutral moisture conditions in southern California and the Southwest. The first two patterns are an El Niño/La Niña signature with the transition zone shifted south (case 1) or north (case 2). The third pattern recalls the 1930s "Dust Bowl" drought, associated with a warm North Atlantic, cool eastern tropical Pacific and a lack of El Niño events (Cook et al., 2007). Analysis of the PDSI maps by Cook et al. (2007) revealed this pattern to be relatively rare over the last 1000 yr. Thus, the early AD 500s drought could be a significant earlier example of this pattern.

Conclusions

The Tavaputs reconstruction provides several insights on local and regional climate history. The frequency and magnitude of wet and dry extremes, both annual and decadal, has changed through time, and only some past droughts and wet periods have analogues in the modern era. The diverse time-series signatures of droughts and wet periods in the tree-ring record emphasize the need to study climate series at multiple temporal scales. The reconstruction presented here helps quantify the natural range of variability, evaluate whether the instrumental record adequately reflects this variability, and identifies periods of time and events potentially significant to ecosystem and human history.

One such period with no analogue is the early AD 500s. A drought in the early AD 500s was identified as the most severe drought in the last 1800 yr of the reconstruction. The runs of dry years experienced then could have severe impacts on a society not prepared to deal with them. The small set of available tree-ring records of moisture conditions in the AD 500s suggests spatial patterns of moisture anomaly like those in El Niño/La Niña events and the 1930s "Dust Bowl". The data also hint at decadal to multi-decadal shifts in the transition zone of the El Niño/La Niña dipole. Increased density of tree-ring coverage during the first millennium AD will be essential for refining these preliminary conclusions. Our reconstruction supports other proxy records in suggesting that the period AD 800–1300 was characterized by a series of prolonged and

severe droughts. On the Tavaputs Plateau, however, these droughts were not unique in length or magnitude. This period does stand out for decreased variance and extremes, both decadal and annual. These characteristics may have important implications for understanding the regional archaeology.

Remnant-wood collections at lower elevations in the West have the potential to greatly extend our knowledge of the climate history of the region and thereby gain further understanding of the range of natural variability and change. Potential applications include identifying analogues for future climate change, examining the effects of climate on ecosystems and human populations, and ultimately assessing the causes and drivers of climate in the region. From collections made in 2005 we discovered three locations in eastern Utah that harbored remnant wood with rings prior to AD 500. In this paper we presented a precipitation reconstruction from the longest and best-replicated of these collections. Despite the already dense network of climatically sensitive tree-ring sites in the western United States, there remains significant potential for extending dendroclimatic reconstructions by focusing future efforts on remnant-wood collection.

Acknowledgments

This work was financially supported by grants from the Explorers Club Exploration Fund, the National Science Foundation IGERT Program in Archaeological Science at the University of Arizona, and the U.S. Bureau of Reclamation (award 04-FG-32-0260). We thank Erica Bigio and Erika Wise for their assistance in the field, and Erin Brannon for her assistance in the lab. We also thank Jeffrey Dean, Connie Woodhouse, and two anonymous reviewers for their valuable comments and suggestions on earlier drafts of this paper.

References

Allen, C.D., Breshears, D.D., 1998. Drought-induced shift of a forest-woodland ecotone: rapid landscape response to a climate variation. Proceedings of the National Academy of Sciences 95, 14839–14842.

Bloomfield, P., 2000. Fourier Analysis of Time Series: An Introduction, second edition. John Wiley & Sons, Inc., New York, p. 261.

Breshears, D.D., Cobb, N.S., Rich, P.M., Price, K.P., Allen, C.D., Balice, R.G., Romme, W.H., Kastens, J.H., Floyd, M.L., Belnap, J., Anderson, J.J., Myers, O.B., Meyer, C.W., 2005. Regional vegetational die-off in response to global-change-type drought. Proceedings of the National Academy of Science 102 (42), 15144–15148.

Benson, L., Kashgarian, M., Rye, R., Lund, S., Paillet, F., Smoot, J., Kester, C., Mensing, S., Meko, D., Lindström, S., 2002. Holocene multidecadal and multicentennial droughts affecting Northern California and Nevada. Quaternary Science Reviews 21, 659–682.

Benson, L.V., Berry, M.S., Jolie, E.A., Spangler, J.D., Stahle, D.W., Hattori, E.M., 2007. Possible impacts of early 11th, middle 12th, and late 13th century droughts on western Native Americans and the Mississippian Cahokians. Quaternary Science Reviews 26, 336–350.

Brown, D.P., Comrie, A.C., 2004. A winter 'dipole' in the western United States associated with multidecadal ENSO variability. Geophysical Research Letters 31, L09203.

Carson, E.C., Munroe, J.S., 2005. Tree-ring based streamflow reconstruction for Ashley Creek, northeastern Utah: implications for palaeohydrology of the southern Uinta Mountains. The Holocene 15 (4), 602–611.

Cook, E.R., 1985. *A Time Series Approach to Tree-Ring Standardization*. Ph.D. dissertation, University of Arizona, Tucson.

Cook, E.R., Peters, K., 1981. The smoothing spline: a new approach to standardizing forest interior tree-ring width series for dendroclimatic studies. Tree-Ring Bulletin 41, 45–53.

Cook, E.R., Briffa, K.R., Meko, D.M., Graybill, D.S., Funkhouser, G., 1995. The 'segment length curse' in long tree-ring chronology development for paleoclimatic studies. The Holocene 5 (2), 229–237.

Cook, E.R., Woodhouse, C.A., Eakin, C.M., Meko, D.M., Stahle, D.W., 2004. Long-term aridity changes in the western United States. Science 306, 1015–1018.

Cook, E.R., Seager, R., Cane, M.A., Stahle, D.W., 2007. North American drought: reconstructions, causes, and consequences. Earth-Science Reviews 81, 91–134.

Cook, E.R., et al., 2008. North American Summer PDSI Reconstructions, Version 2a. IGBP PAGES/World Data Center for Paleoclimatology. Data Contribution Series # 2008-046. NOAA/NGDC Paleoclimatology Program, Boulder CO, USA.

Davies, R.B., Harte, D.S., 1987. Tests for the Hurst effect. Biometrika 74, 95–102.

Dean, J.S., Euler, R.C., Gumerman, G.G., Plog, F., Hevly, R.H., Karlstrom, T.N.V., 1985. Human behavior, demography, and the paleoenvironment on the Colorado Plateaus. American Antiquity 50 (3), 537–554.

Deitrich, C.R., Newsam, G.N., 1997. Fast and exact simulation of stationary Gaussian processes through circulant embedding of the covariance matrix. SIAM Journal on Scientific Computing 18 (4), 1088–1107.

Fritts, H.C., 1976. Tree Rings and Climate. The Blackburn Press, Caldwell, New Jersey.

Fritts, H.C., Guiot, J., Gordon, G.A., 1990. Verification. In: Cook, E.R., Kairiukstis, L.A. (Eds.), Methods of Dendrochronology, Applications in the Environmental Sciences. Kluwer Academic Publishers, pp. 178–185.

Graham, N.E., Hughes, M.K., Ammann, C.M., Cobb, K.C., Hoerling, M.P., Kennett, D.J., Kennett, J.P., Rein, B., Stott, L., Wigand, P.E., Xu, T., 2007. Tropical Pacific – mid latitude teleconnections in medieval times. Climatic Change 83, 241–285.

Gray, S.T., Jackson, S.T., Betancourt, J.L., 2004. Tree-ring based reconstructions of interannual to decadal precipitation variability for northeastern Utah since 1226 A.D. Journal of the American Water Resources Association 40, 940–960.

Grissino-Mayer, H.D., 1996. A 2129-year reconstruction of precipitation for northwestern New Mexico. In: Dean, J.S., Meko, D.M., Swetnam, T.W. (Eds.), Tree-rings, Environment, and Humanity. Radiocarbon, Tucson, pp. 191–204.

Gershunov, A. and Barnett, T.P., 1998. Interdecadal modulation of ENSO teleconnections. Bulletin of the American Meteorological Society.

Herweijer, C., Seager, R., Cook, E.R., Emile-Geay, J., 2007. North American droughts of the last millennium from a gridded network of tree-ring data. Journal of Climate 20, 1353–1376.

Hidalgo, H.G., Dracup, J.A., 2003. ENSO and PDO effects of hydroclimatic variations of the upper Colorado River Basin. Journal of Hydrometeorology 4, 5–23.

Holmes, R.L., 1983. Computer assisted quality control in tree-ring dating and measurement. Tree-Ring Bulletin 43, 69–78.

Hughes, M.K., Brown, P.M., 1992. Drought frequency in central California since 101 B.C. recorded from giant sequoia tree rings. Climate Dynamics 6, 161–167.

Hughes, M.K., Diaz, H.F., 1994. Was there a "Medieval Warm Period", and if so, where and when? Climatic Change 26, 109–142.

Hughes, M.K., Funkhouser, G., 1998. Extremes of moisture reconstructed from tree-rings. In: Beniston, M., Innes, J.L. (Eds.), The Impacts of Climate Variability on Forests. Lecture Notes in the Earth Sciences, 74. Springer-Verlag, Berlin, pp. 99–107.

Hughes, M.K., Graumlich, L.J., 1996. Multimillennial dendroclimatic records from western North America. In: Bradley, R.S., Jones, P.D., Jouzel, J. (Eds.), Climatic Variations and Forcing Mechanisms of the Last 2000 Years. Springer Verlag, Berlin, pp. 109–124.

Kloor, K., 2007. The Vanishing Fremont. Science 318, 1540–1543.

MacDonald, G.M., Tingstad, A.H., 2007. Recent and multicentennial precipitation variability and drought occurrence in the Uinta Mountains region, Utah. Arctic, Antarctic and Alpine Research 39 (4), 549–555.

McCabe, G.J., Wolock, D.M., 2007. Warming may create substantial water supply shortages in the Colorado River basin. Geophysical Research Letters 34, L22708.

McCabe, G.J., Betancourt, J.L., Hidalgo, H.G., 2007. Associations of decadal to multidecadal sea-surface temperature variability with upper Colorado River flow. Journal of the American Water Resources Association 43 (1), 184–192.

Meko, D.M., Woodhouse, C.A., 2005. Tree-ring footprint of joint hydrologic drought in Sacramento and Upper Colorado river basins, western USA. Journal of Hydrology 308, 196–213.

Meko, D.M., Therrell, M.D., Baisan, C.H., Hughes, M.K., 2001. Sacramento River flow reconstructed to A.D. 869 from tree rings. Journal of the American Water Resources Association 37 (4), 1029–1040.

Meko, D.M., Woodhouse, C.A., Baisan, C.A., Knight, T., Lukas, J.L., Hughes, M.K., Salzer, M.W., 2007. Medieval drought in the upper Colorado River Basin. Geophysical Research Letters 34, L10705.

Michaelsen, J., 1987. Cross-validation in statistical climate forecast models. Journal of Climate and Applied Meteorology 26, 1589–1600.

Mitchell, V.L., 1976. The regionalization of climate in the Western United States. Journal of Applied Meteorology 15, 920–927.

Mock, C.J., 1996. Climatic controls and spatial variations of precipitation in the western United States. Journal of Climate 9, 1111–1125.

Percival, D.B., Constantine, W.L.B., 2006. Exact simulation of Gaussian time series from nonparametric spectral estimates with application to bootstrapping. Statistics and Computing 16 (1), 25–35.

Peterson, K.L., 1994. A warm and wet little climatic optimum and a cold and dry Little Ice Age in the southern Rocky Mountains, U.S.A. Climatic Change 26, 243–269.

Seager, R., Graham, N., Herweijer, C., Gordon, A.L., Kushnir, Y., Cook, E., 2007. Blueprints for Medieval hydroclimate. Quaternary Science Reviews 26, 2322–2336.

Snee, R.D., 1977. Validation of regression models: methods and examples. Technometrics 19, 415–428.

Spangler, J.D., 2000. Radiocarbon dates, acquired wisdom, and the search for temporal order in the Uinta Basin. In: Madsen, D.B., Metcalf, M.D. (Eds.), Intermountain Archaeology. University of Utah Anthropological Papers No. 122. University of Utah Press, Salt Lake City, UT, pp. 48–99.

Stahle, D.W., Fye, F.K., Cook, E.R., Griffin, R.D., 2007. Tree-ring reconstructed megadroughts over North America since A.D. 1300. Climatic Change 83, 133–149.

Stine, S., 1994. Extreme and persistent drought in California and Patagonia during medieval time. Nature 269, 546–549.

Stokes, M.A., Smiley, T.L., 1968. An Introduction to Tree-Ring Dating. University of Arizona Press, Tucson.

Swetnam, T.W., 1993. Fire history and climate change in giant sequoia groves. Science 262, 885–889.

Taylor, G.H., Daly, C., and Gibson, W.P., 1995. Development of a model for use in estimating the spatial distribution of precipitation. *Proceedings of the 9th Conference on Applied Climatology, Dallas TX*, American Meteorological Society pp.92–93.

Timilsena, J., Piechota, T., Tootle, G., Singh, A., 2009. Associations of interdecadal/interannual climate variability and long-term Colorado River Basin streamflow. Journal of Hydrology 365, 289–301.

Wigley, T.M.L., Briffa, K.R., Jones, P.D., 1984. On the average value of correlated time series, with applications in dendroclimatology and hydrometeorology. Journal of Climate and Applied Meteorology 23, 201–213.

Woodhouse, C.A., 2003. A 431-yr reconstruction of western Colorado snowpack from tree-rings. Journal of Climate 16, 1551–1561.

Woodhouse, C.A., Gray, S.T., Meko, D.M., 2006. Updated streamflow reconstructions for the Upper Colorado River Basin. Water Resources Research 42, W05415.

Posters

Beagles and Troch, 2010

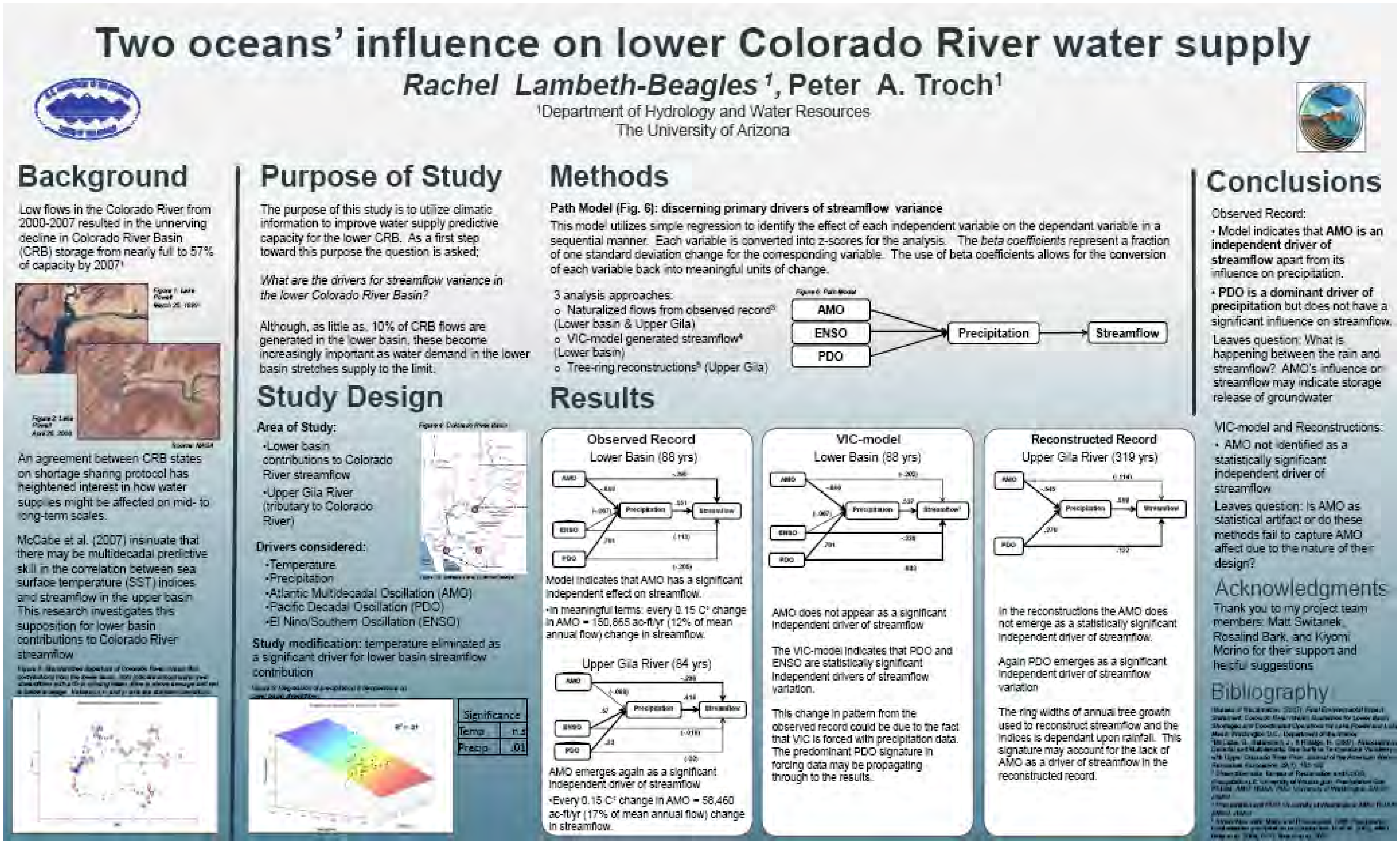

Switanek and Troch, 2010

Decadal Predictability in the Colorado River Basin

Matt Switanek[1], Peter A. Troch[1]

[1]Department of Hydrology and Water Resources, University of Arizona, Tucson, Arizona 85721, USA

Research Incentive

- Decadal to Multi-decadal oscillations in sea surface temperatures (SST) have been recognized to influence and modulate decadal hydroclimatic variability across the United States.
- Two of these oscillations that appear to have a significant influence on the hydroclimatic response are the Atlantic Multi-decadal Oscillation (AMO) and the Pacific Decadal Oscillation (PDO). AMO is the average SST in the central to northern Atlantic, while PDO is the first leading principal component of northern Pacific SSTs.
- Prior research has shown a relationship between streamflow at the outlet of the Upper Colorado River Basin (UCRB) along with AMO and PDO in the same overlapping decades.
- The current work uses the instrumental record to test the hypothesis: can skillful forecasts of streamflow in the UCRB be made a decade in advance knowing the last decade of AMO and PDO?
- Additionally, does the forecast skill obtained in the instrumental record change when using tree-ring reconstructions of streamflow, AMO and PDO?

Study Area and Data

- The Colorado River Basin is the lifeline of the Southwest. It provides approximately 18.5 billion cubic meters (15 million acre-feet) of water to Wyoming, Utah, Colorado, New Mexico, Nevada, Arizona and California. On average, approximately 90 % of this total volume comes from the UCRB.
- The Bureau of Reclamation, the governing body of the river and its dams, has naturalized flows at locations throughout the basin. It is important to attempt to use naturalized flows in this analysis, because these values try to represent the quantity of water that would have been produced in basins without any manmade diversions or dams. The figure below shows the Colorado River Basin with the naturalized flow points in the red circles.

The Colorado River Basin

- Entire Basin Size: 629,000 km^2
- UCRB Size: 290,000 km^2
- 28 naturalized flow points between the period 1906-2007

Figure 1

Methodology and Results

- The left plot of Figure 2 shows the AMO and PDO decadal climate indices on the x and y axes, respectively. While the color of the circles correspond to above average (blue) and below average (red) streamflows at Lee's Ferry (the outflow of the UCRB). The size of the circles reflect how much above or below average the streamflows were. The data used are ten year running means (there are 93 ten year running means with the instrumental record 1906-2007) of AMO and PDO, where the streamflows are shown for the same ten year running means.
- The right plot of Figure 2 shows the same as on the left, except that the streamflows are now lagged a decade behind AMO and PDO. Given the entire period on record, it looks as though when the previous decade of AMO and PDO are both negative, one might expect above average streamflows in the UCRB the next decade. Can this information be used to make useful predictions?

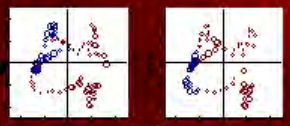

Figure 2

- Figure 3 shows the past information that is used in this relationship to predict the next decade of Lee's Ferry streamflow given the current state of AMO and PDO (shown as the black circle). This is done using Multiple Linear Regression and a Euclidian distance measure.

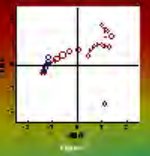

- The resulting forecasts of streamflow, in contrast to the observations, are shown in Figure 4. Using a MSE skill measure, statistically significant skill (99 %) is found in this case.

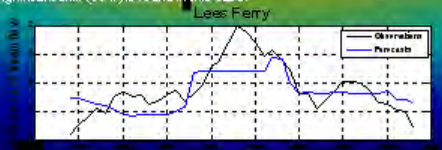

Figure 4

Acknowledgments

This project is funded by the Bureau of Reclamation. Please direct further questions about this poster to Matt Switanek at [redacted] or visit our website at [redacted]

Results

- Does the predictive skill that is observed in the instrumental record hold up using tree-ring reconstructions?
- Reconstructions of streamflow at Lee's Ferry, AMO and PDO are shown as ten year running means (the black lines) in Figure 5. The correlations between the reconstructions and the observations (orange lines) are .95, .93, and .84, respectively.

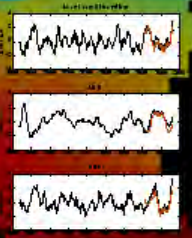

Figure 5

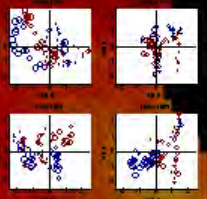

Figure 6

- Figure 6 shows again the relationship between AMO, PDO and streamflow, but this time using hundred year sections of the reconstructed data. The very clear pattern that we observed in the instrumental record does not exist for the reconstructions.
- The forecasts for the last 200 ten year running means using the reconstructions is seen in Figure 7. Though the skill is substantially reduced, it is still statistically significant.

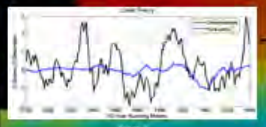

Figure 7

Summary and Discussion

- This study first proved that one could skillfully forecast UCRB decadal streamflows in the observed record using AMO and PDO.
  - However, given the smoothing nature of the running means and the relatively short time span, it is possible that these three frequencies could be randomly aligned.
- The reconstructions show that the relationship does in fact break down over a longer period of time. To be clear, tree-ring reconstructions are not perfect and we cannot trust them completely, but they can provide us with an idea of what might have been.
- So, we appear to have some skill in predicting decadal streamflows in the Colorado River Basin, but probably not as much as what the observed record might indicate.